Delft University of Technology
Faculty of Electrical Engineering, Mathematics and Computer Science
Delft Institute of Applied Mathematics

Mathematical modeling of particle nucleation and growth in metallic alloys

A thesis submitted to the
Delft Institute of Applied Mathematics
in partial fulfillment of the requirements

for the degree

MASTER OF SCIENCE
in
APPLIED MATHEMATICS

by

D. den Ouden

Delft, the Netherlands
December 2009

TU Delft

MSc THESIS APPLIED MATHEMATICS

"Mathematical modeling of particle nucleation and growth in metallic alloys"

D. den Ouden

Delft University of Technology

Abstract: The nucleation and growth of particles in metallic alloys has been studied thoroughly, but the effect of elastic deformation on this process remains unsolved. This work will attempt to incorporate the effect of elastic deformation in a previously proposed model for the nucleation and growth of precipitates. We adapt the KWN-models by Myhr and Grong (2000) and by Robson et al. (2003) to incorporate the effect of strain energy arising from elastic deformation on the nucleation and growth of Mg_2Si particles in an aluminum alloy at constant temperature. Both finite volume and finite element methods are used to simulate the process in regions with various geometries. Simulations of the nucleation and growth of NbC particles in an HSLA steel on the cylindrical region show that the incorporation of elastic strain energies has a noticeable impact on the process. The derived quantities of nucleation and growth, such as the particle volume fraction and the particle nucleation rate, show a clear spatial correlation with the calculated strain energy.

Keywords: KWN-model, nucleation, elastic deformation, strain energy, aluminum alloy, precipitates, Mg_2Si.

Daily supervisor

Dr.ir. F.J. Vermolen

Responsible professor

Prof.dr.ir. C. Vuik

Other thesis committee members

Ir. H.F.M. Corstens

Dr. L.Zhao

December 2009

Delft, the Netherlands

Preface

This thesis is the result of my Master of Science research project at the University of Technology at Delft, The Netherlands. This project has been carried out at the faculty of Electrical Engineering, Mathematics and Computer Science at the chair of Numerical Analysis.

I wish to thank Fred Vermolen for proposing and supervising this project, Lie Zhao for supplying information about the field of metallurgy and Cees Vuik for the opportunity to perform this research at the faculty of Electrical Engineering, Mathematics and Computer Science at the chair of Numerical Analysis. I finally wish to thank Pauline van der Horst for the support she has provided me whilst working on this thesis.

Contents

List of Figures

List of Tables

Chapter 1

Introduction

Metalworking of aluminum alloys is a complex operation that has several factors that influence the usability of the object after metalworking. The influence of most of these factors has been studied and achieved by a process of trial and error. A mathematical approach to investigate these factors could verify the obtained experimental results and extend the knowledge about the behavior of aluminum alloys during metalworking.

This document will focus on the factor regarding nucleation and growth of particles in aluminum alloys during tensile testing, since the presence and size of particles can influence the characteristics of the aluminum alloy object. Nucleation and growth of the particles will be modeled combining the models proposed by Myhr and Grong (2000) and Robson et al. (2003), based on the merits and drawbakcs of both models. Thereafter three systems will be described which model elastic deformations of a material, which will be combined with the model for nucleation and growth of particles, to investigate the influence of the elastic deformations on the nucleation an growth process.

In this paper we show that the model proposed gives reasonable (numerical) results, and thereby verifying that elastic deformations do impose changes to the nucleation and growth of particles for the cases that we studied.

The remainder of this document is structured as follows. First an introduction to the field of metallurgy is given. Chapter 3 will state and compare the separate models for particle nucleation and growth from Myhr and Grong (2000) and Robson et al. (2003). The next chapter will formulate a new model for the process of particle nucleation and growth, as well as three models for elastic deformations. This chapter will end with formulating relations between the deformation and nucleation models. Chapter 5 will present the results from applying numerical techniques, such as finite differences and finite elements, to the derived models. In the next chapter, the processes are simulated using the models, for which the results will be discussed. Finally a summary and some recommendations will be stated.

Chapter 2

Preliminaries in metallurgy

This chapter deals with the basic metallurgy concepts that are required to understand the behavior of alloys during equilibrium and when changing to equilibrium. We begin with a short introduction about the ordering of alloys. Then a discussion is presented about the thermodynamical behavior of alloys and the related phase diagrams. Next the diffusional concepts related to alloys are stated. Thereafter transformations due to diffusion are discussed. Finally some information is presented about metalworking techniques. The information presented in this chapter mostly originates from Porter (1981), especially Chapters 1, 2 and 5.

2.1 Metal alloys

Although the term alloy or metal alloy is unambiguous, one can still order these alloys by their properties. Such an ordering can be made on the solvent metal, but also on the number of components of the alloy. If using the solvent metal for ordering one can distinct the following twenty groups:

Aluminum	Gold	Mercury	Tin
Bismuth	Indium	Nickel	Uranium
Cobalt	Iron	Potassium	Zinc
Copper	Lead	Silver	Zirconium
Gallium	Magnesium	Titanium	Rare earth metals

Another common ordering uses the number of components in the alloy. Although any alloy unintentionally contains all the elements from the periodic table, only traces of most elements are found. If we neglect those elements of which only traces are present, we can number the components of the alloy by decreasing weight percentage or another factor. If only one alloy element is present besides the solvent metal, we speak of binary alloys. Likewise a ternary alloy consist of two alloy elements besides the solvent metal. Quaternary alloys consist of three alloy elements and the solvent metal. Alloys with more then three alloy elements do not have a specific name, which is the reason we call them complex alloys.

Besides the ordering on the number of components of an alloy there exist a subordering for the ternary, quaternary and more complex alloys. This ordering is based on the interaction of the alloy elements with each other. Assume we have a ternary alloy with alloy elements that have the intension to bond in a strict stoichiometric way. As a result we can view this alloy as a binary alloy, since each nucleus that will form, consists of a predefined combination of the two original elements. A ternary alloy with this property will be called a quasi-binary alloy. Likewise a distinction can be made in quaternary and complexer alloys.

Using the last ordering by number of components and the subordering by behavior of the alloy elements the overview in Table 2.1 is gained.

Binary	Ternary	Quaternary	Complex
	Quasi-Binary	Quasi-Binary	Quasi-Binary
		Quasi-Ternary	Quasi-Ternary
			Quasi-Quaternary

Table 2.1: Ordering of alloys by behavior of alloy elements.

2.2 Thermodynamics and Phase diagrams

Before starting with the discussion about thermodynamics and phase diagrams, the definition of three terms need to be given, so that the meaning of these words are clear. These terms are system, phase and component with definitions as below. As a result of these definitions, we can describe the composition of a system or phase by giving the (relative) amounts of the components.

Definition. *A **system** is an alloy that can exist as a mixture of various chemical elements ans states.*

Definition. *A **phase** is a portion of a system with homogeneous properties and a homogeneous composition, which is physically distinct from other phases, e.g. parts of the system.*

Definition. *A **component** is one of the elements or chemical compounds that make up the system.*

The transformations of the phases of a system into other phases can be described by the use of thermodynamics. A phase will transform into another phase or several other phases, depending on the stability of the phase. Eventually the system will be in it's most stable state. Stability in thermodynamics is described by the Gibbs free energy G, measured in joules (J), of the system, defined by

$$G = H - TY,$$

where H is the enthalpy in Joules, T the temperature in Kelvin (K) and Y the entropy of the system in Joules per Kelvin (J/K).The enthalpy H measures the heat content of the system and is given by

$$H = E + PV,$$

where E is the internal energy in Joules, P the pressure in Joules per cubic Meter (J/m^3) and V the volume in cubic Meters (m^3) of the system.

If the temperature and pressure are assumed to be constant, a system will eventually transform to the most stable state characterized by the lowest Gibbs free energy. Potential candidates for this stable state are determined by calculating the conditions such that

$$dG = 0.$$

From these candidates we denote the state with lowest Gibbs free energy as the stable equilibrium state, and the other candidates will be denoted by metastable states. If a system is in a metastable state, it will, given time, transform to the stable equilibrium state.

The above defined Gibbs free energy can be used to derive phase diagrams for alloys. This derivation will not be given, but can be found in Porter (1981). An example of a phase diagram for a binary alloy can be found in Figure 2.1. Here α, β and L are the possible phases the system can be in. The phase

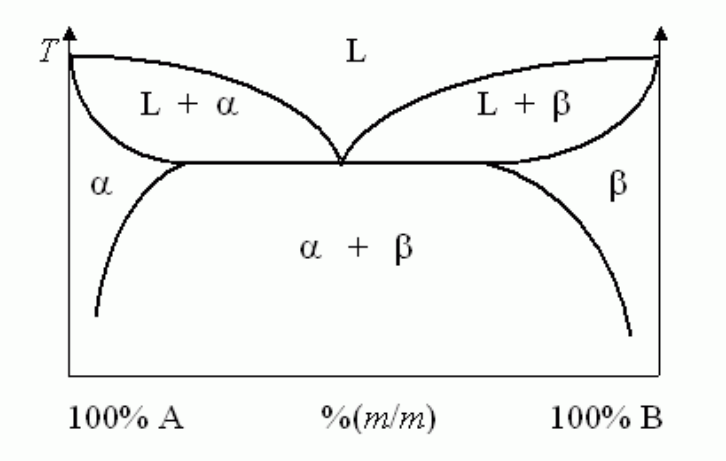

Figure 2.1: An example of a phase diagram. Image from Wikipedia (2002).

diagram has as horizontal axis the composition of the system, measured in the amount or concentration of one of the components. The vertical axis gives the temperature. Inside the diagram lines are drawn that separate the phases that the alloy can be in or can consist of.

Although the Gibbs free energy and phase diagrams can be used to derive information about a system that is in its stable equilibrium state, the probability that one has a system that is in such a state is small. Therefore the concept of diffusion in a system is needed. Besides diffusional transformations also martensitic transformations can occur. These transformations change the crystal structure, but do not use diffusion to achieve these transformations. Martensitic transformations will not be further discussed in this thesis.

2.3 Diffusion

If a system is not in a stable equilibrium state, an important process that influences the time and manner in which the equilibrium state is reached, is the diffusion of atoms in the system. There are two types of diffusion that occur in systems. The first type is interstitial diffusion, the second type substitutional diffusion. Interstitial diffusion occurs when the solute atoms are significantly smaller than the atoms of the solvent. The difference in size of the atoms allows the solute atoms to force their way between the atoms of the solvent atoms. If the solute atoms are as large or larger then the atoms of the solvent, substitutional diffusion occurs. Substitutional diffusion is characterized by a vacancy mechanism. Here a solute atom will move to a vacant place in the solvent matrix. A schematic interpretation of the two diffusion types can be found in Figure 2.2.

It is clear that interstitial diffusion can take place without influencing the ordering of the solvent atoms and thus the concentration of the solvent. This type of diffusion can therefore be modeled by Fick's second law. During substitutional diffusion it is likely that solvent atoms will also move to other locations in the matrix, thereby altering the concentration of the solvent. This means that the diffusion of solute atoms cannot be described by Fick's second law. If we assume on the other hand that we have a dilute solution, we may assume according to Porter (1981) that the solvent concentration is constant. As a result, also substitutional diffusion can be modeled by Fick's second law. Since substitutional diffusion requires the presence of vacancies, that are available in small numbers only, substitutional diffusion rates are much lower than interstitial diffusion rates in general.

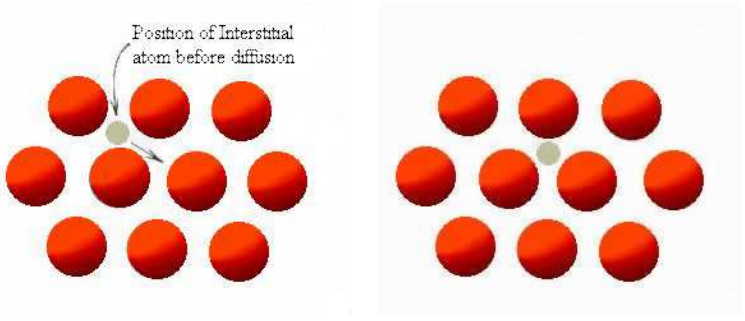

(a) Atom arrangement before interstitial diffusion.

(b) Atom arrangement after interstitial diffusion.

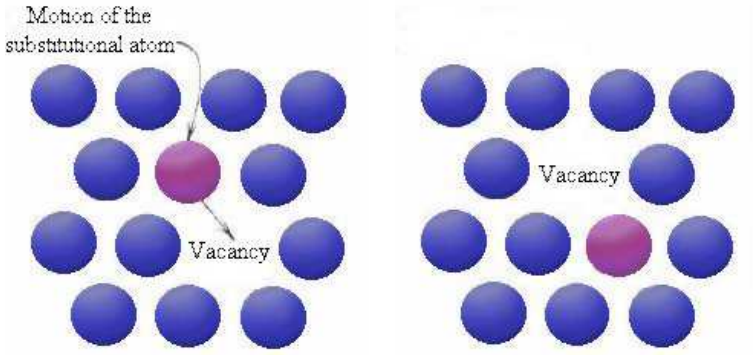

(c) Atom arrangement before substitutional diffusion.

(d) Atom arrangement after substitutional diffusion.

Figure 2.2: Interstitial and substitutional diffusion. Image from Seagrave and Canty (1999).

2.4 Diffusional transformations in solids

Due to diffusion, interstitial or substitutional, caused by a change in temperature the phases of a system can transform. There are five types of phase transformations possible, namely precipitation reactions, eutectoid transformations, ordering reactions, massive transformations and polymorphic changes. Precipitation reactions are those reactions that describe the transformation of a single solid phase into a mixture of two solid phases. If α is the phase before transformation and α' and β the phases after transformation, precipitation reaction can be expressed as

$$\alpha \rightarrow \alpha' + \beta.$$

If we have a system in a supersaturated metastable solid phase α and a precipitation reaction has occured, the resulting system will consist of two phases, α' and β. Here α' is a solid phase with lower Gibbs free energy than α but with the same crystal structure as α. β is a (meta)stable precipitate phase.

Eutectoid transformations describe the change of a phase consisting of two components into a mixture of two solid phases. If γ is the phase before transformation and α and β the phases after transformation, a general eutectoid transformation can be expressed as

$$\gamma \rightarrow \alpha + \beta.$$

In this case the mixture of phases α and β is more stable then the single phase γ. Both eutectoid transformations and precipitation reactions influence the matrix of the system. As a result these transformations can only occur if long-range diffusion is present in the system. Phase transformations that do not require long-range diffusion are the three remaining transformations.

Ordering reactions describe the transformation of a single phase α to the single phase α' and where the phase α has an disordered matrix structure and α' a ordered matrix structure. Reactions of these types can be expressed as

$$\alpha(\text{disordered}) \rightarrow \alpha'(\text{ordered}).$$

If a phase transforms into several other phases that have different crystal structures than the original phase, but with the same overall composition, a massive transformation has occurred. A simple example of this type of transformation can be described by the transformation

$$\beta \rightarrow \alpha.$$

In single component systems there can exist crystal structures that are stable in some temperature ranges. If the temperature changes in such a way that the present phase becomes unstable, a polymorphic transformation will occur. After this transformation the system will be in a stable phase with different crystal structure then the starting phase. Such a reaction can be described by

$$\gamma \rightarrow \alpha.$$

A schematic representation of the above discussed phase transformations can be found in Figure 2.3.

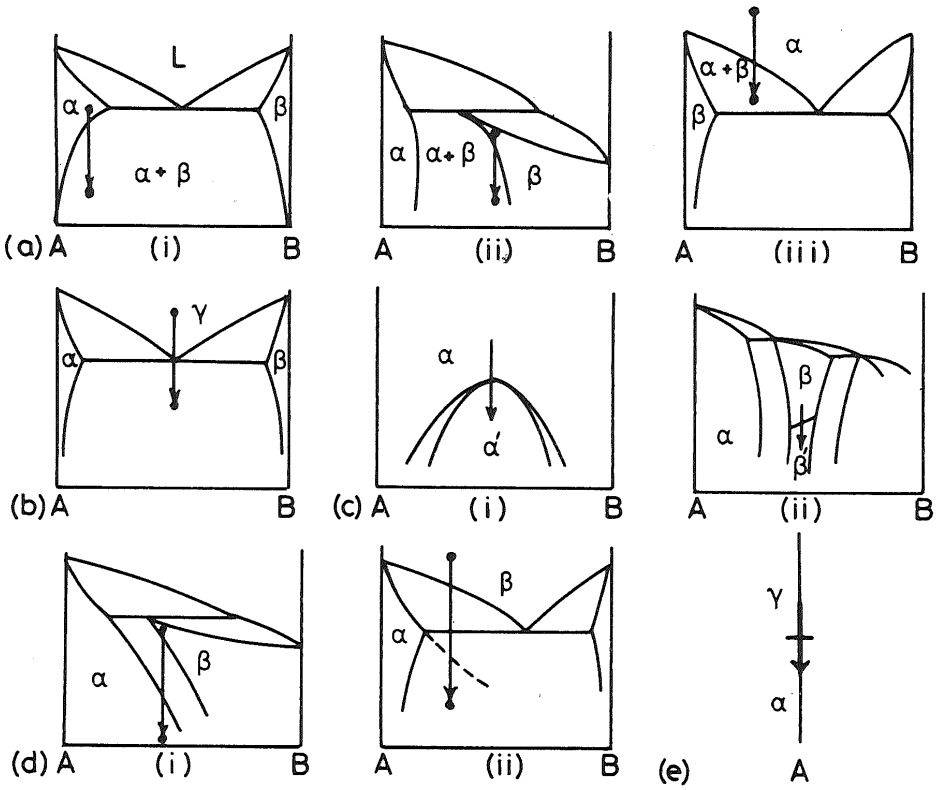

Figure 2.3: Examples of diffusional phase transformations. Image from Porter (1981).

In this thesis only phase transformations caused by precipitation reactions are modeled. These transformations are characterized by diffusional nucleation and growth. There are two types of nucleation, namely homogeneous and heterogeneous. The latter is the most occurring type and therefore will be used to model the nucleation in a system. After nuclei are formed, the nuclei will grow or shrink. This growth will also be modeled to describe the behavior of the system under time. The models for nucleation and growth will not be derived here, but can for example be found in Porter (1981).

2.5 Metalworking techniques

There exist several metalworking techniques, such as (flat) rolling, extrusion, pressing and casting. In this thesis only flat rolling and extrusion will be of importance. Both of these methods involve reforming the metal object by pressure.

Flat rolling is used to lower the thickness of a metal plate as in Figure 2.4. If the temperature of the plate is below the temperature at which nucleation stops, this method is referred to as cold rolling. If the temperature is higher, we speak of hot rolling. Extrusion is a method that reforms a block of metal into another shape by pressing it through a die. An example can be found in Figure 2.5. This methods can be also be distinguished by the temperature at which the metal is reformed.

Both methods can influence the nucleation and growth of particles as it changes the location of these particles, but also the volume of the metal object and as a result the concentrations influence nucleation and growth. The reforming of the metal is an application of an inelastic deformation, which means that it can be modeled by stress and strain. The relation between stress and strain cannot be described by Hook's Law, as this law only is applicable to elastic deformations.

The stress-strain relation for aluminum can be described by Figure 2.6. In this figure point 2 indicates the yield strength for aluminum. If a force is applied with resulting stress above this yield strength, inelastic deformations will occur. Forces with resulting stress below the yield strength result in elastic deformations. Point 1 depicts the maximum amount of stress a material can endure. Point 3 is the proportional limit stress, which indicates the maximum stress for which a material remains behaving elastic. Point 4 indicates the level of stress and strain to obtain a fracture or rupture of the material. Point 5 is used to determine point 2, the yield strength. It is called the offset strain and has typically a value of 0.2%.

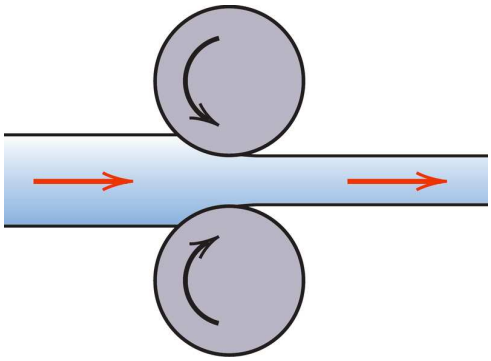

Figure 2.4: Flat rolling. Image from Wikipedia (2005).

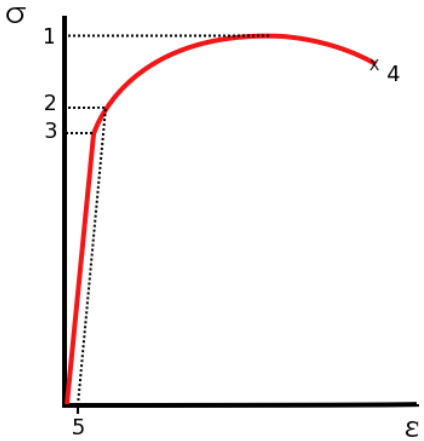

Figure 2.6: Stress-strain relation for aluminum. Image from Wikipedia (2003).

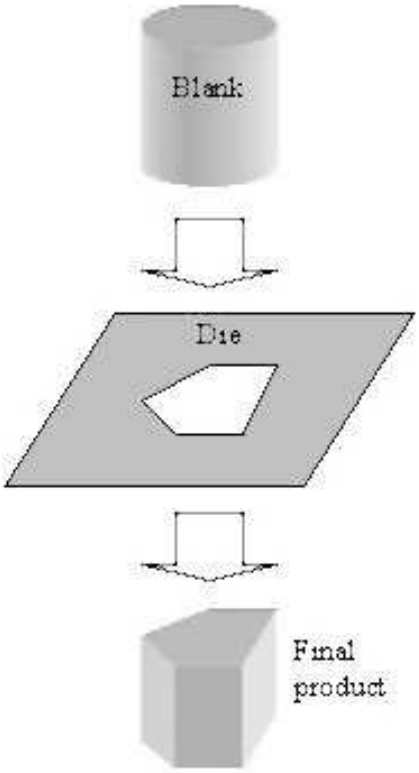

Figure 2.5: Extrusion. Image from Wikipedia (2004).

Chapter 3

Basic mathematical models

This chapter will discuss the derivation and formulation of two different models. Both models will be concerned with the precipitation, growth and coarsening of particles in binary and quasi-binary alloys and are based on the original model proposed by Kampmann et al. (1987), Wagner and Kampmann (1991) and Langer and Schwartz (1980). The first model has previously been discussed and simulated by Myhr and Grong (2000), the second model by Robson et al. (2003). These models differ in the type of nucleation that is modeled. The first model only describes heterogeneous nucleation, whereas the second model also includes homogeneous nucleation. We will only describe the heterogeneous part of Robson et al. (2003), as this is the only type of nucleation investigated during this thesis.

3.1 Nucleation and growth of particles according to Myhr and Grong (2000)

The model described in this section consists of three parts, each of them related to each other. We will state these parts individually in the next sections.

3.1.1 Heterogeneous nucleation of particles

In Section 2.4 the phase transformation precipitation reaction was discussed. This transformation is characterized by nucleation and growth of particles. From Myhr and Grong (2000) we can assume that the number of particles that are created, the heterogeneous nucleation rate, can be described by:

$$j = j_0 \exp\left(-\left(\frac{A_0}{RT}\right)^3 \left(\frac{1}{\ln(\bar{C}/C_e)}\right)^2\right) \exp\left(-\frac{Q_d}{RT}\right), \tag{3.1}$$

where j is measured in the number of particles per cubic meter per second ($\#/m^3 s$). In this formula $\bar{C}$ is the mean solute concentration in the system and C_e the equilibrium solute concentration at the particle/matrix interface, which can vary with time, both given in weight percentages (wt%). The factors j_0 and A_0 are parameters that are related to the energy barrier for heterogeneous nucleation and scale the nucleation to the correct proportions. Further R, T and Q_d are respectively the universal gas constant (8.314 J/Kmol), the absolute temperature (K) and the activation energy for diffusion (J/mol). The meaning of these quantities and any other terms can be found in the nomenclature at the end of this document.

The term C_e can be calculated using the phase diagrams as discussed in Section 2.2. In Myhr and Grong (2000) the Arrhenius rate relation, which describes the rate at which the concentration changes with temperature, is used. This relation gives as result the formula

$$C_e = C_s \exp\left(-\frac{Q_s}{RT}\right),$$

where C_s can be derived from either the phase diagram or estimated from experimental results (Porter, 1981).

3.1.2 Growth of particles

Besides a nucleation rate that predicts the number of new particles that will be created per second, the growth of the present particles will influence the precipitation reaction. For the sake of simplicity, Myhr and Grong (2000) assume that a particle has a spherical shape, with radius r. For this particle its radius will change in time at the rate

$$v = \frac{dr}{dt} = \frac{\bar{C} - C_i}{C_p - C_i} \frac{D}{r}, \tag{3.2}$$

where C_i is the particle/matrix interface concentration and C_p the concentration of the solute of interest inside the particle. It can be shown that C_i can be related to the equilibrium concentration C_e, which results in

$$C_i = C_e \exp\left(\frac{2\gamma_{\alpha\beta} V_m}{rRT}\right), \tag{3.3}$$

where $\gamma_{\alpha\beta}$ is the particle-matrix interface energy in J/m^2.

For each combination of possible concentrations $C_e, \bar{C}$, there is a particle that will neither grow or dissolve. From (3.2) and (3.3) we can derive that this particle has radius

$$r^* = \frac{2\gamma_{\alpha\beta} V_m}{RT} \left(\ln\left(\frac{\bar{C}}{C_e}\right)\right)^{-1}, \tag{3.4}$$

which we will call the critical particle radius of the system. From this result we can also conclude that v is negative for radii smaller than r^* and that v is positive for radii larger than r^*. This means that the smaller particles will dissolve and the larger will grow.

The diffusion coefficient D can be calculated by means of another Arrhenius relation depending on Q_d, R and T and is given by

$$D = D_0 \exp\left(-\frac{Q_d}{RT}\right),$$

where D_0 is derived from experimental results. For the derivation of this formula one is referred to Chapter 2 of Porter (1981).

3.1.3 The particle size distribution

During this study, we are interested in the number of particles in a certain system as a function of time. One way to describe this is the use of a particle concentration function. If we denote this concentration by N with the definition that $N(r,t)$ indicates the number op particles per cubic meter with particle radius between $r - \Delta r/2$ and $r + \Delta r/2$ at time t, we may derive a model for N. Δr is the size of a control interval.

Let $\Omega = (r - \Delta r/2, r + \Delta r/2) \subseteq [0, \infty)$ be an arbitrary domain. Let F be the flux of transport of particles over radii from this domain. If we assume that F has a positive orientation, the flow of particles into Ω is defined by $F(r - \Delta r/2)$. Similar the flow out of Ω equals $F(r + \Delta r/2)$. The change of particles with radii from Ω can also be due to a source term S. As a result, the change in time of the number of particles with radii from Ω can be expressed as

$$\Delta r \frac{\partial N}{\partial t} = F(r - \Delta r/2) - F(r + \Delta r/2) + \Delta r S.$$

Dividing by Δr and letting Δr tend to zero, we arrive with the use of the definition of the partial derivative at

$$\frac{\partial N}{\partial t} = -\frac{\partial F}{\partial r} + S.$$

The flux F is defined as the collective growth rate of particles with a certain size. We also formally know the rate at which the particles grow, namely v. This means that the flux F is given by $F = Nv$. Substituting this relation into the derived partial differential equation, results in

$$\frac{\partial N}{\partial t} = -\frac{\partial (Nv)}{\partial r} + S. \tag{3.5}$$

In the field of metallurgy one is often not interested in the number of particles per cubic meter (N), but in the particle size distribution function ϕ. To simplify things N is calculated numerically, after which ϕ can be determined by the relation $\Delta r\phi(r,t) = N(r,t)$ where r is the center of a control interval and Δr the size of this control interval.

3.1.4 The complete model for the particle distribution

Although we have formulated three formal expressions about the nucleation and growth of particles, we do not have a closed system yet. Closing this system requires the definition of the source term S in (3.5) and the definition of boundary and initial conditions for N.

We will start with defining the source term S. This term represents the number of particles that nucleate per second per cubic meter. In Section 3.1.1 we have formulated the function j, that has this same meaning. So a logical step is to relate S to j, but $S = j$ is not useful, since then the overall production over the real axis can become infinitely large. Research by Kampmann et al. (1987) has indicated that the particles that are being formed have a radius that is slightly larger then the critical radius r^*. Let Δr^* be a small positive number and denote by $r^* + \Delta r^*$ the radius of particles that are being formed. Now we can formally say that S is given by

$$S(r,t) = \begin{cases} j(t) & \text{if } r = r^* + \Delta r^*, \\ 0 & \text{otherwise.} \end{cases} \tag{3.6}$$

Although we now have defined the source term S, yet no relation between j and N has been given. This relation can be made easily if we define the mean concentration $\bar{C}$ as a function of N. In the above section we have formally defined the function ϕ as the size distribution function, which is related to N and will be used in the needed relation.

First define the particle volume fraction f as

$$f(t) = \int_0^\infty \frac{4}{3}\pi r^3 \phi dr. \tag{3.7}$$

Note that f is dimensionless. At any point in time, the total mass of solute atoms should remain constant. This indicates that we must have

$$\bar{C}(1-f) + C_p f = C_0,$$

where C_0 is the concentration of the solute in the overall system. Solving for $\bar{C}$ results in:

$$\bar{C} = \frac{C_0 - C_p f}{1-f}. \tag{3.8}$$

Using equations (3.7) and (3.8) to obtain j and S we have related S to our function N, which was needed to close the system. A fortunate result of the derived relation, is that we also have found a relation between v and N, by means of $\bar{C}$.

On inspecting the partial differential equation (3.5), we see that exactly one initial condition and at most one boundary condition is needed. The initial condition is of the form

$$N(r,0) = N_0(r),$$

where N_0 is a known positive function or identically zero. If we investigate the characteristics of the system, we see that these can be divided into to regions, to the left of r^* and to the right of r^*. The characteristics plane with the division line r^* is sketched in Figure 3.1. The region left of r^* has a negative growth rate v, to the right a positive growth rate v. Due to these characteristics, no boundary condition need to be specified.

We now have formulated a closed system that can predict the number of particles per cubic meter in an alloy. This system is given by

$$\begin{cases} \dfrac{\partial N}{\partial t} = -\dfrac{\partial (Nv)}{\partial r} + S & \text{for } r \in [0,\infty), t \in (0,\infty), \\ N(r,0) = N_0(r) & \text{for } r \in [0,\infty). \end{cases} \tag{3.9}$$

Note that this is a non-linear partial differential equation due to the relations between N, v and S.

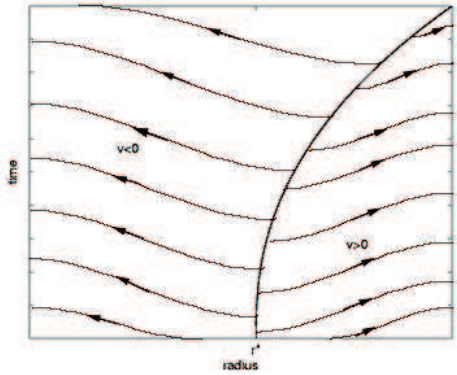

Figure 3.1: Characteristics of system (3.5).

3.1.5 Several derived quantities

Although a complete model has been formulated from which multiple quantities can be derived, other quantities are also of interest. These quantities are the total number of particles present in the system, the mean particle radius of the system and the standard deviation of the radii of the system. Both the total number of particles as the mean particle radius can be expressed as the moments of the size distribution function ϕ.

Let $n = n(t)$ be the total number of particles per cubic meter present in the system. This quantity can be calculated by the first moment of ϕ:

$$n(t) = \int_0^\infty \phi(r,t)dr.$$

Let $\bar{r} = \bar{r}(t)$ be the mean particle radius of the system. This quantity can be calculated by dividing the second moment of ϕ by the first moment of ϕ:

$$\bar{r}(t) = \frac{1}{n(t)} \int_0^\infty r\phi(r,t)dr.$$

Let $\rho(t) = \rho$ be the standard deviation of radii of the system. This quantity can be calculated by the next formula:

$$\rho(t) = \sqrt{\frac{1}{n(t)} \int_0^\infty (r - \bar{r}(t))^2 \phi(r,t)dr}.$$

3.2 Nucleation and growth of particles according to Robson et al. (2003)

The model described in this section also consists of three parts, each of them related to each other. This model is similar to the model discussed above, so some parts will not be discussed in detail.

3.2.1 Heterogeneous nucleation of particles

In Section 2.4 the phase transformation precipitation reaction was discussed. This transformation is characterized by nucleation and growth of particles. From Robson et al. (2003) we can assume that the number of particles that nucleate heterogeneously, can be described by:

$$j = N_v^* Z \beta^* \exp\left(-\frac{\Delta G_{\text{het}}^*}{kT}\right) \exp\left(-\frac{\tau}{t}\right), \tag{3.10}$$

where j is measured in the number of particles per cubic meter per second ($\#/m^3 s$). In this formula N_v^*, Z, β^* and τ are respectively the number of heterogeneous nucleation sites per unit volume, the

Zeldovich nonequilibrium factor*, the atomic attachment to a growing particle* and the incubation time for nucleation*. Further k and T are respectively the Boltzman constant ($1.3806504 \times 10^{-23} J/K$) and the absolute temperature (K). The meaning of these quantities and any other terms can be found in the nomenclature at the end of this document. The formulas for Z, β^* and τ can be found in Robson et al. (2003).

The term ΔG^*_{het} (in J) represents the energy barrier for heterogeneous nucleation, which can be expressed as a function of the critical radius r^*

$$\Delta G^*_{\text{het}} = \frac{4\pi}{3}\gamma_{\alpha\beta}(r^*)^2,$$

where r^* is given by (Robson et al., 2003)

$$r^* = \frac{-2\gamma_{\alpha\beta}}{\Delta G_v + \Delta G_s - \Delta G_{\text{dis}}}.$$

The energies ΔG_v, ΔG_s and ΔG_{dis} are respectively the change in chemical volume free energy driving nucleation, the strain energy per unit volume of a particle and the dislocation strain energy destroyed during nucleation. All three energies are given in J/m^3. As the term ΔG_{dis} is approximately equal to ΔG_s, as stated by Robson et al. (2003), we will follow this assumption by setting $\Delta G_s - \Delta G_{\text{dis}} = 0$.

The change in chemical volume free energy ΔG_v is chosen by Robson et al. (2003) to be described best by a formula containing the chemical potentials and mole fractions of all presents phases during nucleation. Following Aaronson et al. (1970) this formula can be replaced by the approximation

$$\Delta G_v = -\frac{RT}{V_m}\left(x_p \ln\left(\frac{\bar{C}}{C_e}\right) + (1-x_p)\ln\left(\frac{100-\bar{C}}{100-C_e}\right)\right), \tag{3.11}$$

where x_p is the molar fraction of the solute inside a particle.

Robson et al. (2003) has followed the discussion of Barnett et al. (1974) to model the term ΔG_s, by using the (simplified) formula

$$\Delta G_s = 3\varepsilon_m^2 \delta_p \left(1 - \left(1 + \frac{\delta_m}{\delta_p}\left(3\frac{1-\nu_m}{1+\nu_m} - 1\right)\right)^{-1}\right). \tag{3.12}$$

Here δ_p and δ_m are functions related to the elastic moduli of the matrix and the particle and can be found in Robson et al. (2003). The parameter ν_m represents the Poisson ratio of the matrix. The misfit strain ε_m represents the strain present in the system due to misfit between the matrix and the particle and can be expressed as (Ratel et al., 2006)

$$\varepsilon_m = \frac{a_p - a_m}{a_m},$$

where a_m and a_p are respectively the lattice parameter of the matrix and the particle.

The number of potential heterogeneous nucleation sites per unit volume N_v^* can be directly related to N_v, the number of homogeneous nucleation sites per unit volume, and the dislocation density ρ_D. The latter variable is measured in the length of dislocations per unit volume, i.e. in $1/m^2$. Following Robson et al. (2003) we set

$$N_v^* = (N_v)^{1/3}\rho_D.$$

The variable N_v can be calculated by using the concentrations of all elements and their properties at a given time and represents the number of solute atoms in the matrix.

3.2.2 Growth of particles

Although above two different nucleation rates have been proposed, the growth of a particle is independent of the type of nucleation by which it has come to existence. This means we can model the growth of the particles by assuming the same formula as proposed by Myhr and Grong (2000). These formulas can be found in the previous section.

*Which will not be discussed in detail here, but can be found in Robson et al. (2003).

3.2.3 The particle size distribution

As in the previously discussed model we are interested in the number of particles as a function of time. The model proposed by Robson et al. (2003) can be described by the same partial differential equation (3.9) as in the model by Myhr and Grong (2000). All other theories and relations discussed in Sections 3.1.4 and 3.1.5 also apply to the model proposed by Robson et al. (2003) so those will not be discussed here.

3.3 Comparison of the models

The heterogeneous nucleation aspects of the models proposed by Myhr and Grong (2000) and Robson (2004), as stated in the previous sections contain various similar elements, but differ to great extent on the area of the heterogeneous nucleation rate j. To investigate the differences of the models, both models are used in two numerical simulations. The numerical schemes for these simulations can be found in Chapter 5, where the parameters needed for both models can be found in Table 3.1 below. If any value of the parameters is changed, this value will be stated.

Parameter	**Value**	**Comments**
Both models		
C_0	0.63	Myhr and Grong (2000)
C_p	63.4	Myhr and Grong (2000)
C_s	970	Myhr and Grong (2000)
D_0	2.2×10^{-4}	Myhr and Grong (2000)
Q_d	130,000	Myhr and Grong (2000)
Q_s	47,175	Myhr and Grong (2000)
$\gamma_{\alpha\beta}$	0.2	Myhr and Grong (2000)
V_m	3.95×10^{-5}	Myhr and Grong (2000)
Myhr and Grong (2000)		
j_0	9.66×10^{34}	Myhr and Grong (2000)
A_0	16,220	Myhr and Grong (2000)
Robson et al. (2003)		
x_p	2/3	Chosen
a_m	4.049×10^{-10}	Uguz (2003)
a_p	6.295×10^{-10}	Tani and Kido (2008)
δ_m	1.1013×10^{11}	Hyland (1992)
δ_p	8.4250×10^{10}	Tani and Kido (2008)
ν_m	0.34	Hyland (1992)
ν_p	0.161	Tani and Kido (2008)
V_a	13.97×10^{-6}	Molar volume of Mg
ρ_D	1.5×10^{11}	Robson et al. (2003)

Table 3.1: Parameters used for simulations.

The first simulation in Myhr and Grong (2000) investigates the long term behavior of a system of the alloy AA 6082 under influence of a temperature of $180°C$ or the equivalent temperature $453.15K$. This method is called prolonged artificial ageing in the field of metallurgy. During the simulation, we will let the time run from 1 to 3×10^6 seconds, which corresponds to approximately 35 days. This simulation will be performed with both models discussed above. The value of $\gamma_{\alpha\beta}$ will also be changed to 0.1275 in the simulation of the model by Robson et al. (2003), to achieve behavior similar (not equal) to those with the model by Myhr and Grong (2000) with regard to the initial nucleation rate. The results of these simulations can be found in Figures 3.2 and 3.3.

As can be seen from the results, both models show the same similar shape in behavior, but do have different outcomes. This is clearly visible at times beyond 10^3, at which the nucleation stage is replaced by the growth and coarsening stages of the process. This indicates that the interface energy present in both models should be distinguished to have two different facets. First the model by Myhr and Grong

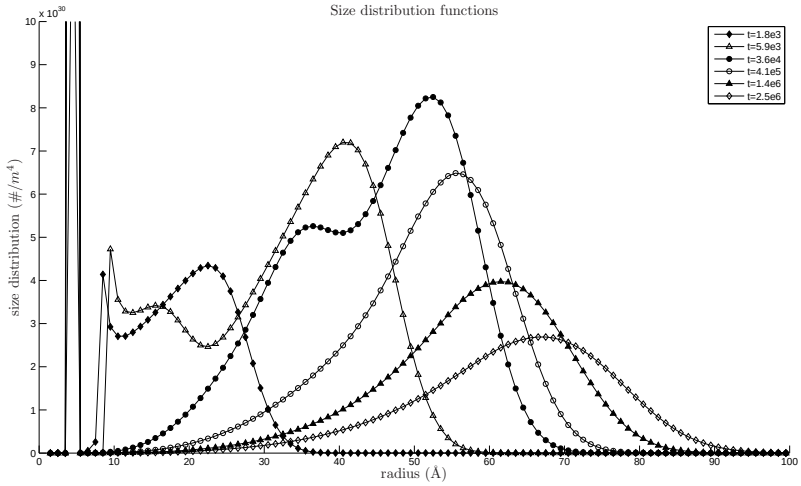

(a) Myhr and Grong (2000).

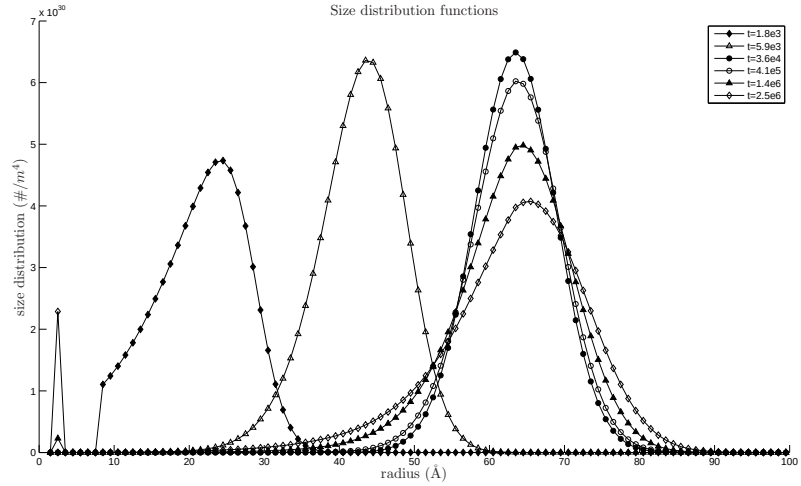

(b) Robson et al. (2003), $\gamma_{\alpha\beta} = 0.1275$.

Figure 3.2: Particle size distribution functions from simulations of long term behavior.

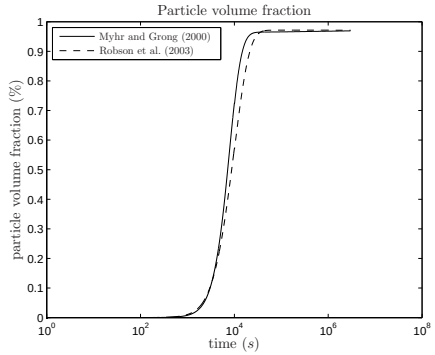

(a) Evolution of the particle volume fraction f.

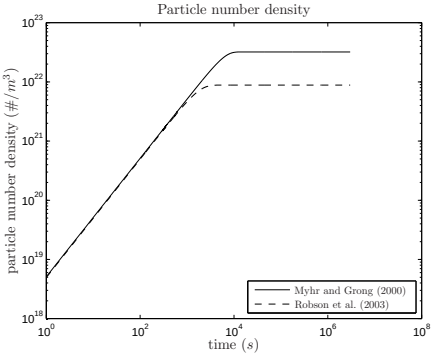

(b) Evolution of the particle number density n.

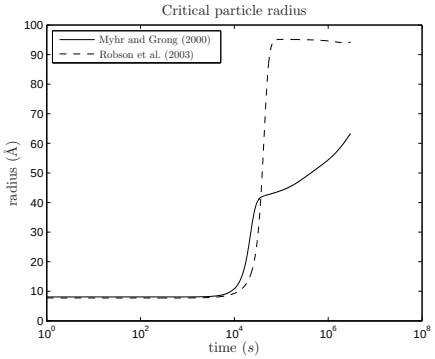

(c) Evolution of the critical particle radius r^*.

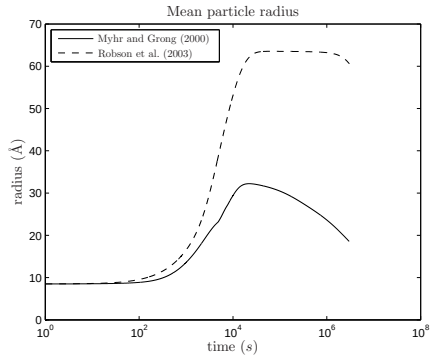

(d) Evolution of the mean particle radius $\bar{r}$.

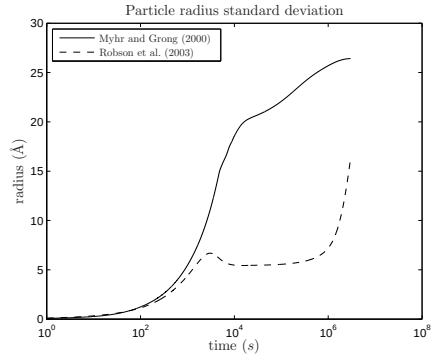

(e) Evolution of the particle radius standard deviation ρ.

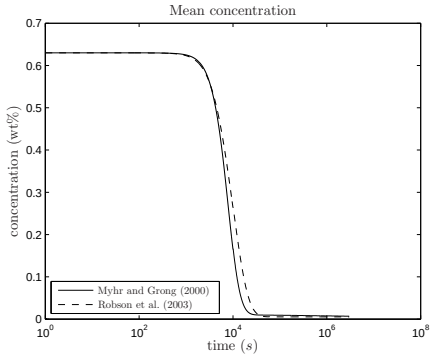

(f) Evolution of the concentrations $\bar{C}$ and C_e.

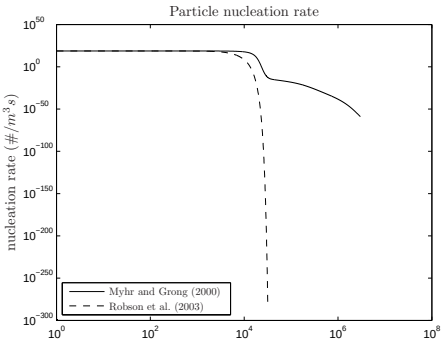

(g) Evolution of the nucleation rate j.

Figure 3.3: Results from simulations of long term behavior.

(2000) does not incorporate the value of $\gamma_{\alpha\beta}$ in the nucleation rate, whereas the model by Robson et al. (2003) does. This means that with regard to nucleation the model proposed by Robson et al. (2003) can be adapted to simulate specific behavior, where the nucleation rate by Myhr and Grong (2000) is static. With regard to the coarsening behavior, i.e. the growth of the precipitates, it can be seen that the lower value of $\gamma_{\alpha\beta}$ in the simulation with the model by Robson et al. (2003) causes different values of the concentration at the particle/matrix interface C_i and subsequently different growth rates for the particles. This can be seen back in the values for the critical radius obtained by the simulation. Assuming that the results from the model by Myhr and Grong (2000) give correct predictions, the coarsening behavior of the model by Robson et al. (2003) should be corrected. As this is beyond the scope of this project, we refer to Robson et al. (2003) as this paper contains a discussion on this subject.

3.4 Merits and drawbacks of both models

Both models have several strong and weak points. An understanding of these points can be of interest to achieve a better model, both physically and mathematically. For each model we will state their merits and drawbacks, accompanied with a short clarification.

3.4.1 Model by Myhr and Grong (2000)

The model proposed by Myhr and Grong (2000) has the following merits:

- Correct nucleation rate: The value of the nucleation rate during the nucleation stage are in good agreement with experimental research and theories.
- Correct coarsening behavior: The coarsening of particles appears to behave as should be expected from experminental results and theories.
- Low information needed to compute: Although the model describes a complete system, it does not require the calculation of large numbers of variables.

And the following drawbacks:

- No incorporation of misfit strains between matrix and particles: This term can effect the nucleation behavior significantly, so should be taken into account.
- Simplified version of the chemical volume free energy: Although not apparent in the model as stated above, the chemical volume free energy is simplified by neglecting the latter part of formula (3.11).

3.4.2 Model by Robson et al. (2003)

The model proposed by Robson et al. (2003) has the following merits:

- Incorporation of misfit strains between matrix and particles: This term can effect the nucleation behavior significantly, so it is correct to account for it.
- Full version of the chemical volume free energy: No parts of (3.11) are neglected, but it should be noted that this formula is already an approximation (Aaronson et al., 1970).

And the following drawbacks:

- Incorrect coarsening behavior: The results above suggest that the coarsening of particles is incorrectly described and should be adapted.
- Various variables needing additional information: This model describes the system using a single element as main catalyst, but to calculate some variables also information is needed about the other elements and thereby increasing the complexity of this method.

3.5 Conclusion

The models discussed in the previous sections, proposed by Myhr and Grong (2000) and Robson et al. (2003), both predict heterogeneous nucleation to a fair degree, bot also have some flaws. These flaws can be seen by examining the results from simulation and the theoretical drawbacks as stated in the last section. The next chapter of this thesis will use the merits of both models to derive a new model that has fewer drawbacks than those proposed here.

Chapter 4

Mathematical modeling

This chapter will start with the derivation of a new model based on the models proposed by Myhr and Grong (2000) and Robson et al. (2003), as discussed in Chapter 3. As the purpose of this thesis is to model the influence of elastic deformations on the nucleation process of particles in (quasi-)binary alloys, three models for elastic deformations are derived. The first model will describe one dimensional deformations in a three dimensional context, the second model will directly model three dimensional deformations. The final model will describe three dimensional deformations in cylindrical coordinates. After the derivation of the deformation models, a relation between the nucleation model and the deformation models are constructed.

4.1 A new model for nucleation

As discussed in Chapter 3 both the model by Myhr and Grong (2000) as those by Robson et al. (2003) contain various merits and drawbacks. On of the drawbacks of the model by Robson et al. (2003) is that it does not incorporate the correct coarsening behavior. As this behavior is crucial to the overall behavior, we will take the model by Myhr and Grong (2000) as starting point.

4.1.1 The volume free energy

A drawback of the model by Myhr and Grong (2000) is that it contains a simplified version of the chemical volume free energy ΔG_v. To incorporate formula (3.11) into the model, we must first derive the formula used in the definition of (3.1) for the heterogeneous nucleation energy barrier ΔG^*_{het}. Assuming that the exponential factor used in this model is of the form*

$$\exp\left(-\frac{\Delta G^*_{\text{het}}}{RT}\right),$$

we derive that ΔG^*_{het} is given by

$$\Delta G^*_{\text{het}} = \frac{A_0^3}{\left(RT\ln(\bar{C}/C_e)\right)^2}.$$

The simplified version of ΔG_v used in the model by Myhr and Grong (2000) is

$$\Delta G_v = -x_p \frac{RT}{V_m} \ln\left(\frac{\bar{C}}{C_e}\right),$$

which gives using the theoretical heterogeneous nucleation energy barrier, ignoring any other energies

$$\Delta G^*_{\text{het}} = \frac{16\pi}{3} \frac{N_A \gamma^3_{\alpha\beta}}{(\Delta G_v)^2}.$$

*Using RT instead of kT as used in the model by Robson et al. (2003) does not influence the model as this can be easily recovered by multiplication by N_A, the Avogadro constant.

This gives the full version:

$$\Delta G^*_{\text{het}} = \frac{16\pi}{3} \frac{N_A V_m^2 \gamma_{\alpha\beta}^3}{x_p^2 (RT)^2 (\ln(\bar{C}/C_e))^2}.$$

Comparing the two version for ΔG^*_{het}, we see that A_0 is an approximation given by

$$A_0^3 \approx \frac{16\pi}{3} \frac{N_A V_m^2 \gamma_{\alpha\beta}^3}{x_p^2}.$$

To incorporate the correct formula (3.11), we define the parameter $\tilde{A}_0$ by

$$\tilde{A}_0^3 = \frac{A_0^3 x_p^2}{V_m^2}.$$

Setting

$$\Delta G^*_{\text{het}} = \frac{\tilde{A}_0^3}{(\Delta G_v)^2}$$

and using the simplified formula for ΔG_v results in the same formulas as in Myhr and Grong (2000). This indicates that our model is now consistent and can be used with the correct formula (3.11).

To summarize, we replace the nucleation rate formula (3.1) from Myhr and Grong (2000) by

$$j = j_0 \exp\left(-\frac{\Delta G^*_{\text{het}}}{RT}\right) \exp\left(-\frac{Q_d}{RT}\right), \tag{4.1}$$

where ΔG^*_{het}, $\tilde{A}_0^3$ and ΔG_v are given by

$$\begin{aligned}
\Delta G^*_{\text{het}} &= \frac{\tilde{A}_0^3}{(\Delta G_v)^2} \\
\tilde{A}_0^3 &= \frac{A_0^3 x_p^2}{V_m^2} \\
\Delta G_v &= -\frac{RT}{V_m}\left(x_p \ln\left(\frac{\bar{C}}{C_e}\right) + (1-x_p)\ln\left(\frac{100-\bar{C}}{100-C_e}\right)\right).
\end{aligned}$$

4.1.2 Incorporating misfit strain energy

The second drawback of the model proposed by Myhr and Grong (2000) is that it neglects the possible misfit strain energy between the matrix and particles. This drawback can be lifted by using part of the model by Robson et al. (2003). Ignoring any dislocation energy destroyed during nucleation we set

$$\Delta G^*_{\text{het}} = \frac{\tilde{A}_0^3}{(\Delta G_v + \Delta G_s)^2},$$

where ΔG_s is again the elastic strain energy per particle, modeled by (3.12):

$$\Delta G_s = 3\varepsilon_m^2 \delta_p \left(1 - \left(1 + \frac{\delta_m}{\delta_p}\left(3\frac{1-\nu_m}{1+\nu_m} - 1\right)\right)^{-1}\right).$$

4.1.3 Overview of the new model

The models by Myhr and Grong (2000) and Robson et al. (2003) are combined above to resolve their drawbacks and better simulate the behavior of alloys with regard to the nucleation and coarsening of particles. This model for heterogeneous nucleation is described by the initial value problem (3.9):

$$\begin{cases} \dfrac{\partial N}{\partial t} = -\dfrac{\partial (Nv)}{\partial r} + S & \text{for } r \in [0,\infty), t \in (0,\infty), \\ N(r,0) = N_0(r) & \text{for } r \in [0,\infty), \end{cases} \tag{4.2}$$

with the source term S given by (3.6)

$$S(r,t) = \begin{cases} j(t) & \text{if } r = r^* + \Delta r^*, \\ 0 & \text{otherwise,} \end{cases}$$

and the nucleation rate j by (4.1)

$$j = j_0 \exp\left(-\frac{\Delta G^*_{\text{het}}}{RT}\right) \exp\left(-\frac{Q_d}{RT}\right).$$

4.2 Elastic deformations

This section will be concerned with the formulation of three models for elastic deformations, starting with a model for one dimensional deformations in a three dimensional context. Thereafter a model for three dimensional deformations will be derived. This section will be concluded with a model for deformations in cylindrical coordinates.

4.2.1 One dimensional deformations

Assume a hypothetical plate with finite dimensions is given, where the thickness is significantly smaller than the width and depth of the plate, for example a plate with width and depth equal to one meter and a thickness of one centimeter. Further more assume this plate is fixed at the bottom face and a force is applied to the top face.

As the ratio between thickness and width is small, it is likely the plate will only deform along the the direction of the force. Denote by x the location variable in this direction[†]. The variable x is from the range 0 to d where d is the thickness of the plate.

Derivation of the model

Let $u \equiv u(x,t)$ be the displacements in the plate at location x and time t in meters m. The strain $\varepsilon \equiv \varepsilon(x,t)$ due to these deformations is, in this one dimensional situation, given by:

$$\varepsilon = \frac{\partial u}{\partial x}. \tag{4.3}$$

Besides strain plays the stress $\sigma \equiv \sigma(x,t)$ an important role in the deformation of a material. In one dimension the relation between stress σ and strain ε is given by Hooke's Law

$$\sigma = E\varepsilon, \tag{4.4}$$

where $E \equiv E(x,t)$ is the time and place dependent Young's modulus, one of the several elastic moduli of materials. Both σ and E denote an amount of force per unit area with dimension N/m^2.

Under the assumption that an equilibrium is at all times obtained for the deformation of the plate, Newton's Second Law gives the equation

$$\frac{\partial}{\partial t}\left(\rho_m \frac{\partial u}{\partial t}\right) = \frac{\partial \sigma}{\partial x} + b,$$

where $\rho_m \equiv \rho_m(x,t)$ is the density of the material in kg/m^3 and $b \equiv b(x,t)$ is the total of internal body forces per unit volume in N/m^3. Application of the relations between u, ε and σ result in the partial differential equation

$$\frac{\partial}{\partial t}\left(\rho_m \frac{\partial u}{\partial t}\right) = \frac{\partial}{\partial x}\left(E\frac{\partial u}{\partial x}\right) + b.$$

As this system has a second derivative in time, two initial conditions should be applied. If a system is deformed, this deformation is relative to the original configuration at which no deformations are present. This suggest setting

$$u(x,0) = 0 \quad \text{for all } x \in [0,d].$$

[†]Although y could be a more appropriate choice, x is chosen so that when comparing the one dimensional model with the three dimensional model the differences can be seen more easily.

An initial velocity of the system could be given, which is given by the condition

$$\frac{\partial u}{\partial t}(x,0) = G(x) \quad \text{for all } x \in [0,d],$$

with $G(x)$ some given function with dimension m/s.

Besides a second order time derivative also a second order spatial derivative is present. This means that at each boundary of the domain $[0,d]$ a boundary condition should be imposed. These boundary conditions could either reflect a fixed boundary, possibly with a time-dependent special displacement, a boundary with a force on its surface or a mixture of the first two. For clarification assume a fixed boundary at $x = 0$ and a force at $x = d$. This suggest setting the boundary conditions

$$\begin{cases} u(0,t) &= 0 & \text{for } t > 0, \\ E(d,t)\dfrac{\partial u}{\partial x}(d,t) &= F(t) & \text{for } t > 0, \end{cases}$$

where F has dimension N/m^2.

The overall system is now given by

$$\begin{cases} \dfrac{\partial}{\partial t}\left(\rho_m \dfrac{\partial u}{\partial t}\right) &= \dfrac{\partial}{\partial x}\left(E\dfrac{\partial u}{\partial x}\right) + b & \text{for } x \in (0,d), t > 0, \\ u(x,0) &= 0 & \text{for all } x \in [0,d], \\ \dfrac{\partial u}{\partial t}(x,0) &= G(x) & \text{for all } x \in [0,d], \\ u(x,t) &= 0 & \text{for } t > 0, \text{ for } x \in \Gamma_1 \subseteq \{0,d\}, \\ E(x,t)\dfrac{\partial u}{\partial x}(x,t) &= F(t) & \text{for } t > 0, \text{ for } x \in \Gamma_2 \subseteq \{0,d\}, \end{cases} \tag{4.5}$$

where $\Gamma_1 \cup \Gamma_2 = \{0,d\}$ and $\Gamma_1 \cap \Gamma_2 = \emptyset$.

Simplification of the model

Although model (4.5) is time dependent, the time dependency can be ignored by reasoning as follows. Assume for simplicity that ρ_m and E are constant in time and place and that no body forces are present. This simplifies (4.5) to

$$\begin{cases} \rho_m \dfrac{\partial^2 u}{\partial t^2} &= E\dfrac{\partial^2 u}{\partial x^2} & \text{for } x \in (0,d), t > 0, \\ u(x,0) &= 0 & \text{for all } x \in [0,d], \\ \dfrac{\partial u}{\partial t}(x,0) &= G(x) & \text{for all } x \in [0,d], \\ u(x,t) &= 0 & \text{for } t > 0, \text{ for } x \in \Gamma_1 \subseteq \{0,d\}, \\ E\dfrac{\partial u}{\partial x}(x,t) &= F(t) & \text{for } t > 0, \text{ for } x \in \Gamma_2 \subseteq \{0,d\}, \end{cases}$$

Assume furthermore that a fixed boundary is present at $x = 0$ is and a force $F(t)$ at $x = d$. Replacing $u(x,t)$ with $v(x,t) + w(x,t)$ where v satisfies the same equation as u, but with homogeneous boundary conditions and w satisfies $\partial^2 w/\partial x^2 = 0$ and homogeneous initial conditions. The system for w is given by:

$$\begin{cases} \dfrac{\partial^2 w}{\partial x^2} &= 0 & \text{for } x \in (0,d), t > 0, \\ w(x,0) &= 0 & \text{for all } x \in [0,d], \\ \dfrac{\partial w}{\partial t}(x,0) &= 0 & \text{for all } x \in [0,d], \\ w(0,t) &= D(t) & \text{for } t > 0, \\ E\dfrac{\partial w}{\partial x}(d,t) &= F(t) & \text{for } t > 0. \end{cases}$$

The solution of this system can easily be found and is given by

$$w(x,t) = \frac{F(t)}{E}x + D(t).$$

The system for v is given by

$$\begin{cases} \rho_m \dfrac{\partial^2 v}{\partial t^2} &= E\dfrac{\partial^2 v}{\partial x^2} & \text{for } x \in (0,d), t>0, \\ v(x,0) &= 0 & \text{for all } x \in [0,d], \\ \dfrac{\partial v}{\partial t}(x,0) &= G(x) & \text{for all } x \in [0,d], \\ v(0,t) &= 0 & \text{for } t>0, \\ E\dfrac{\partial v}{\partial x}(d,t) &= 0 & \text{for } t>0. \end{cases}$$

This system can be solved by separation of variables, which gives the solution

$$v(x,t) = \sum_{k=0}^{\infty} B_k \sin(\lambda_k x) \sin\left(\frac{\sqrt{E}}{\sqrt{\rho_m}}\lambda_k t\right),$$

where

$$B_k = \frac{\sqrt{\rho_m}}{\sqrt{E}} \frac{2}{d\lambda_k} \int_0^d G(x)\sin(\lambda_k x)\mathrm{d}x,$$

and

$$\lambda_k = \frac{(2k+1)\pi}{2d}.$$

On investigation of B_k we see that

$$\lim_{\sqrt{E/\rho_m}\to\infty} B_k = 0.$$

As E is in most scenarios several orders larger than ρ_m this means that $v(x,t)$ will become small and close to zero.

The above shows that u will tend rapidly to w if $\sqrt{E/\rho_m}$ is large, which indicates that any time dependence will only follow from the boundary conditions. This indicates that the one dimension model can be replaced by the model

$$\begin{cases} -\dfrac{\partial}{\partial x}\left(E\dfrac{\partial u}{\partial x}\right) &= b & \text{for } x \in (0,d), t>0, \\ u(x,t) &= 0 & \text{for } t>0, \text{ for } x \in \Gamma_1 \subseteq \{0,d\}, \\ E(x,t)\dfrac{\partial u}{\partial x}(x,t) &= F(t) & \text{for } t>0, \text{ for } x \in \Gamma_2 \subseteq \{0,d\}, \end{cases} \tag{4.6}$$

4.2.2 Three dimensional elastic deformations

This section will derive a model for three dimensional elastic deformations for which the time dependency of the model is neglected, by analogy with the one dimension model (4.6).

Assume a hypothetical block or plate with finite dimensions is given in which deformations $\boldsymbol{u} \equiv \boldsymbol{u}(\boldsymbol{x})$ occur. Denote by Ω the domain of the block or plate. The linear strain $\underline{\underline{\boldsymbol{\varepsilon}}} \equiv \underline{\underline{\boldsymbol{\varepsilon}}}(\boldsymbol{x})$ is given by

$$\underline{\underline{\boldsymbol{\varepsilon}}} = \frac{1}{2}\left(\boldsymbol{u}\nabla^T + \nabla\boldsymbol{u}^T\right), \tag{4.7}$$

or equivalent

$$\varepsilon_{pq} = \frac{1}{2}\left(\frac{\partial u_p}{\partial x_q} + \frac{\partial u_q}{\partial x_p}\right) \quad \text{for } p,q = 1,2,3.$$

Hooke's Law for multiple dimensions relates the strain $\underline{\underline{\boldsymbol{\varepsilon}}}$ with the stress $\underline{\underline{\boldsymbol{\sigma}}} \equiv \underline{\underline{\boldsymbol{\sigma}}}(\boldsymbol{x})$:

$$\underline{\underline{\boldsymbol{\sigma}}} = \lambda \operatorname{Tr}(\underline{\underline{\boldsymbol{\varepsilon}}})I + 2\mu\underline{\underline{\boldsymbol{\varepsilon}}}, \tag{4.8}$$

where $\lambda \equiv \lambda(\boldsymbol{x})$ and $\mu \equiv \mu(\boldsymbol{x})$ are the the Lamé parameters, with μ also known as the shear modulus.

Application of these identities in combination with a balance of forces gives the following system of partial differential equations:

$$-\nabla \cdot \left(\lambda\left(\nabla\cdot\boldsymbol{u}\right)I + \mu\left(\boldsymbol{u}\nabla^T + \nabla\boldsymbol{u}^T\right)\right) = \boldsymbol{b},$$

where $\boldsymbol{b} \equiv \boldsymbol{b}(\boldsymbol{x})$ are the internal body forces in Newton per cubic meter, in row vector notation.

The boundary conditions for this system at the boundary Γ of the domain Ω can be given by either a fixed boundary, or a boundary on which a force is applied[‡], or a mixture of the to, as the radial deformations can be fixed, but a force is exerted in the axial direction, or vice versa. Let $\Gamma_i^0 \subseteq \Gamma$ be those points for which no deformation is imposed in the i-th direction and $\Gamma_i^f \subseteq \Gamma$ those points for which a force is described in the i-th direction. This gives that the boundary conditions can be expressed as:

$$\begin{aligned} u_i(\boldsymbol{x},t) &= 0 && \text{for } t>0, \text{ for } \boldsymbol{x} \in \Gamma_i^0, \\ \left(\underline{\underline{\boldsymbol{\sigma}}}(\boldsymbol{x},t)\cdot\boldsymbol{n}\right)_i &= f_i(\boldsymbol{x},t) && \text{for } t>0, \text{ for } \boldsymbol{x} \in \Gamma_i^f. \end{aligned}$$

Combining the system for $\boldsymbol{u}$, combined with the boundary condition gives the final three dimensional system:

$$\left\{\begin{array}{rcll} -\nabla\cdot\left(\lambda\left(\nabla\cdot\boldsymbol{u}\right)I+\mu\left(\boldsymbol{u}\nabla^T+\nabla\boldsymbol{u}^T\right)\right) &=& \boldsymbol{b} & \text{for } \boldsymbol{x}\in\Omega, t>0, \\ u_i(\boldsymbol{x},t) &=& 0 & \text{for } t>0, \text{ for } \boldsymbol{x}\in\Gamma_i^0, \\ \left(\underline{\underline{\boldsymbol{\sigma}}}(\boldsymbol{x},t)\cdot\boldsymbol{n}\right)_i &=& f_i(\boldsymbol{x},t) & \text{for } t>0, \text{ for } \boldsymbol{x}\in\Gamma_i^f. \end{array}\right. \tag{4.9}$$

4.2.3 Cylindrical model

Although the above model for three dimensional simulations is correct, this system can be replaced by two partial differential equations, if some assumptions are made. First of all assume a cylindrical shaped region Ω with outher boundary Γ, with cylindrical coordinates (η,θ,z), where η denotes the distance of a point to the z-axis, θ the angle with respect to the x_1 axis and z resembles x_3[§]. Also assume that the region has circle symmetry, which means that all functions are constant with respect to θ, and no deformations in the direction of θ are present.

Let the deformations inside the cylindrical region Ω be defined as u_η, u_θ and u_z, where the subscript represents the direction of the deformation. Then the strains, following Chau and Wei (2000), can be expressed as

$$\begin{aligned} \varepsilon_{\eta\eta} &= \frac{\partial u_\eta}{\partial\eta} & \varepsilon_{\theta\theta} &= \frac{u_\eta}{\eta}+\frac{1}{\eta}\frac{\partial u_\theta}{\partial\theta} & \varepsilon_{zz} &= \frac{\partial u_z}{\partial z} \\ \varepsilon_{\eta\theta} &= \frac{1}{2}\left(\frac{\partial u_\theta}{\partial\eta}+\frac{1}{\eta}\frac{\partial u_\theta}{\partial\theta}-\frac{u_\theta}{\eta}\right) & \varepsilon_{\eta z} &= \frac{1}{2}\left(\frac{\partial u_\eta}{\partial z}+\frac{\partial u_z}{\partial\eta}\right) & \varepsilon_{\theta z} &= \frac{1}{2}\left(\frac{1}{\eta}\frac{\partial u_z}{\partial\theta}+\frac{\partial u_\theta}{\partial z}\right). \end{aligned}$$

Using circle symmetry, this can be simplified to:

$$\begin{array}{rclrclrcl} \varepsilon_{\eta\eta} &=& \frac{\partial u_\eta}{\partial\eta} & \varepsilon_{\theta\theta} &=& \frac{u_\eta}{\eta} & \varepsilon_{zz} &=& \frac{\partial u_z}{\partial z} \\ \varepsilon_{\eta\theta} &=& 0 & \varepsilon_{\eta z} &=& \frac{1}{2}\left(\frac{\partial u_\eta}{\partial z}+\frac{\partial u_z}{\partial\eta}\right) & \varepsilon_{\theta z} &=& 0. \end{array} \tag{4.10}$$

Similar to the three dimensional model, the relations between stresses and strains can be expressed, assuming an isotropic material, by

$$\sigma_{\alpha\beta} = \delta_{\alpha\beta}\lambda\left(\varepsilon_{\eta\eta}+\varepsilon_{\theta\theta}+\varepsilon_{zz}\right)+2\mu\varepsilon_{\alpha\beta}, \tag{4.11}$$

for $\alpha,\beta = \eta,\theta,z$.

Applying an equilibrium force balance in the radial direction gives the differential equation (Jaeger et al., 2007)

$$\frac{\partial\sigma_{\eta\eta}}{\partial\eta}+\frac{\partial\sigma_{\eta z}}{\partial z}+\frac{\sigma_{\eta\eta}-\sigma_{\theta\theta}}{\eta}+b_\eta = 0,$$

where b_η are the body forces acting in radial direction. Similar an equation can be derived for the axial direction (Jaeger et al., 2007)

$$\frac{\partial\sigma_{\eta z}}{\partial\eta}+\frac{\partial\sigma_{zz}}{\partial z}+\frac{\sigma_{\eta z}}{\eta}+b_z = 0,$$

where b_z are the body forces acting in axial direction. No equation has to be derived for the tangential direction, as circle symmetry implies no forces in that direction.

[‡]Note that a free boundary can be assumed to be of the latter form, but with a force equal to zero

[§]Although in most cases r is used, we will use η, as r is already used in the particle nucleation model.

Using the stress-strain relations and the strain-deformation relations, we arrive at the set of differential equations:

$$\begin{cases} \frac{\partial}{\partial \eta}\left[(\lambda+2\mu)\frac{\partial u_\eta}{\partial \eta}+\lambda\frac{u_\eta}{\eta}+\lambda\frac{\partial u_z}{\partial z}\right]+\frac{\partial}{\partial z}\left[\mu\frac{\partial u_\eta}{\partial z}+\mu\frac{\partial u_z}{\partial \eta}\right]+\frac{2\mu}{\eta}\left[\frac{\partial u_\eta}{\partial \eta}-\frac{u_\eta}{\eta}\right]+b_\eta &= 0 \\ \frac{\partial}{\partial z}\left[(\lambda+2\mu)\frac{\partial u_z}{\partial z}+\lambda\frac{u_\eta}{\eta}+\lambda\frac{\partial u_\eta}{\partial \eta}\right]+\frac{\partial}{\partial \eta}\left[\mu\frac{\partial u_\eta}{\partial z}+\mu\frac{\partial u_z}{\partial \eta}\right]+\frac{\mu}{\eta}\left[\frac{\partial u_\eta}{\partial z}+\frac{\partial u_z}{\partial \eta}\right]+b_z &= 0 \end{cases}$$

Although these equations are correct, some boundary conditions are needed, both natural and symmetry boundary conditions. The symmetry boundary condition arises due to the circle symmetry imposed on the problem. This boundary condition can be expressed as:

$$u_\eta(0,z)=0.$$

The boundary conditions for this system at the boundary Γ of the domain Ω can be given by either a fixed boundary, or a boundary on which a force is applied¶, or a mixture of the to, as the radial deformations can be fixed, but a force is exerted in the axial direction, or vice versa. Let $\Gamma_1 \subseteq \Gamma$ be those points for which no radial deformation is imposed, $\Gamma_2 \subseteq \Gamma$ those points for which no axial deformation is imposed, $\Gamma_3 \subseteq \Gamma$ those points for which a radial force is described and $\Gamma_4 \subseteq \Gamma$ those points for which an axial force is described. This gives that the boundary conditions can be expressed as, including the boundary condition above:

$$\begin{aligned} u_\eta(\eta,\theta,z,t) &= 0 && \text{for } t>0,\ (\eta,\theta,z)\in\Gamma_1, \\ u_z(\eta,\theta,z,t) &= 0 && \text{for } t>0,\ (\eta,\theta,z)\in\Gamma_3, \\ \left(\underline{\underline{\boldsymbol{\sigma}}}(\eta,\theta,z,t)\cdot\boldsymbol{n}\right)_\eta &= f_\eta(\eta,\theta,z,t) && \text{for } t>0,\ (\eta,\theta,z)\in\Gamma_2, \\ \left(\underline{\underline{\boldsymbol{\sigma}}}(\eta,\theta,z,t)\cdot\boldsymbol{n}\right)_z &= f_z(\eta,\theta,z,t) && \text{for } t>0,\ (\eta,\theta,z)\in\Gamma_4. \end{aligned}$$

Note that we must have $\Gamma_1\cup\Gamma_2=\Gamma_3\cup\Gamma_4=\Gamma$ and $\Gamma_1\cap\Gamma_2=\Gamma_3\cap\Gamma_4=\emptyset$.

At this moment we have a complete model for the deformation of a cylindrical region:

$$\begin{aligned} -\frac{\partial}{\partial \eta}\left[(\lambda+2\mu)\frac{\partial u_\eta}{\partial \eta}+\lambda\frac{u_\eta}{\eta}+\lambda\frac{\partial u_z}{\partial z}\right]-\frac{\partial}{\partial z}\left[\mu\frac{\partial u_\eta}{\partial z}+\mu\frac{\partial u_z}{\partial \eta}\right]-\frac{2\mu}{\eta}\left[\frac{\partial u_\eta}{\partial \eta}-\frac{u_\eta}{\eta}\right] &= b_\eta && \text{for } (\eta,z)\in\Omega, \\ -\frac{\partial}{\partial z}\left[(\lambda+2\mu)\frac{\partial u_z}{\partial z}+\lambda\frac{u_\eta}{\eta}+\lambda\frac{\partial u_\eta}{\partial \eta}\right]-\frac{\partial}{\partial \eta}\left[\mu\frac{\partial u_\eta}{\partial z}+\mu\frac{\partial u_z}{\partial \eta}\right]-\frac{\mu}{\eta}\left[\frac{\partial u_\eta}{\partial z}+\frac{\partial u_z}{\partial \eta}\right] &= b_z && \text{for } (\eta,z)\in\Omega, \\ u_\eta(\eta,\theta,z,t) &= 0 && \text{for } t>0,\ (\eta,\theta,z)\in\Gamma_1, \\ u_z(\eta,\theta,z,t) &= 0 && \text{for } t>0,\ (\eta,\theta,z)\in\Gamma_2, \\ \left(\underline{\underline{\boldsymbol{\sigma}}}(\eta,\theta,z,t)\cdot\boldsymbol{n}\right)_\eta &= f_\eta(\eta,\theta,z,t) && \text{for } t>0,\ (\eta,\theta,z)\in\Gamma_3, \\ \left(\underline{\underline{\boldsymbol{\sigma}}}(\eta,\theta,z,t)\cdot\boldsymbol{n}\right)_z &= f_z(\eta,\theta,z,t) && \text{for } t>0,\ (\eta,\theta,z)\in\Gamma_4. \end{aligned} \tag{4.12}$$

4.3 Relating the models

This section will have as goal to relate the model for nucleation and coarsening to the models for elastic deformations describe in the previous sections. We will start with modeling the influence of elastic deformations on the nucleation process, followed by a method to model the influence of the nucleation on the elastic deformations.

4.3.1 Influence of elastic strain and stresses

Upon investigation of the model for nucleation, one term is related to stresses and strains in the system, namely the elastic strain energy per unit volume ΔG_s. Although this energy term is only used to model misfit strain energies between the matrix and particles, it can be extended to incorporate other strain energies.

The energy present in a system due to elastic deformations can be calculated by first deriving the solution u of (4.6), the solution $\boldsymbol{u}$ of (4.9) or the solution (u_η, u_z) of (4.12). Thereafter the strain and

¶Note that a free boundary can be assumed to be of the latter form, but with a force equal to zero

stress in the system can be calculated by using identities (4.3) and (4.4) for the one-dimensional model, identities (4.7) and (4.8) for the three-dimensional model or identities (4.10) and (4.11) for the cylindrical model. Following basic theory for elasticity, elastic strain energy in the system is than given (at a point in the material) as:

$$\Delta G_s^{el} = \frac{1}{2}\sigma\varepsilon,$$

for one-dimensional deformations, and

$$\Delta G_s^{el} = \frac{1}{2}\underline{\underline{\boldsymbol{\sigma}}} : \underline{\underline{\boldsymbol{\varepsilon}}},$$

for three-dimensional and cylindrical deformations. Here : represents the Frobenius inner product, given for two $n \times m$-matrices A and B:

$$A : B = \sum_{i=1}^{n}\sum_{j=1}^{m} A_{ij}B_{ij}.$$

Let ΔG_s now be redefined by

$$\Delta G_s = \Delta G_s^m + \Delta G_s^{el},$$

where ΔG_s^{el} as defined above and ΔG_s^m by (3.12):

$$\Delta G_s^m = 3\varepsilon_m^2\delta_p\left(1 - \left(1 + \frac{\delta_m}{\delta_p}\left(3\frac{1-\nu_m}{1+\nu_m} - 1\right)\right)^{-1}\right),$$

where $\varepsilon_m, \delta_p, \delta_m$ and ν_m were defined just after (3.12).

4.3.2 Influence of particles

Although the amount of particles that are present during nucleation can be expected to be low, the presence of particles can influence the elastic behavior of the alloy. To model this influence we follow Pal (2005) by letting the particle volume fraction f influence the elastic moduli of the alloy.

The elastic moduli used in both the one-dimensional model, the three-dimensional model and the cylindrical model are the shear modulus μ, the Young's modulus E and the first Lamé parameter λ. As all elastic moduli can be calculated by knowing only two of these elastic moduli, we will only model the influence on the parameters E and μ and calculate λ from these results by using the formula:

$$\lambda = \mu\frac{E - 2\mu}{3\mu - E}.$$

Pal (2005) state and discuss that the shear modulus μ of the alloy can be described by the formula

$$\mu = \mu_m + \left(\frac{15(1-\nu_m)(\mu_p - \mu_m)}{2\mu_p(4-5\nu_m) + \mu_m(7-5\nu_m)}\right)\mu_m\, f.$$

In this formula the subscript m refers to the matrix, the subscript p to the particles and ν is the Poisson ratio. Using this formula and others Pal (2005) derived a formula for the Young's modulus of the alloy:

$$E = E_m + (10\beta_1(1+\nu_m) + \beta_2(1-2\nu_m))\; E_m\, f,$$

where β_1, β_2 are functions of E_m, E_p and the functions $\alpha_i, i = 1, \ldots, 6$, which are in turn functions of the Poisson's ratios ν_m and ν_p. These functions can be found in Pal (2005), so will not be stated here.

During this Master thesis project we will assume that the elastic moduli of the matrix are determined by the element that is in excess present. This means that for the alloy used for the simulations in Section 3.3, this elements is aluminum and therefore we use the values of aluminum for the elastic moduli of the matrix. This approach can be incorrect, but as no information can be found on the exact value for mixtures without particles present, we use this approach.

4.3.3 Consequences

In the two sections above we have related model (4.2) to model (4.6) and (4.9). As the latter two models are spacial, with time dependent constants and boundary conditions and the first a model is in a stochastic domain, model (4.2) should be solved for each time at each point of the spacial domains on which models (4.6) and (4.9) are solved. Thereafter the results of (4.2) are used to recalculate models (4.6) and (4.9).

Chapter 5

Numerical methods

This chapter will deal with the discretization of all models that have been formulated in Chapter 4. The model for nucleation and growth of particles will be discretized by means of finite volume methods, all other models by means of finite element methods.

5.1 Nucleation and growth of particles

This section will continue on the previous two chapters by discretizing the partial differential equation (4.2) in time and place. The derivation of the discretized model will not be stated here but can be found in Chapter 4 of den Ouden (2009). We will use an IMEX* θ-method with $\theta = 1/2$ for the time integration, as the comparison of the discussed methods in Chapter 5 of den Ouden (2009) suggest that this leads to a second order accuracy in time at minimal computational costs.

The numerical scheme is characterized by solving the system

$$\left(I - \frac{1}{2}\frac{\Delta t}{\Delta r}A^n\right)\vec{N}^{n+1} = \left(I + \frac{1}{2}\frac{\Delta t}{\Delta r}A^n\right)\vec{N}^n + \Delta t\vec{S}^n, \tag{5.1}$$

iteratively with starting value

$$\vec{N}^0 = \vec{N}_0,$$

and definitions

$$\begin{array}{rcll} \vec{N}_i^n & = & N(t^n, r_i) & \text{for } i = 1, \ldots, G-1 \\ A_{ii}^n & = & -((v_{i-1/2}^n)^- + (v_{i+1/2}^n)^+) & \text{for } i = 1, \ldots, G-1 \\ A_{i,i-1}^n & = & (v_{i-1/2}^n)^+ & \text{for } i = 2, \ldots, G-1 \\ A_{i,i+1}^n & = & (v_{i+1/2}^n)^- & \text{for } i = 1, \ldots, G-1 \\ \vec{S}_i^n & = & S(t^n, r_i) & \text{for } i = 1, \ldots, G-1, \end{array}$$

and $A_{ij}^n = 0$ if not defined above. This matrix equation will be solved by using the Thomas algorithm for tri-diagonal matrices (CFD-Online, 2005). For any number a, a^+ stands for $\max(a, 0)$, the positive part of a, and a^- for $\max(-a, 0)$, the negative part of a.

The time step Δt used during simulations is not restricted if no linearization is applied, due to the real and negative eigenvalues of the matrix A^n. A derivation of the value of the eigenvalues can be found in Appendix A.

This method has been assumed to be of second order time accuracy in den Ouden (2009). However, the linearization used in the above method decreases the order to first order time accuracy. This can be seen by studying the test differential equation:

$$\frac{dy}{dt}(t) = f(t)y(t) + g(t).$$

Application of the IMEX θ-method above to this equation gives the numerical scheme:

$$w^{n+1} = w^n + hf(t^n)\left(\theta w^{n+1} + (1-\theta)w^n\right) + hg(t^n),$$

*IMEX stands for IMplicit-EXplicit.

where w^n is the approximation of $y(t^n)$ and h is the (time) step size. If we assume that w^n is the exact solution of the differential equation, so $w^n = y(t^n)$, and apply a Taylor expansion around t^n of w^{n+1}, we see the following:

$$w^{n+1} = y(t^n) + h\frac{dy}{dt}(t^n) + \theta f(t^n)\left(h^2\frac{dy}{dt}(t^n) + \frac{h^3}{2}\frac{d^2y}{dt^2}(t^n) + \mathcal{O}(h^4)\right). \tag{5.2}$$

The exact solution $y(t^{n+1})$ can also be expanded in a Taylor series. This gives

$$y(t^{n+1}) = y(t^n) + h\frac{dy}{dt}(t^n) + h^2\frac{d^2y}{dt^2}(t^n) + \frac{h^3}{6}\frac{d^3y}{dt^3}(t^n) + \mathcal{O}(h^4). \tag{5.3}$$

Subtracting (5.3) from (5.2) and division by h gives the local error e_l^n:

$$e_l^n = h\left(\theta f(t^n)\frac{dy}{dt}(t^n) - \frac{d^2y}{dt^2}(t^n)\right) + h^2\left(\frac{\theta}{2}f(t^n)\frac{d^2y}{dt^2}(t^n) - \frac{1}{6}\frac{d^3y}{dt^3}(t^n)\right) + \mathcal{O}(h^3).$$

This indicates that the global accuracy is of order 2 if for each time t^n holds

$$\theta f(t^n)\frac{dy}{dt}(t^n) - \frac{d^2y}{dt^2}(t^n) = 0.$$

In all other cases only first order accuracy is achieved. As the above equation is in most cases not true, we can assume only first order accuracy is achieved on theoretical grounds.

The upwind scheme used to derive the matrix A^n is of first order accuracy in place, which indicates that if we set

$$\frac{\Delta t}{\Delta r} = \text{constant},$$

an overall accuracy of first order is achieved.

5.2 Elastic deformations

This section will state the result of the application of finite element methods on (4.5) and (4.9). Thereafter a system will be derived to obtain additional information of the system.

5.2.1 One dimensional model

The application of finite element methods to the one dimensional model (4.5) results in the system

$$S\boldsymbol{u} = \boldsymbol{q}, \tag{5.4}$$

with element matrices and vectors

$$\begin{aligned}
(S^e)_{ij} &= \frac{|l|}{2}a_i^1 a_j^1 \sum_{k=1}^{2} E(x_k) && \text{for } i,j = 1,2\\
(q^e)_i &= \frac{|l|}{2}b(x_i) && \text{for } i = 1,2\\
(S^{x=0}) &= \alpha_1\\
(S^{x=d}) &= \alpha_2\\
(q^{x=0}) &= F_1\\
(q^{x=d}) &= F_2,
\end{aligned}$$

where e is a linear line element and a_k^1 refers to the 1-th component of the linear basis function of the k-th point of an element. Here we have replaced the boundary conditions of (4.5) with the general boundary condition:

$$\begin{aligned}
-E(0,t)\frac{\partial u}{\partial x}(0,t) &= F_1 - \alpha_1 u(0,t)\\
E(d,t)\frac{\partial u}{\partial x}(d,t) &= F_2 - \alpha_2 u(d,t)
\end{aligned}$$

5.2.2 Three dimensional model

The application of finite element methods to the three dimensional variant of (4.9) results in the system

$$\begin{bmatrix} S_{11} & S_{12} & S_{13} \\ S_{21} & S_{22} & S_{23} \\ S_{31} & S_{32} & S_{33} \end{bmatrix} \begin{bmatrix} \boldsymbol{u}_1 \\ \boldsymbol{u}_2 \\ \boldsymbol{u}_3 \end{bmatrix} = \begin{bmatrix} \boldsymbol{q}_1 \\ \boldsymbol{q}_2 \\ \boldsymbol{q}_3 \end{bmatrix}, \tag{5.5}$$

with element matrices and vectors

$$\begin{aligned}
(S^e_{ij})_{kl} &= \frac{|V|}{24} a^i_k a^j_l \sum_{m=1}^{4} \lambda(\boldsymbol{x}_m) + \frac{|V|}{24} a^j_k a^i_l \sum_{m=1}^{4} \mu(\boldsymbol{x}_m) \\
&\quad + \delta_{ij} \frac{|V|}{24} \sum_{m=1}^{3} a^m_k a^m_l \sum_{m=1}^{4} \mu(\boldsymbol{x}_m) && \text{for } i,j = 1,2,3 \quad \text{and for } k,l = 1,2,3,4 \\
(q^e_i)_k &= \frac{|V|}{24} b_i(\boldsymbol{x}_k) && \text{for } i = 1,2,3 \quad \text{and for } k = 1,2,3,4 \\
(S^b_{ij})_{kl} &= \alpha_i \delta_{ij} \delta_{kl} \frac{|\Delta|}{6} && \text{for } i,j = 1,2,3 \quad \text{and for } k,l = 1,2,3 \\
(q^b_i)_k &= \frac{|\Delta|}{6} f_i(\boldsymbol{x}_k) && \text{for } i = 1,2,3 \quad \text{and for } k = 1,2,3,
\end{aligned}$$

where e is a linear tetrahedron, b a linear triangle and a^i_k refers to the i-th component of the linear basis function of the k-th point of an element. The derivation of this numerical scheme can be found at den Ouden (2009). Here we have replaced the boundary conditions of (4.9) with the general boundary condition:

$$\underline{\underline{\boldsymbol{\sigma}}} \cdot \boldsymbol{n} = \boldsymbol{f} - \text{Diag}\left(\boldsymbol{\alpha} \boldsymbol{u}^T\right)$$

To avoid false propagation of displacements in the block simulated, we will use a three-dimensional mesh based on an odd-even decomposition. Let the region of interest be divided into a number of similar cuboids, where each cuboid has been assigned a number. If the number of cuboids in the x_i-th direction is given by n_i and a cuboid is the j_i-th cuboid in the i-th direction, this cuboid will have the number C

$$C = j_1 + (j_2 - 1)n_1 + (j_3 - 1)n_1 n_2.$$

Each cuboid will be given a decomposition into five tetrahedra, based on the parity of C. The decompositions used in this paper can be found in Figure 5.1.

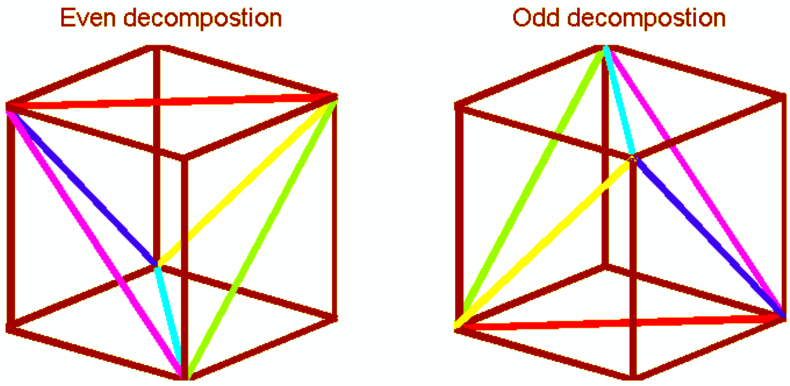

Figure 5.1: Topology for odd-even decomposition for three dimensional mesh.

5.2.3 Cylindrical model

To derive the numerical scheme of (4.12), first multiply the left hand side of the first equation of (4.12) by a test function v_η with $v_\eta = 0$ on the boundary Γ_1 and $\eta^\dagger$ and integrate over the cylindrical domain Ω. We will use the stresses in this step, as this simplifies things:

$$
\begin{aligned}
-\int_\Omega \left[\frac{\partial \sigma_{\eta\eta}}{\partial \eta} + \frac{\partial \sigma_{\eta z}}{\partial z} + \frac{1}{\eta}\left(\sigma_{\eta\eta} - \sigma_{\theta\theta}\right)\right] \eta v_\eta \,\mathrm{d}\Omega &= -\int_\Omega \left\{ \begin{bmatrix} \frac{\partial}{\partial \eta} \\ \frac{1}{\eta}\frac{\partial}{\partial \theta} \\ \frac{\partial}{\partial z} \end{bmatrix} \cdot \begin{bmatrix} \sigma_{\eta\eta} \\ 0 \\ \sigma_{\eta z} \end{bmatrix} + \frac{1}{\eta}\left(\sigma_{\eta\eta} - \sigma_{\theta\theta}\right) \right\} \eta v_\eta \,\mathrm{d}\Omega \\
&= \int_\Omega \begin{bmatrix} \sigma_{\eta\eta} \\ 0 \\ \sigma_{\eta z} \end{bmatrix} \cdot \begin{bmatrix} \frac{\partial (\eta v_\eta)}{\partial \eta} \\ \frac{1}{\eta}\frac{\partial (\eta v_\eta)}{\partial \theta} \\ \frac{\partial (\eta v_\eta)}{\partial z} \end{bmatrix} - \left(\sigma_{\eta\eta} - \sigma_{\theta\theta}\right) v_\eta \,\mathrm{d}\Omega \\
&\quad - \int_\Gamma \begin{bmatrix} \sigma_{\eta\eta} \\ 0 \\ \sigma_{\eta z} \end{bmatrix} \cdot \boldsymbol{n} \eta v_\eta \,\mathrm{d}\Gamma \\
&= \int_\Omega \left((\lambda + 2\mu)\frac{\partial u_\eta}{\partial \eta} + \lambda \frac{u_\eta}{\eta} + \lambda \frac{\partial u_z}{\partial z}\right)\left(\eta \frac{\partial v_\eta}{\partial \eta} + v_\eta\right) \mathrm{d}\Omega \\
&\quad + \int_\Omega \eta\mu \left(\frac{\partial u_\eta}{\partial z} + \frac{\partial u_z}{\partial \eta}\right)\frac{\partial v_\eta}{\partial z} \,\mathrm{d}\Omega \\
&\quad - \int_\Omega 2\mu \left(\frac{\partial u_\eta}{\partial \eta} - \frac{u_\eta}{\eta}\right) v_\eta \,\mathrm{d}\Omega - \int_{\Gamma_3} \eta f_\eta v_\eta \,\mathrm{d}\Gamma.
\end{aligned}
$$

Applying the same procedure to the right hand side of the first equation of (4.12) and repeating for the second equation, gives the system:

$$
\begin{aligned}
&\int_\Omega \left((\lambda + 2\mu)\frac{\partial u_\eta}{\partial \eta} + \lambda \frac{u_\eta}{\eta} + \lambda \frac{\partial u_z}{\partial z}\right)\left(\eta \frac{\partial v_\eta}{\partial \eta} + v_\eta\right) + \eta\mu \left(\frac{\partial u_\eta}{\partial z} + \frac{\partial u_z}{\partial \eta}\right)\frac{\partial v_\eta}{\partial z} - 2\mu \left(\frac{\partial u_\eta}{\partial \eta} - \frac{u_\eta}{\eta}\right) v_\eta \,\mathrm{d}\Omega \\
&\qquad = \int_{\Gamma_3} \eta f_\eta v_\eta \,\mathrm{d}\Gamma + \int_\Omega \eta b_\eta v_\eta \,\mathrm{d}\Omega \\
&\int_\Omega \mu \left(\frac{\partial u_z}{\partial \eta} + \frac{\partial u_\eta}{\partial z}\right)\left(\eta \frac{\partial v_z}{\partial \eta} + v_z\right) + \eta \left((\lambda + 2\mu)\frac{\partial u_z}{\partial z} + \lambda \frac{u_\eta}{\eta} + \lambda \frac{\partial u_\eta}{\partial \eta}\right)\frac{\partial v_z}{\partial z} - \mu \left(\frac{\partial u_\eta}{\partial z} + \frac{\partial u_z}{\partial \eta}\right) v_z \,\mathrm{d}\Omega \\
&\qquad = \int_{\Gamma_4} \eta f_z v_z \,\mathrm{d}\Gamma + \int_\Omega \eta b_z v_z \,\mathrm{d}\Omega.
\end{aligned}
$$

These equations can further be simplified using circle symmetry to:

$$
\begin{aligned}
&\int_{\Omega_{\eta z}} \left((\lambda + 2\mu)\frac{\partial u_\eta}{\partial \eta} + \lambda \frac{u_\eta}{\eta} + \lambda \frac{\partial u_z}{\partial z}\right)\left(\eta^2 \frac{\partial v_\eta}{\partial \eta} + \eta v_\eta\right) + \eta^2\mu \left(\frac{\partial u_\eta}{\partial z} + \frac{\partial u_z}{\partial \eta}\right)\frac{\partial v_\eta}{\partial z} - 2\eta\mu \left(\frac{\partial u_\eta}{\partial \eta} - \frac{u_\eta}{\eta}\right) v_\eta \,\mathrm{d}\eta\mathrm{d}z \\
&\qquad = \int_{\Gamma_{3,\eta z}} \eta^2 f_\eta v_\eta \,\mathrm{d}\eta\mathrm{d}z + \int_{\Omega_{\eta z}} \eta^2 b_\eta v_\eta \,\mathrm{d}\eta\mathrm{d}z \\
&\int_{\Omega_{\eta z}} \mu \left(\frac{\partial u_z}{\partial \eta} + \frac{\partial u_\eta}{\partial z}\right)\left(\eta^2 \frac{\partial v_z}{\partial \eta} + \eta v_z\right) + \eta^2 \left((\lambda + 2\mu)\frac{\partial u_z}{\partial z} + \lambda \frac{u_\eta}{\eta} + \lambda \frac{\partial u_\eta}{\partial \eta}\right)\frac{\partial v_z}{\partial z} - \eta\mu \left(\frac{\partial u_\eta}{\partial z} + \frac{\partial u_z}{\partial \eta}\right) v_z \,\mathrm{d}\eta\mathrm{d}z \\
&\qquad = \int_{\Gamma_{4,\eta z}} \eta^2 f_z v_z \,\mathrm{d}\eta\mathrm{d}z + \int_{\Omega_{\eta z}} \eta^2 b_z v_z \,\mathrm{d}\eta\mathrm{d}z.
\end{aligned}
$$

Approximating $u_\alpha, \alpha = \eta, z$ with

$$
u_\alpha = \sum_{j=1}^{n} u_{\alpha,j} \varphi_j,
$$

where $\varphi_j, j = 1, \ldots, n$ are basis functions that are constant with respect to θ. Setting $v_\alpha = \varphi_i, \alpha = \eta, z$, results in the system:

$$
\begin{bmatrix} S_{\eta\eta} & S_{\eta z} \\ S_{z\eta} & S_{zz} \end{bmatrix} \begin{bmatrix} u_\eta \\ u_z \end{bmatrix} = \begin{bmatrix} q_\eta \\ q_z \end{bmatrix}, \tag{5.6}
$$

†Note that this is not the Jacobian of integration over cylindrical coordinates.

with definitions:

$$
\begin{aligned}
(S_{\eta\eta})_{ij} &= \int_{\Omega_{\eta z}} \left((\lambda+2\mu)\frac{\partial\varphi_j}{\partial\eta} + \lambda\frac{\varphi_j}{\eta}\right)\left(\eta^2\frac{\partial\varphi_i}{\partial\eta} + \eta\varphi_i\right) + \eta^2\mu\frac{\partial\varphi_j}{\partial z}\frac{\partial\varphi_i}{\partial z} - 2\eta\mu\left(\frac{\partial\varphi_j}{\partial\eta} - \frac{\varphi_j}{\eta}\right)\varphi_i \,\mathrm{d}\eta\mathrm{d}z \\
(S_{\eta z})_{ij} &= \int_{\Omega_{\eta z}} \lambda\frac{\partial\varphi_j}{\partial z}\left(\eta^2\frac{\partial\varphi_i}{\partial\eta} + \eta\varphi_i\right) + \eta^2\mu\frac{\partial\varphi_j}{\partial\eta}\frac{\partial\varphi_i}{\partial z}\,\mathrm{d}\eta\mathrm{d}z \\
(S_{z\eta})_{ij} &= \int_{\Omega_{\eta z}} \mu\frac{\partial\varphi_j}{\partial z}\left(\eta^2\frac{\partial\varphi_i}{\partial\eta} + \eta\varphi_i\right) + \lambda\eta^2\left(\frac{\varphi_j}{\eta} + \frac{\partial\varphi_j}{\partial\eta}\right)\frac{\partial\varphi_i}{\partial z} - \eta\mu\frac{\partial\varphi_j}{\partial z}\varphi_i \,\mathrm{d}\eta\mathrm{d}z \\
(S_{zz})_{ij} &= \int_{\Omega_{\eta z}} \mu\frac{\partial\varphi_j}{\partial\eta}\left(\eta^2\frac{\partial\varphi_i}{\partial\eta} + \eta\varphi_i\right) + \eta^2(\lambda+2\mu)\frac{\partial\varphi_j}{\partial z}\frac{\partial\varphi_i}{\partial z} - \eta\mu\frac{\partial\varphi_j}{\partial\eta}\varphi_i \,\mathrm{d}\eta\mathrm{d}z \\
(q_\eta)_i &= \int_{\Gamma_{3,\eta z}} \eta^2 f_\eta\varphi_i \,\mathrm{d}\eta\mathrm{d}z + \int_{\Omega_{\eta z}} \eta^2 b_\eta\varphi_i \,\mathrm{d}\eta\mathrm{d}z \\
(q_z)_i &= \int_{\Gamma_{4,\eta z}} \eta^2 f_z\varphi_i \,\mathrm{d}\eta\mathrm{d}z + \int_{\Omega_{\eta z}} \eta^2 b_z\varphi_i \,\mathrm{d}\eta\mathrm{d}z.
\end{aligned}
$$

Application of linear triangles and linear line elements in the (η, z)-domain results in basis functions of the form:

$$\phi_i = a_i^0 + a_i^\eta\eta + a_i^z z,$$

and element matrices and vectors:

$$
\begin{aligned}
(S^e_{\eta\eta})_{ij} &= a_i^\eta a_j^\eta\frac{|\Delta|}{6}\sum_{k=1}^{3}\left[\eta^2(\lambda+2\mu)\right]_{(\eta_k,z_k)} + a_i^z a_j^z\frac{|\Delta|}{6}\sum_{k=1}^{3}\left[\eta^2\mu\right]_{(\eta_k,z_k)} + a_j^\eta\frac{|\Delta|}{6}\left[\lambda\eta\right]_{(\eta_i,z_i)} \\
&\quad + a_i^\eta\frac{|\Delta|}{6}\left[\lambda\eta\right]_{(\eta_j,z_j)} + \delta_{ij}\frac{|\Delta|}{6}\left[\lambda+2\mu\right]_{(\eta_i,z_i)} \\
(S^e_{\eta z})_{ij} &= a_i^\eta a_j^z\frac{|\Delta|}{6}\sum_{k=1}^{3}\left[\eta^2\lambda\right]_{(\eta_k,z_k)} + a_i^z a_j^\eta\frac{|\Delta|}{6}\sum_{k=1}^{3}\left[\eta^2\mu\right]_{(\eta_k,z_k)} + a_j^z\frac{|\Delta|}{6}\left[\eta\lambda\right]_{(\eta_i,z_i)} \\
(S^e_{z\eta})_{ij} &= a_i^\eta a_j^z\frac{|\Delta|}{6}\sum_{k=1}^{3}\left[\eta^2\mu\right]_{(\eta_k,z_k)} + a_i^z a_j^\eta\frac{|\Delta|}{6}\sum_{k=1}^{3}\left[\eta^2\lambda\right]_{(\eta_k,z_k)} + a_j^z\frac{|\Delta|}{3}\left[\eta\mu\right]_{(\eta_i,z_i)} - a_i^z\frac{|\Delta|}{6}\left[\eta\lambda\right]_{(\eta_j,z_j)} \\
(S^e_{zz})_{ij} &= a_i^\eta a_j^\eta\frac{|\Delta|}{6}\sum_{k=1}^{3}\left[\eta^2\mu\right]_{(\eta_k,z_k)} + a_i^z a_j^z\frac{|\Delta|}{6}\sum_{k=1}^{3}\left[\eta^2(\lambda+2\mu)\right]_{(\eta_k,z_k)} \\
(q^e_\eta)_i &= \frac{|\Delta|}{6}\eta_i^2 b_\eta(\eta_i,z_i) \\
(q^e_z)_i &= \frac{|\Delta|}{6}\eta_i^2 b_z(\eta_i,z_i) \\
(q^b_\eta)_i &= \frac{L}{2}\eta_i^2 f_\eta(\eta_i,z_i) \\
(q^b_z)_i &= \frac{L}{2}\eta_i^2 f_z(\eta_i,z_i).
\end{aligned}
$$

After assembly of the large matrix and vector, those rows and columns of associated with a fixed boundary, the points from boundary Γ_1 and Γ_2, should be deleted. To this end let $I_{\Gamma_i} \subset \mathbb{N}$ be the set of indices associated with the points from boundary Γ_i. Then we must delete the rows and columns with an index from I_{Γ_1} from the large matrix and vector and subsequently the rows and columns with an index from $I_{\Gamma_2} + n$, where n is the total number of points.

5.2.4 Derived quantities

Although the systems (5.4), (5.5) and (5.6) give a solution of the models (4.5), (4.9) and (4.12), the values of the stress and strain in the system are also of importance. In this elastic model the stresses σ and $\underline{\underline{\boldsymbol{\sigma}}}$ can be directly calculated from the strains ε and $\underline{\underline{\boldsymbol{\varepsilon}}}$ by using equations (4.4), (4.8) and (4.11), but the latter variables must be calculated from the numerical solution of (5.4), (5.5) or (5.6).

The one dimensional strain ε is defined by equation (4.3)

$$\varepsilon = \frac{\partial u}{\partial x}.$$

Multiplication of both sides with a test function v and integration over the whole domain of interest $[0, d]$ gives

$$\int_0^d \varepsilon v \mathrm{d}x = \int_0^d \frac{\partial u}{\partial x} v \mathrm{d}x.$$

If we substitute, analogous to the derivation of (5.4), the approximations

$$u(x) = \sum_{j=1}^{n} u_j \varphi_j(x)$$
$$\varepsilon(x) = \sum_{j=1}^{n} \varepsilon_j \varphi_j(x),$$

and set $v = \phi_j$ for $j = 1, \ldots, n$ we arrive at the system

$$\Lambda \boldsymbol{\varepsilon} = U \boldsymbol{u},$$

with

$$\Lambda_{ij} = \int_0^d \varphi_i \varphi_j \mathrm{d}x \qquad \text{for } i, j = 1, \ldots, n$$
$$U_{ij} = \int_0^d \varphi_i \frac{\partial \varphi_j}{\partial x} \mathrm{d}x \qquad \text{for } i, j = 1, \ldots, n.$$

Application of linear elements to the one dimensional model results in the element matrices

$$(\Lambda^e)_{ij} = \frac{l}{2}\delta_{ij} \qquad \text{for } i, j = 1, 2$$
$$(U^e)_{ij} = \frac{l}{2} a_j^1 \qquad \text{for } i, j = 1, 2.$$

Using the same approach as above with the three dimensional model and (4.7) results in the system

$$\begin{bmatrix} \Lambda_{11} & & & & & \\ & \Lambda_{12} & & & & \\ & & \Lambda_{13} & & & \\ & & & \Lambda_{22} & & \\ & & & & \Lambda_{23} & \\ & & & & & \Lambda_{33} \end{bmatrix} \begin{bmatrix} \boldsymbol{\varepsilon}_{11} \\ \boldsymbol{\varepsilon}_{12} \\ \boldsymbol{\varepsilon}_{13} \\ \boldsymbol{\varepsilon}_{22} \\ \boldsymbol{\varepsilon}_{23} \\ \boldsymbol{\varepsilon}_{33} \end{bmatrix} = \begin{bmatrix} 2U_1 & & \\ U_2 & U_1 & \\ U_3 & & U_1 \\ & 2U_2 & \\ & U_3 & U_2 \\ & & 2U_3 \end{bmatrix} \begin{bmatrix} \boldsymbol{u}_1 \\ \boldsymbol{u}_2 \\ \boldsymbol{u}_3 \end{bmatrix},$$

with element matrices

$$(\Lambda_{ij}^e)_{kl} = \frac{|\Delta|}{6}\delta_{kl} \qquad \text{for } i = 1, 2, 3, j = i, \ldots, 3 \qquad \text{and for } k, l = 1, 2, 3, 4$$
$$(U_i^e)_{kl} = \frac{|\Delta|}{3} a_l^i \qquad \text{for } i = 1, 2, 3 \qquad \text{and for } k, l = 1, 2, 3, 4.$$

Using the same approach as above with the cylindrical model and (4.7) results in the system

$$\begin{bmatrix} \Lambda & & & \\ & \Lambda & & \\ & & \Lambda & \\ & & & \Lambda \end{bmatrix} \begin{bmatrix} \varepsilon_{\eta\eta} \\ \varepsilon_{\theta\theta} \\ \varepsilon_{zz} \\ \varepsilon_{\eta z} \end{bmatrix} = \begin{bmatrix} 2U_\eta & \\ U_\theta & \\ & 2U_z \\ U_z & U_\eta \end{bmatrix} \begin{bmatrix} \boldsymbol{u}_\eta \\ \boldsymbol{u}_z \end{bmatrix},$$

with element matrices

$$(\Lambda^e)_{ij} = \frac{|\Delta|}{6}\delta_{ij}\eta_i$$
$$(U^e_\eta)_{ij} = \frac{|\Delta|}{12}a^\eta_j\eta_i$$
$$(U^e_z)_{ij} = \frac{|\Delta|}{12}a^z_j\eta_i$$
$$(U^e_\theta)_{ij} = \delta_{ij}\frac{|\Delta|}{6},$$

and all other strains equal to zero due to circle symmetry.

The resulting systems are easily calculated after which the result can be used to calculate the numerical values $\boldsymbol{\sigma}$ and $\boldsymbol{\sigma}_{ij}$ of the physical quantities σ and $\underline{\underline{\boldsymbol{\sigma}}}$. These quantities can thereafter be used to calculate the strain energy ΔG^{el}_s. In the case of one dimension the vector containing the (numerical) values of ΔG^{el}_s at certain points in the domain $[0, d]$ can be calculated by performing a point-wise product of the vectors $1/2\boldsymbol{\sigma}$ and $\boldsymbol{\varepsilon}$ with values at the same spacial locations. This can be formulated as

$$\boldsymbol{\Delta G}^{el}_s = \frac{1}{2}\boldsymbol{\sigma}.\boldsymbol{\varepsilon},$$

where . represents the point-wise product. In three dimensions at each point in space a Frobenius inner product should be calculated. This inner product is for two square matrices $A, B \in \mathbb{R}^{n\times n}$ defined as

$$A : B = \sum_{i=1}^{n}\sum_{j=1}^{n} A_{ij}B_{ij}.$$

If at any point in space σ_{ij} and ε_{ij} for $i, j = 1, 2, 3$ are known, ΔG^{el}_s can easily be calculated by a Frobenius inner product. This should then be repeated for all other points in space for which ΔG^{el}_s is required. Although this is a correct approach, a faster calculation can be constructed. As $\boldsymbol{\sigma}_{ij}$ and $\boldsymbol{\varepsilon}_{ij}$ represent the numerical values at points in space with the same ordering, the Frobenius inner product can be combined with the point-wise product to give an expression for ΔG^{el}_s at all points in space, which can be denoted by $\boldsymbol{\Delta G}^{el}_s$. This expression is given by:

$$\boldsymbol{\Delta G}^{el}_s = \frac{1}{2}\sum_{i=1}^{3}\sum_{j=1}^{3}\boldsymbol{\sigma}_{ij}.\boldsymbol{\varepsilon}_{ij}.$$

A similar equation can be derived for the cylindrical model.

5.3 Combined algorithm

As the model for nucleation (3.9) and the elastic models (4.5), (4.9) and (4.12) are converted to a finite set of equations that can be solved, the couplings between the two models impose a specific algorithm that simulates the behavior of a system under nucleation and elastic deformation. This algorithm is:

1. Set all constants;
2. Set all initial values;
3. For each time step:
   (a) Calculate elastic parameters;
   (b) Build matrices for elastic deformation;
   (c) Calculate elastic deformations;
   (d) Calculate elastic strain energy;
   (e) For each point:

i. Calculate nucleation parameters;
ii. Calculate matrices for nucleation;
iii. Calculate nucleation.

The length of the outer for-loop is determined by the time range of interest and the size of the time step used. This length cannot be altered in, as a restriction on the time step could be present. The length of the inner for-loop is uniquely determined by the number of points used to discretize the spacial domain of interest. As the number of points is in most cases high, this for-loop could become large and of high computational costs. If a reduction in length of the for-loop is wanted, two approaches could be taken. The first option is to lower the number of points, but as this lowers the accuracy of the model, this seems not a good approach. Second, the nucleation model could be calculated at a fraction of the points, after which an interpolation of the results could be imposed. This reduces the length of the loop and the total computational costs of the loop by some fixed ratio, but the application of the interpolation step should be well defined and based on the physics of the problem. This suggests performing simulations with the non-simplified algorithm with a low number of points, after which the number of points can be increased and an interpolation based on the results of the first simulation could be implemented.

Chapter 6

Numerical results

This chapter will perform various simulations with the models presented in Chapter 4 and the corresponding discretizations in Chapter 5. We will start with determining the experimental order of accuracy of scheme (5.1), with as goal to determine if the theoretical order of accuracy is achieved. Thereafter various simulations will be performed to investigate the effect of elastic deformations on the nucleation process and vice versa. All simulations will be based on the same physical setting.

6.1 Physical setting

The simulations performed in this chapter will all simulate prolonged artificial ageing at $T = 180°$ C for 3×10^3 seconds. The parameters used for the simulation can be found in Table 6.1. The value of Δr^* is chosen to be five percent of r^*.

Parameter	**Value**	**Comments**
C_0	0.63	Myhr and Grong (2000)
C_p	63.4	Myhr and Grong (2000)
C_s	970	Myhr and Grong (2000)
D_0	2.2×10^{-4}	Myhr and Grong (2000)
Q_d	130,000	Myhr and Grong (2000)
Q_s	47,175	Myhr and Grong (2000)
$\gamma_{\alpha\beta}$	0.2	Myhr and Grong (2000)
V_m	3.95×10^{-5}	Myhr and Grong (2000)
j_0	9.66×10^{34}	Myhr and Grong (2000)
A_0	16,220	Myhr and Grong (2000)
x_p	2/3	Chosen
a_m	4.049×10^{-10}	Uguz (2003)
a_p	6.295×10^{-10}	Tani and Kido (2008)
δ_m	1.1013×10^{11}	Hyland (1992)
δ_p	8.4250×10^{10}	Tani and Kido (2008)
ν_m	0.34	Hyland (1992)
ν_p	0.161	Tani and Kido (2008)
μ_m	26.3×10^9	Hyland (1992)
μ_p	49.2×10^9	Tani and Kido (2008)
E_m	70.7×10^9	Hyland (1992)
E_p	113.5×10^9	Tani and Kido (2008)

Table 6.1: Parameters used for simulations.

The region of radii we will simulate will be between 1Å and 100Å, and will be divided into regions of size $\Delta r = 1/2$Å, unless otherwise mentioned. The time step Δt used in all simulations will be 0.5

seconds, unless otherwise mentioned. In case of the one dimensional deformations, we will use a grid of length 30 millimeter, divided into a 100 evenly spaced elements, centered around zero. In case of the three dimensional deformations, we will use a grid with dimensions $6 \times 6 \times 30$ millimeter, using a cubic decomposition using $4 \times 4 \times 20$ cubes, centered around the origin. Although these number of cubes is low, it will give preliminary results on the behavior of the nucleation under elastic deformations. The number of cubes used is low due to the high computational costs needed to run the three dimensional simulation. The cylindrical simulations will be performed by modeling a cylinder of height 30 millimeter and radius 3 millimeter. The number of grid points in the radial direction will be 10, those in the axial direction will be 20.

6.2 Order determination

In Section 5.1 a theoretical discussion resulted in the conclusion that the scheme (5.1) is of first order accuracy in both time and place. To support this conclusion, we will perform simulations to determine the accuracy of this scheme, independent of the order determined by the theory. To determine the experimental order of the scheme, a method must be derived to determine the order. This will be done in the next section. Thereafter several results will be obtained by simulation and a discussion of these results.

6.2.1 Determination method

Let $\Delta t_i, i = 1, 2, 3$ and $\Delta r_i, i = 1, 2, 3$ be given, fulfilling the relations:

$$\begin{aligned} \frac{\Delta t_i}{\Delta r_i} &= C && \text{for } i = 1, 2, 3 \\ \Delta r_{i+1} &= \lambda \Delta r_i && \text{for } i = 1, 2, \end{aligned}$$

where C and λ are constants, with $\lambda > 1$ and integer. Let $N_i, i = 1, 2, 3$ be the numerical solutions of (5.1) by using Δt_i and Δr_i.

These solutions can be seen as an approximation of the exact solution $N(r, t)$ to some order of magnitude p in time and place. This can be written as

$$N(r, t) = N_i(r, t) + \alpha \Delta r_i^p, \tag{6.1}$$

due to the relations imposed on Δt_i and Δr_i and α is a constant independent of the grid size.

The exact total number density $n(t)$ can be calculated using the formula:

$$n(t) = \int_0^\infty \phi(r, t) \mathrm{d}r.$$

Using the relation $N(r, t) = \phi(r, t)/\Delta r_i$ for any Δr_i, we can derive the following:

$$\begin{aligned} n(t) &= \frac{1}{\Delta r_i} \int_0^\infty N(r, t) \mathrm{d}r \\ &= \frac{1}{\Delta r_i} \int_0^\infty \left(N_i(r, t) + \alpha \Delta r_i^p \right) \mathrm{d}r \\ &= \frac{1}{\Delta r_i} \int_0^\infty N_i(r, t) \mathrm{d}r + \Delta r_i^{p-1} \int_0^\infty \alpha \mathrm{d}r, \end{aligned}$$

in which the integrals are replaced by discrete integrals using an order $m \geq p$ accurate integration rule:

$$\begin{aligned} &= \frac{1}{\Delta r_i} \sum_{j=1}^{P} w_j N_i(r_j, t) \Delta r_i + \Delta r_i^{p-1} \sum_{j=1}^{P} \alpha \Delta r_i + \mathcal{O}(\Delta r_i^m) \\ &= \sum_{j=1}^{P} w_j N_i(r_j, t) + \Delta r_i^p \alpha P + \mathcal{O}(\Delta r_i^m). \end{aligned}$$

The sum can be seen as the discrete form n_i of $n(t)$ using grid i, with the w_j indicating the weights to achieve order m accuracy in integration. As the order of the integration m is assumed to be equal or of higher than p, we have the following identity for $i = 1, 2, 3$:

$$n(t) = n_i(t) + \bar{\alpha}\Delta r_i^p, \tag{6.2}$$

for some grid independent constant $\bar{\alpha}$.

Now choose a discrete time t^n for the coarsest grid ($i = 3$). This discrete time corresponds with the discrete time $t^{\lambda n}$ for $i = 2$ and with $t^{\lambda^2 n}$ for $i = 1$. Comparing equation (6.2) for $i = 1$ at time $t^{\lambda^2 n}$ with equation (6.2) for $i = 2$ at $t^{\lambda n}$ gives:

$$n_2(t^{\lambda n}) - n_1(t^{\lambda^2 n}) = \bar{\alpha} P \Delta r_1^p \left(1 - \lambda^p\right).$$

Comparing equation (6.2) for $i = 2$ at time $t^{\lambda n}$ with equation (6.2) for $i = 3$ at t^n gives:

$$n_3(t^n) - n_2(t^{\lambda n}) = \bar{\alpha} P \Delta r_1^p \lambda^p \left(1 - \lambda^p\right).$$

Division of the latter by the first equation and taking absolute values gives:

$$\lambda^p = \frac{|n_3(t^n) - n_2(t^{\lambda n})|}{|n_2(t^{\lambda n}) - n_1(t^{\lambda^2 n})|},$$

or solved for p:

$$p = \frac{\log\left(\frac{|n_3(t^n) - n_2(t^{\lambda n})|}{|n_2(t^{\lambda n}) - n_1(t^{\lambda^2 n})|}\right)}{\log \lambda}. \tag{6.3}$$

Note that (6.3) can be evaluated for each discrete time t^n of the coarsest grid.

Instead of using the total number density of the to determine the order of the IMEX-θ method, we can also use formula (6.1) to determine the order of the method. This will lead to the formula:

$$p = \frac{\log\left(\frac{|N_3(r_i, t^n) - N_2(r_i, t^{\lambda n})|}{|N_2(r_i, t^{\lambda n}) - N_1(r_i, t^{\lambda^2 n})|}\right)}{\log \lambda},$$

where r_i is any grid point from the coarsest grid, shared by the two finer grids. We choose not to use this method, as this choosing a correct grid point can be difficult due to the nature of the differential equation (4.2).

6.2.2 Experimental results

This section will contain the results from simulations with three grid sizes and time step combinations and the order determined from these results. We choose for the finest grid the value $\Delta r_1 = 0.125$Å and as relational parameters for the other grids the values $C = 1s/$Å and $\lambda = 2$. A combination of the time dependent variables, with no deformations imposed, can be found in Figure 6.1. To calculate $n_i, i = 1, 2, 3$, we use the second order accurate integration method known as the Compound Midpoint Rule. As the theoretical discussion of the accuracy of the IMEX θ-method is order 1, this should not pose any restriction on the order of accuracy determined by the experiments.

As can be seen from these figures are the results for the chosen grid sizes and time steps close to each other. Using the results from Figure 6.1(b), the time dependent order can be calculated using formula (6.3). These results can be seen in Figure 6.2. In this figure one can see that the order of the method is calculated to be of approximately first order ($p \approx 1$).

We can conclude that the experimental results give an order of approximately 1, which is in good agreement with the theoretical results obtained in Section 5.1.

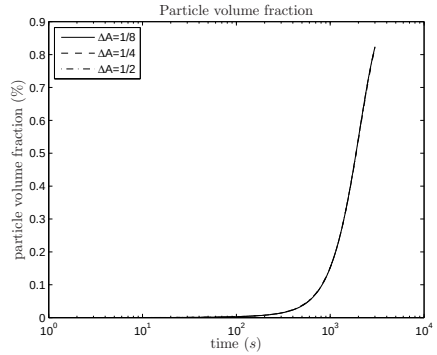

(a) Evolution of the particle volume fraction f.

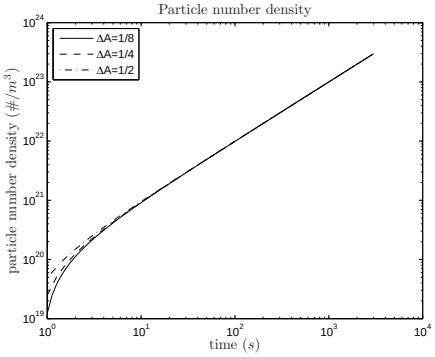

(b) Evolution of the particle number density n.

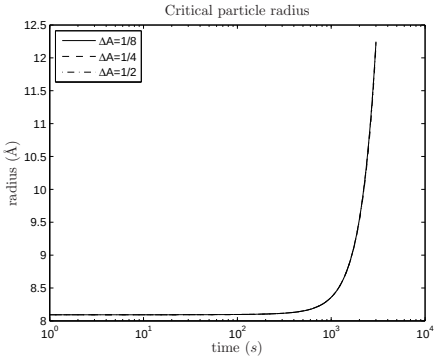

(c) Evolution of the critical particle radius r^*.

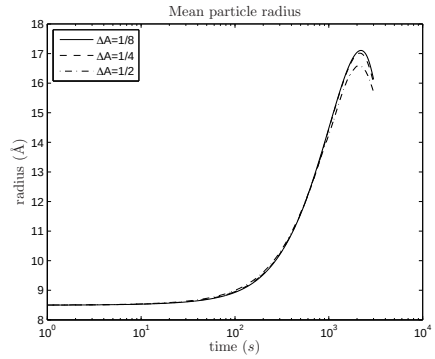

(d) Evolution of the mean particle radius $\bar{r}$.

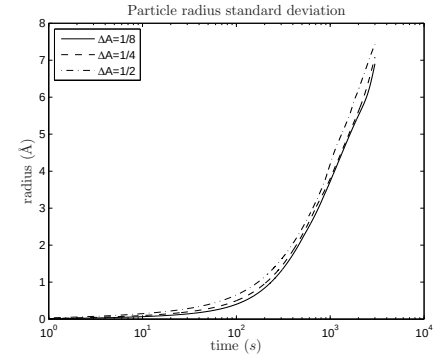

(e) Evolution of the particle radius standard deviation ρ.

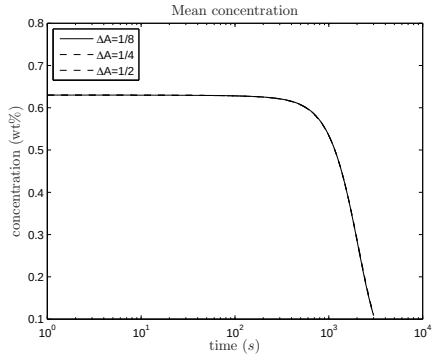

(f) Evolution of the concentrations $\bar{C}$ and C_e.

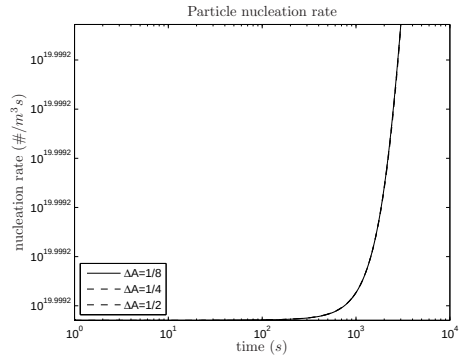

(g) Evolution of the nucleation rate j.

Figure 6.1: Results from simulations for order determination.

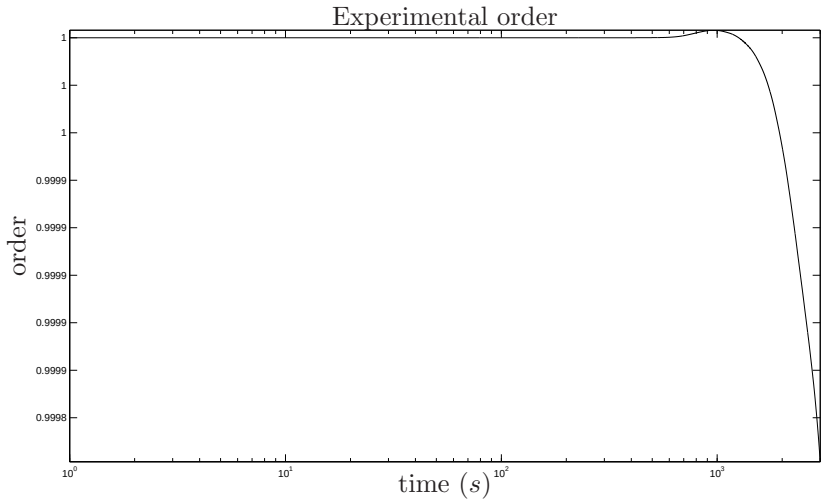

Figure 6.2: Time dependent experimental order.

6.3 Reference simulation

In order to determine the influence of incorporating elastic deformations into the nucleation process, a reference simulation is needed. The results from various deformations can than be compared with the reference results. If we investigate a bar, either one or three dimensional or cylindrical, where no deformations are imposed on, we see that all points should behave similarly with regard to nucleation due to the absence of ΔG_s^{el}. The results from simulating with the absence of elastic deformations can be seen in Figure 6.3.

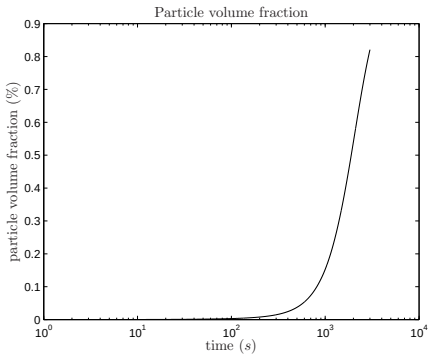

(a) Evolution of the particle volume fraction f.

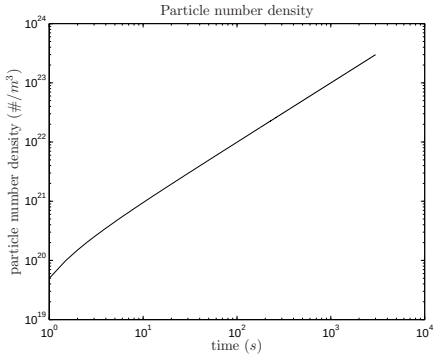

(b) Evolution of the particle number density n.

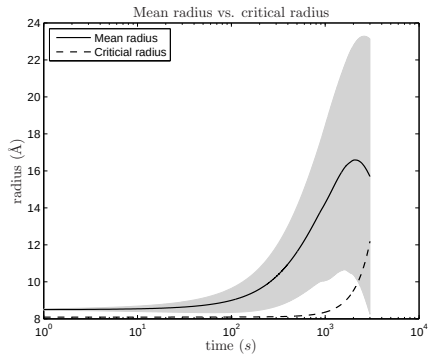

(c) Evolution of the critical particle radius r^* and mean radius $\bar{r}$. Gray area implicates the standard deviation ρ.

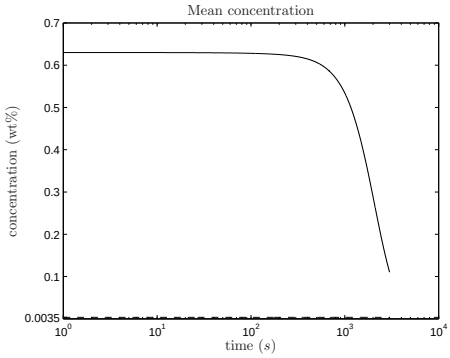

(d) Evolution of the concentrations $\bar{C}$ and C_e.

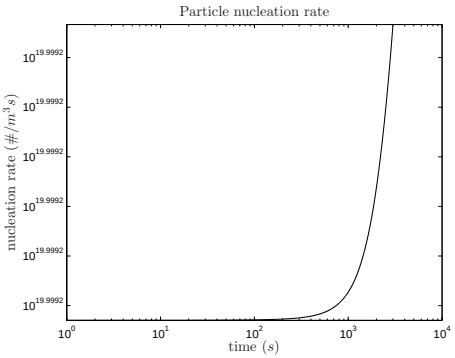

(e) Evolution of the nucleation rate j.

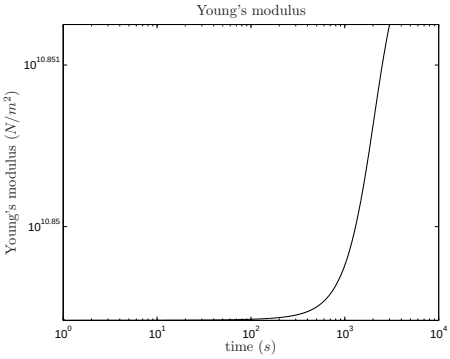

(f) Evolution of the Young's modulus E.

Figure 6.3: Results from reference simulation.

6.4 Influence of gravity

The simplest form of elastic deformations is due to gravitational forces. To investigate these forces, we set the body forces b in the one dimensional model (4.5) to

$$b = -2700 * 9.81,$$

where the value 2700 represents the density of aluminum, which is approximately the same as that for the alloy of interest. The value 9.81 represents the gravitational acceleration. Results from the simulation with the one dimensional model can be seen in Figure B.1. If we calculate the difference with the results from the reference simulation in percentages of the latter, we see that all variables have the same values as the reference values. This can be explained by looking at the value of the elastic strain energy ΔG_s^{el}, which can be seen in Figure 6.4, and that of the misfit strain energy ΔG_s^m, which has an approximate value of

$$2.9892 \times 10^{10},$$

in these simulations. As we can see the value of ΔG_s^{el} is less than 5×10^{-15} percent of ΔG_s^m, which explains the lack of visible influences in the results. This indicates that the influence of gravitational forces can be neglected.

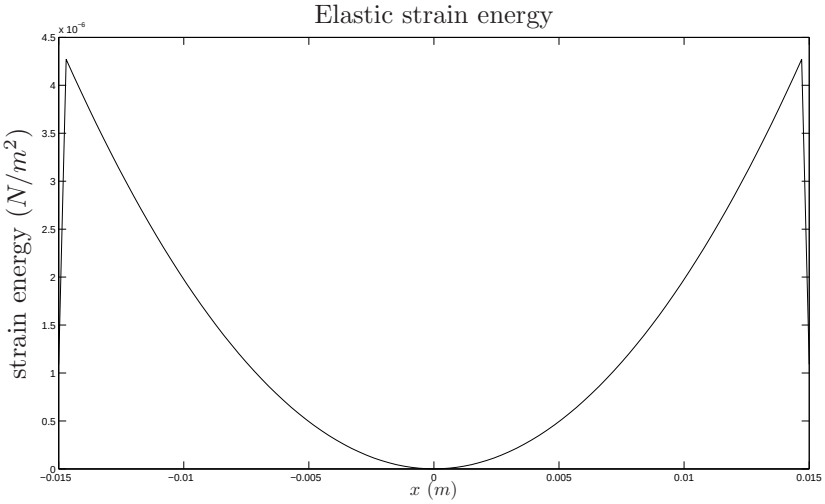

Figure 6.4: Elastic strain energy due to gravitational forces.

To indicate the correct working of the algorithm in the presence of gravitational forces, we multiplied the gravitational acceleration with 10^6 and recalculated the results. These can be seen in Figures B.2. The percent differences with the reference results can be found in Figure 6.5.

These figures indicate that differences with the reference simulation occur, but are still at most 10^{-5} percent of these results. This indicates that our conclusion that the gravitational forces can be ignored is correct, as a million times larger gravity indicates only slight changes in comparison with no gravitational forces.

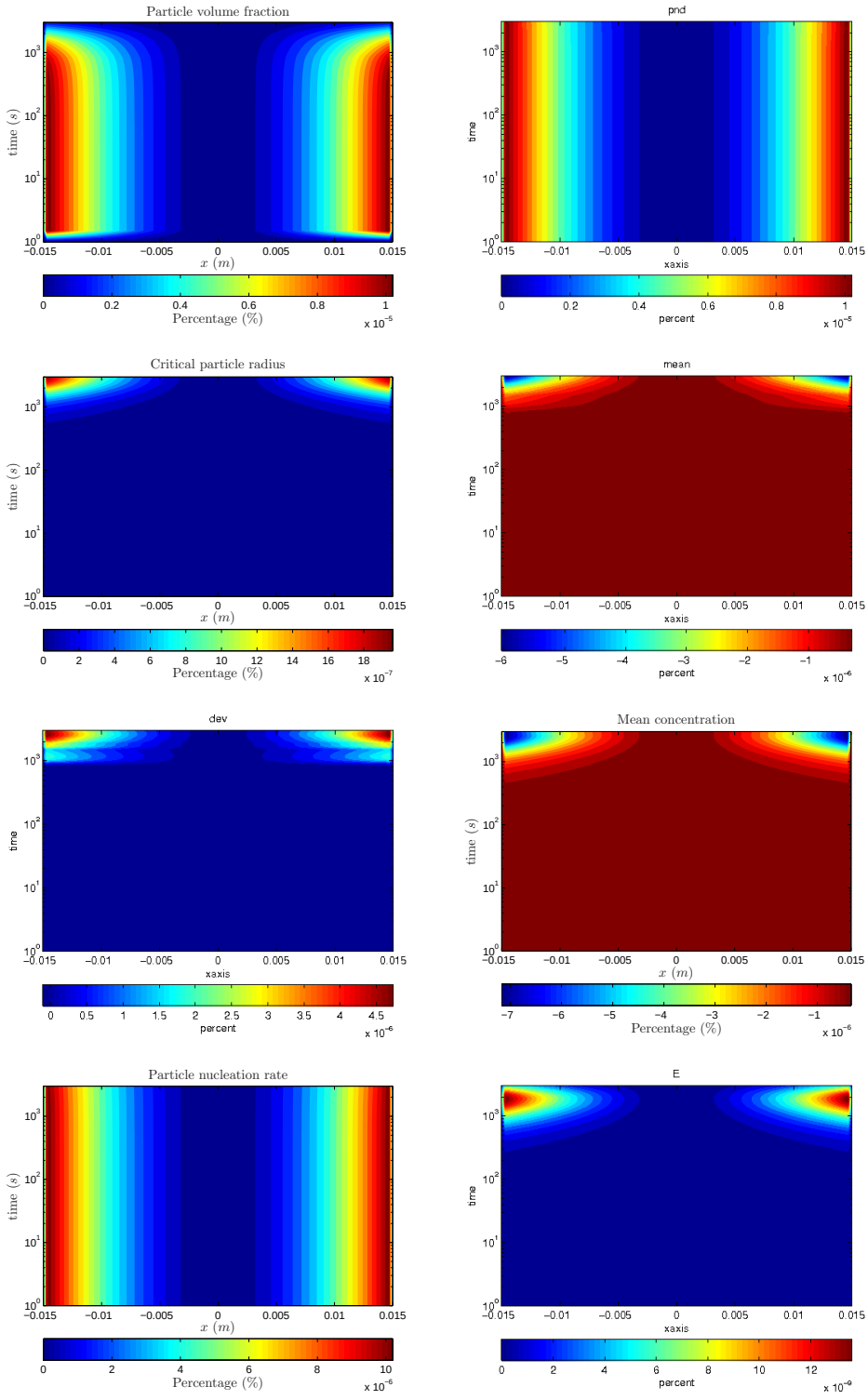

Figure 6.5: Percent differences under amplified gravity.

6.5 One-dimensional deformation

As the previous section has shown, the influences of gravitational forces can be neglected. This does not indicate that all deformations can be ignored. To this end we will perform a tensile test with the one-dimension model. This indicates setting the boundary conditions to

$$u(-d,t) = 0$$
$$E(d,t)\frac{\partial u}{\partial x}(d,t) = F_2(t),$$

where $F_2(t)$ will be assumed constant in time. As only realistic results can be obtained if F_2 does not give rise to strains and stress beyond the yielding point of the material, F_2 cannot be chosen lightly. Following Abrantes et al. (2006), we set the yield stress σ_Y to be

$$\sigma_Y = 160 \times 10^6 \frac{N}{m^2}.$$

Simulation of the one-dimensional model, ignoring nucleation, with various values for F_2 give that the value of F_2 should approximately lie between zero and $7.915 \times 10^9 N/m^2$. To ensure results below the yielding point, we set:

$$F_2 = 7.5 \times 10^9 \frac{N}{m^2}.$$

The results from the simulations of the tensile test can be found in Figures B.3 and 6.6, where the latter depicts the percent differences with the reference simulations. Figure 6.7 depicts the difference of the total strain energy ΔG_s due to tensile testing with the reference simulation in percentages of the latter.

From the figures presented we can see that the total strain energy differs at most 5.5×10^{-4} percent, which results in differences with the reference simulation in all variables. The highest differences can be found away from the edges of the stretched bar, where no differences are found at the edges. This behavior coincides with the difference with the reference simulation, as at the edges of the stretched bar no deformations are present, resulting in no stresses, strains and strain energy. With regard to time, we can see that the difference with the reference simulation reduces to zero at the later stage of the nucleation process. This can be explained by the fact that although the nucleation process evolves slightly differently, still an equilibrium situation is achieved, which is the same as for the reference simulation.

The results above indicate that increasing the total strain energy forces influences the nucleation process. To further investigate this influence, we increase the applied tension force to it's thousandfold

$$F_2 = 7.5 \times 10^{12} \frac{N}{m^2}.$$

This means that in theory the material should stop behaving linear elastic, but at this moment we assume that linear elasticity holds. The results from this test can be found in Figures B.4, 6.8 and 6.9.

These results show that increasing the elastic stress en resulting elastic strain energy, do influence the nucleation process to high extent. This indicates that materials with a higher region of elasticity and conforming yield stress will have a different behavior under (tensile) elastic deformations.

The results from one dimensional tension testing indicate that using a force, which results in less stress than the yield stress at any point, influences the behavior and outcome of nucleation, but only slight, as the results differ up to at most 4×10^{-7} percent if no tensile test is performed. If a material with a higher yield stress is used, it can be expected from Figure 6.8 that higher differences in comparison with no deformations will occur using the proposed model.

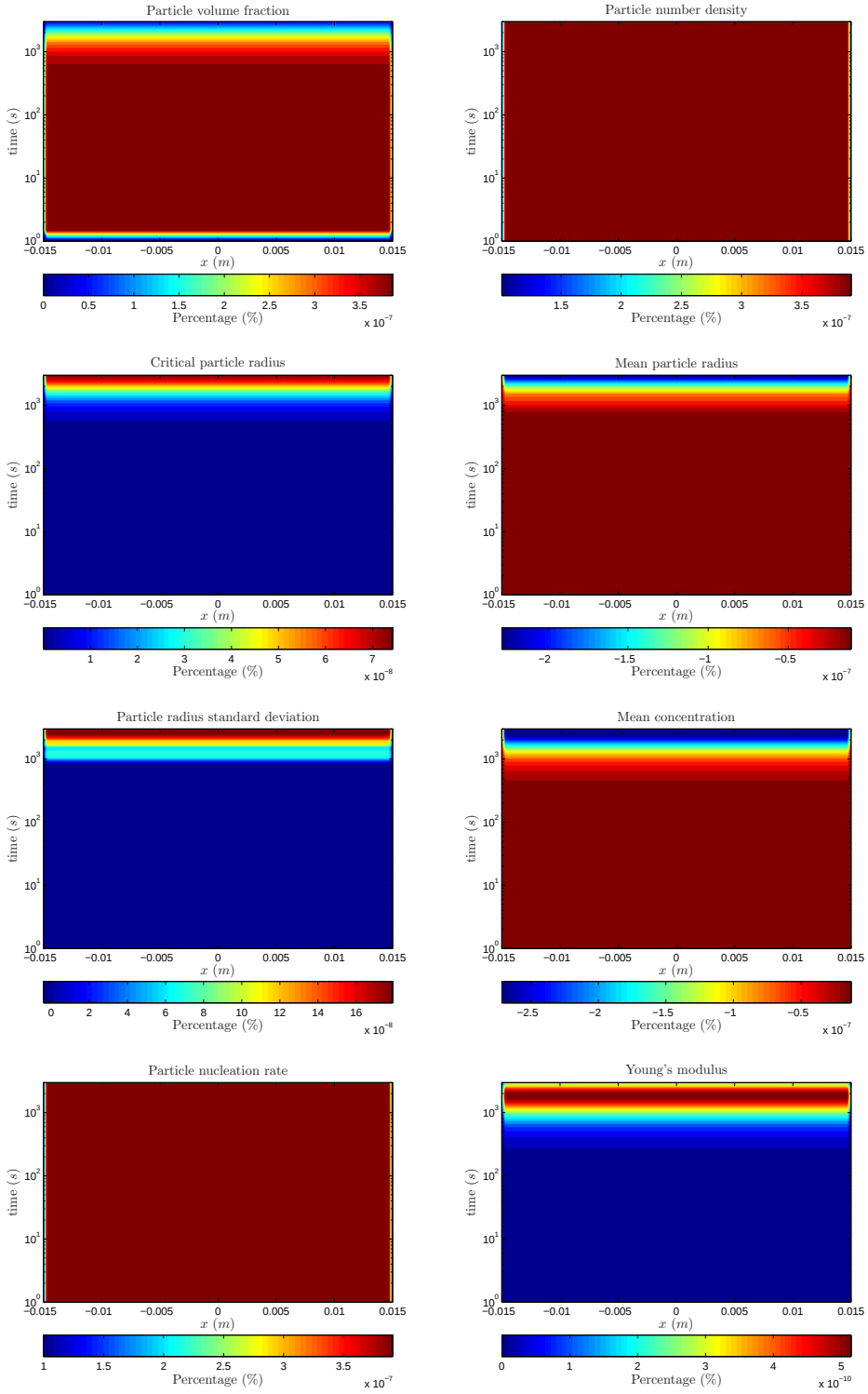

Figure 6.6: Percent differences under tensile test.

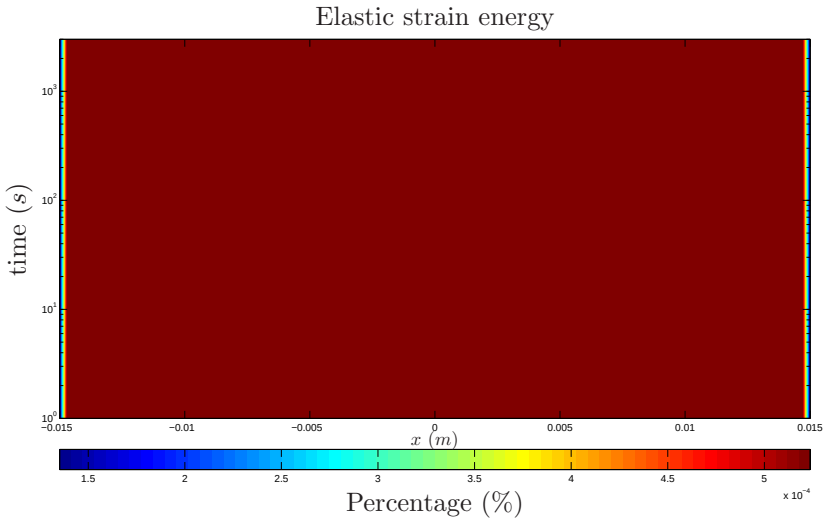

Figure 6.7: Percent differences of total strain energy with respect to the reference simulation.

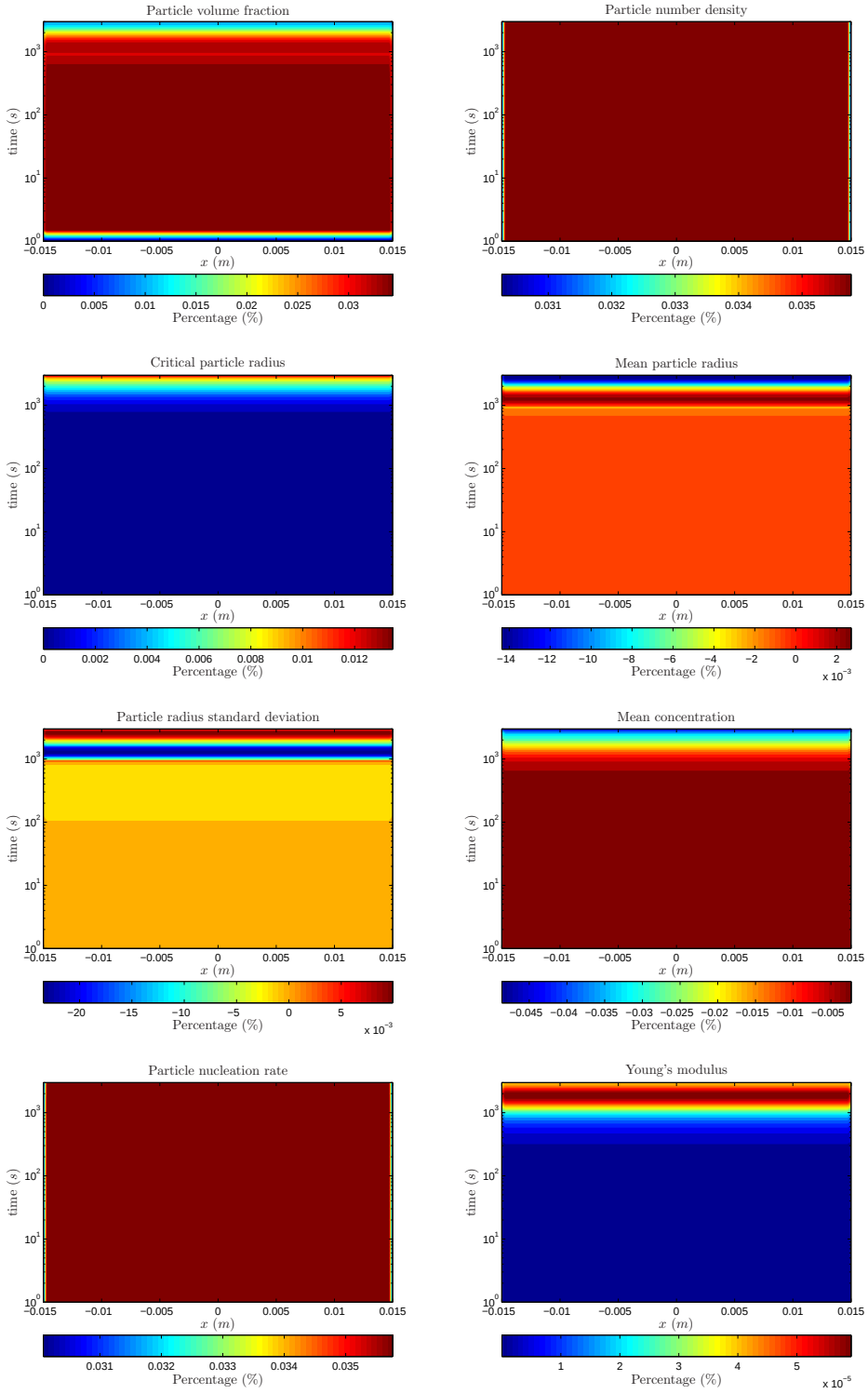

Figure 6.8: Percent differences under amplified tensile test.

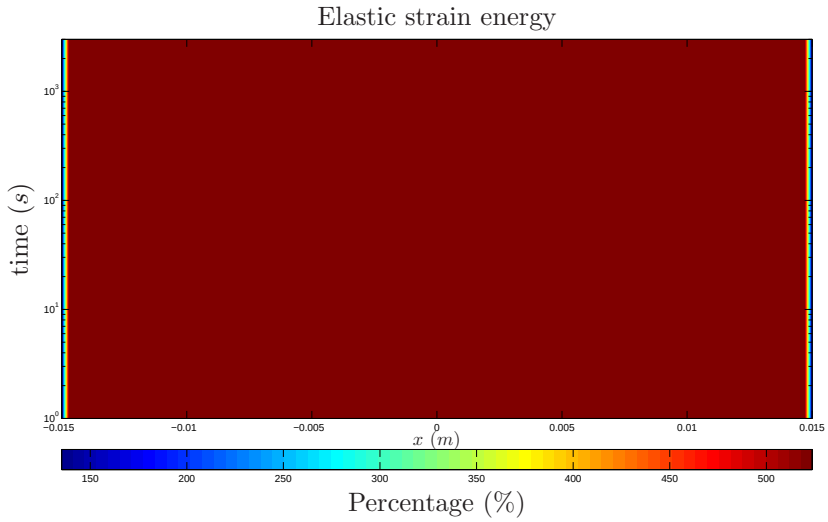

Figure 6.9: Percent differences of total strain energy with respect to the reference simulation under amplified tensile test.

6.6 Three-dimensional deformation

As with the one-dimensional tensile test, we will perform a similar simulation with the three-dimensional model. Demanding no deformations at the boundary plane given by $x_3 = -d_3$, where $2d_3$ equals the height of the block, a normal force exerted at the boundary plane given by $x_3 = d_3$ and a free boundary at all other boundary planes, give the following boundary conditions:

$$\begin{aligned} &\boldsymbol{u}(\boldsymbol{x}) = \boldsymbol{0} && \forall \boldsymbol{x} : x_3 = -d_3 \\ &\underline{\underline{\boldsymbol{\sigma}}} \cdot \boldsymbol{n} = \begin{bmatrix} 0 \\ 0 \\ F \end{bmatrix} && \forall \boldsymbol{x} : x_3 = d_3 \\ &\underline{\underline{\boldsymbol{\sigma}}} \cdot \boldsymbol{n} = \boldsymbol{0} && \forall \boldsymbol{x} : x_1 = \pm d_1 \vee x_2 = \pm d_2, \end{aligned}$$

where F represents the force exerted on the top face of the bar. To ensure again elastic deformations a value for F has been chosen such that in each point the stress does not exceed the yield stress σ_Y. This value is:

$$F = 3.5 \times 10^6 \, \frac{N}{m^2}.$$

As the nucleation variables computed are given in each point of the block at each simulated discrete time, depicting these results is difficult. In Figure 6.10 the initial deformation and elastic strain energy with no nucleation influence is depicted. To depict the results from nucleation, we will choose eight two-dimensional planes of the simulated block, for which pictures similar to Figure 6.10 will be constructed for each variable, but with one of the coordinates x_1, x_2 or x_3 replaced by the time variable. Five of the planes will be perpendicular to x_3 and three will be perpendicular to x_1. The choice of these planes has been based on the results in Figure 6.10 and the symmetry of these results. The planes $P_i, i = 1, \ldots, 6$ chosen are described by:

$$\begin{aligned} P_1 &= \{\boldsymbol{x} : x_1 = 0\} \\ P_2 &= \{\boldsymbol{x} : x_1 = d_1/2\} \\ P_3 &= \{\boldsymbol{x} : x_1 = d_1\} \\ P_4 &= \{\boldsymbol{x} : x_3 = -d_3\} \\ P_5 &= \{\boldsymbol{x} : x_3 = -d_3/2\} \\ P_6 &= \{\boldsymbol{x} : x_3 = 0\} \\ P_7 &= \{\boldsymbol{x} : x_3 = d_3/2\} \\ P_8 &= \{\boldsymbol{x} : x_3 = d_3\}, \end{aligned}$$

and can be seen in Figure 6.10(f).

The results from simulations can be found in Figures B.5 to B.20. Due to time constraint of this master thesis we have chosen to simulate only 500 seconds, instead of the mentioned 3000 seconds. As can be seen from these figures the results differ slightly from those obtained with the one dimensional simulation. We again note that these are preliminary results, as we used a very coarse grid.

No simulations are performed using finer grids, as the computations to obtain the results will use a large amount of time. We therefore propose to implement the model using a programming language that has been optimized for these type of computations and applying specific optimized algorithms for solving the various matrix equations.

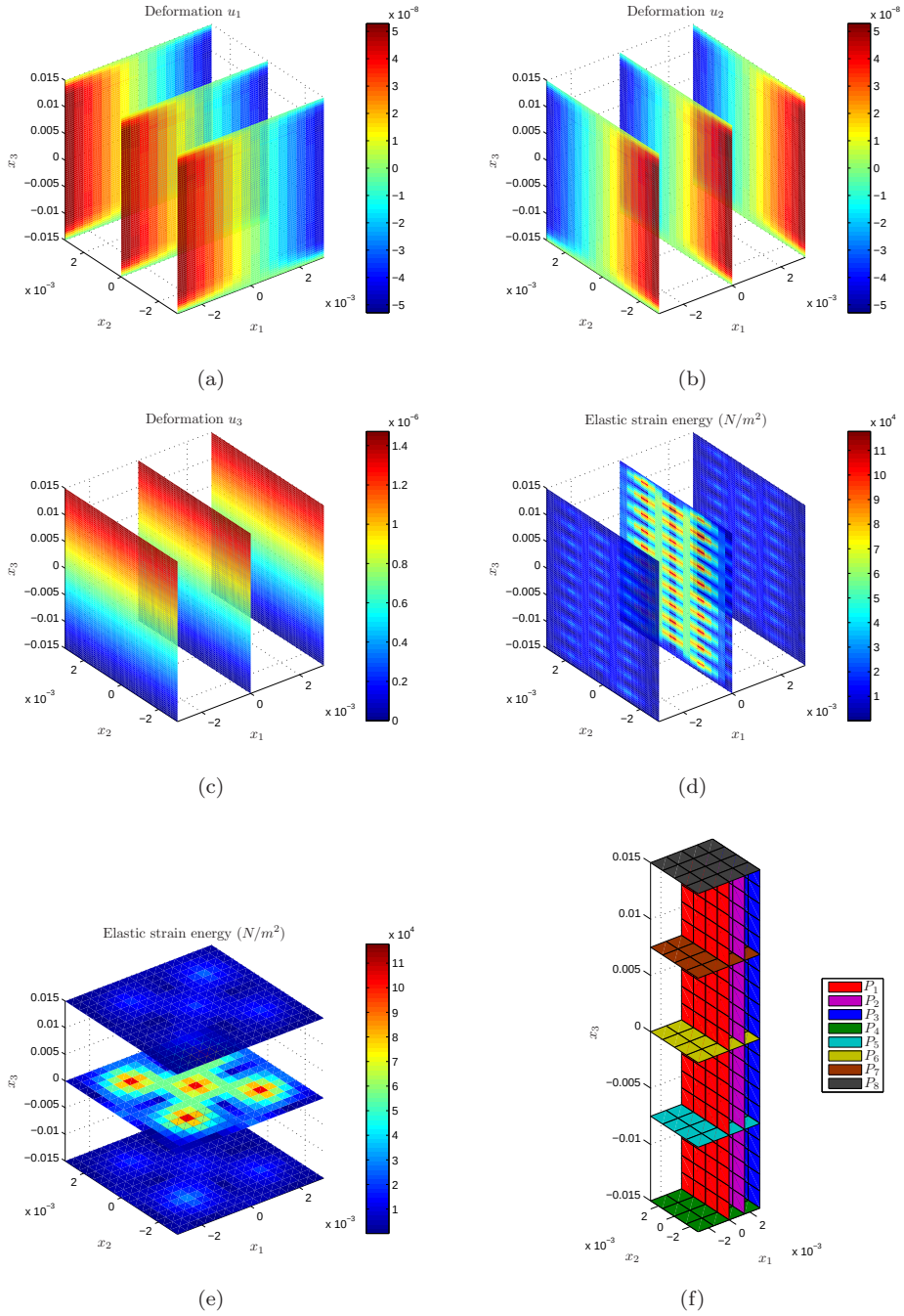

(a) (b) (c) (d) (e) (f)

Figure 6.10: (a)-(e): Initial deformations and energies under tensile test. (f): Planes used to depict results.

6.7 Cylindrical deformations

As with the one-dimensional tensile test, we will perform a similar simulation with the cylindrical model. Demanding no deformations at the boundary plane given by $z = 0$, a normal force exerted at the boundary plane given by $z = h$ and no radial deformations at this plane, with h the height of the cylinder, no radial deformations and no axial forces at $\eta = 0$ and a free boundary at all outer boundary planes, give the following boundary conditions:

$$\begin{aligned}
u_\eta(\eta, z) &= 0 && \forall(\eta, z) : \eta = 0 \vee z = 0 \vee z = h \\
u_z(\eta, z) &= 0 && \forall(\eta, z) : z = 0 \\
\underline{\underline{\boldsymbol{\sigma}}} \cdot \boldsymbol{n}\Big|_{(\eta,z)} &= \mathbf{0} && \forall(\eta, z) : \eta = \eta_{\max} \\
\underline{\underline{\boldsymbol{\sigma}}} \cdot \boldsymbol{n}\Big|_{(\eta,z)} &= [0, F]^T && \forall(\eta, z) : z = h \\
\underline{\underline{\boldsymbol{\sigma}}}_z \cdot \boldsymbol{n}\Big|_{(\eta,z)} &= 0 && \forall(\eta, z) : \eta = 0,
\end{aligned}$$

where F represents the force exerted on the top face of the bar. To ensure again elastic deformations a value for F has been chosen such that in each point the stress does not exceed the yield stress σ_Y. This value is:

$$F = 6 \times 10^6 \, \frac{N}{m^2}.$$

Using the above conditions, the results from the simulations can be found in Figures 6.11, B.21, 6.12 and 6.13. Figure 6.11 presents the deformation and resulting strain at the beginning of the simulation. Figure B.21 depicts the results for the various variables from the simulation with respect to time and Figures 6.12 and 6.13 depict the latter results as percent differences with the reference simulation.

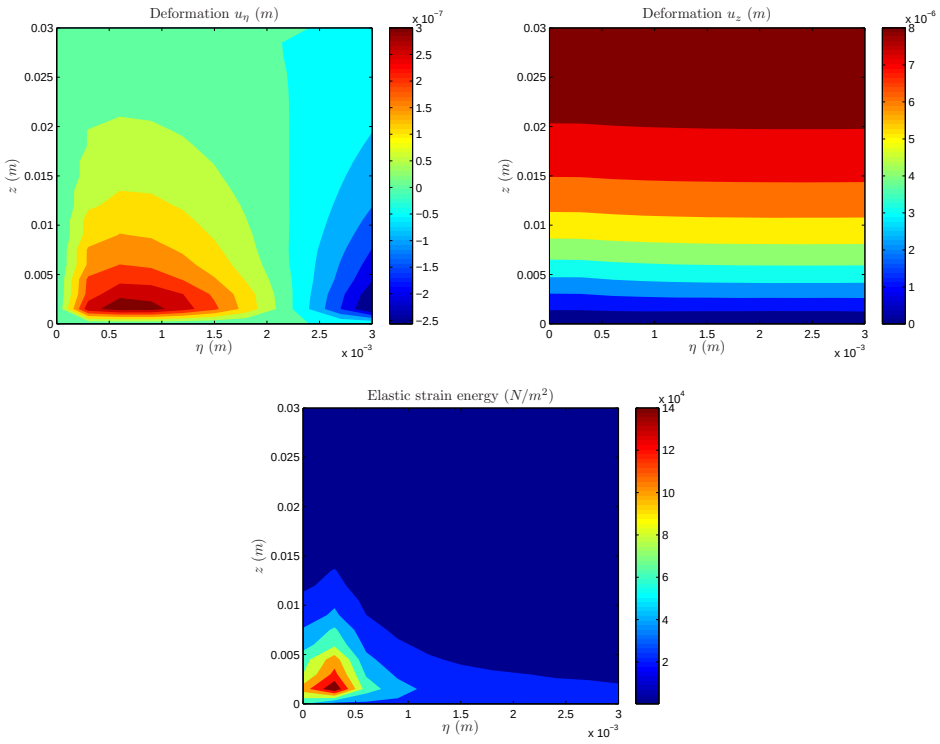

Figure 6.11: Initial deformations and energies under tensile test.

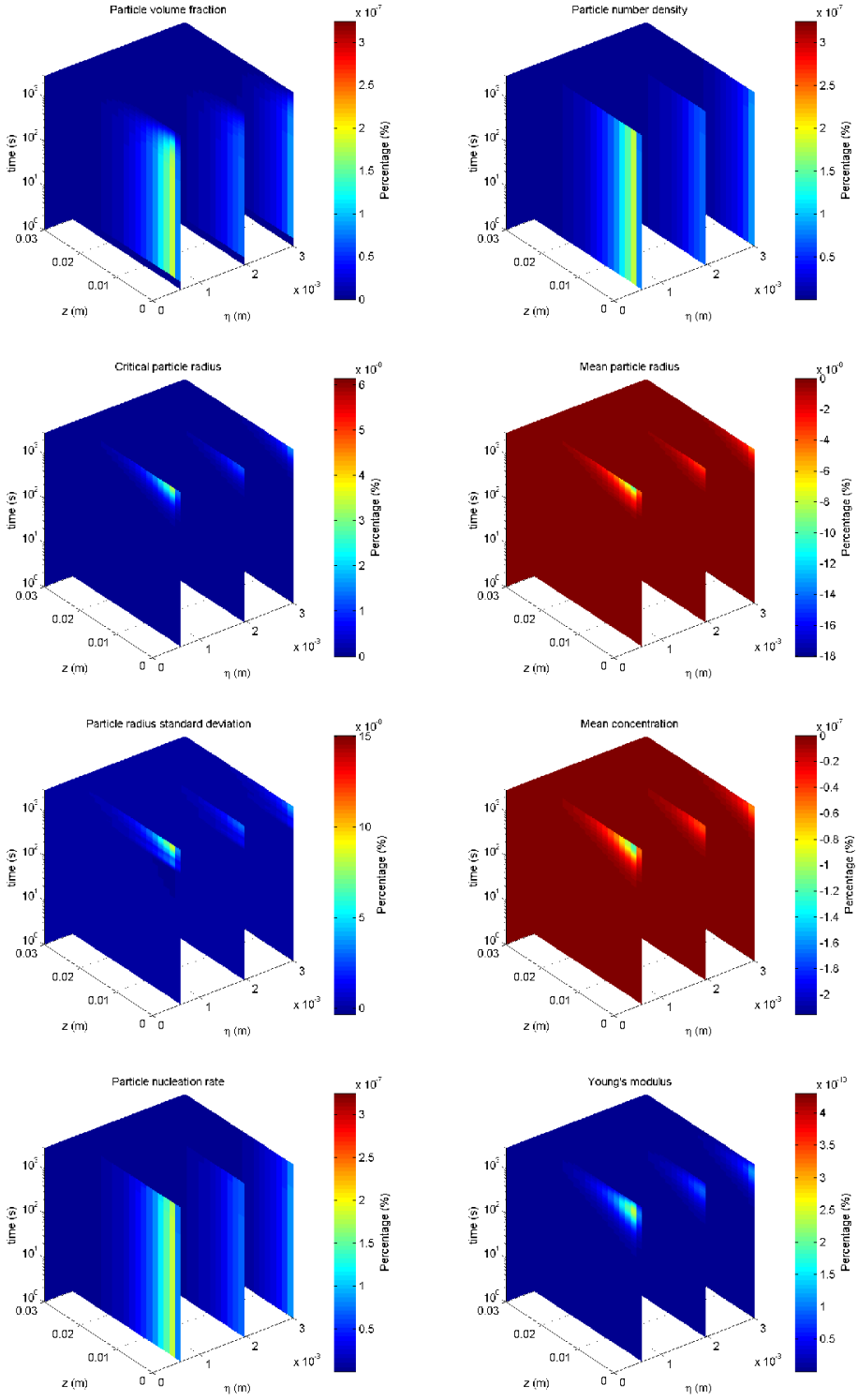

Figure 6.12: Percent differences under tensile test.

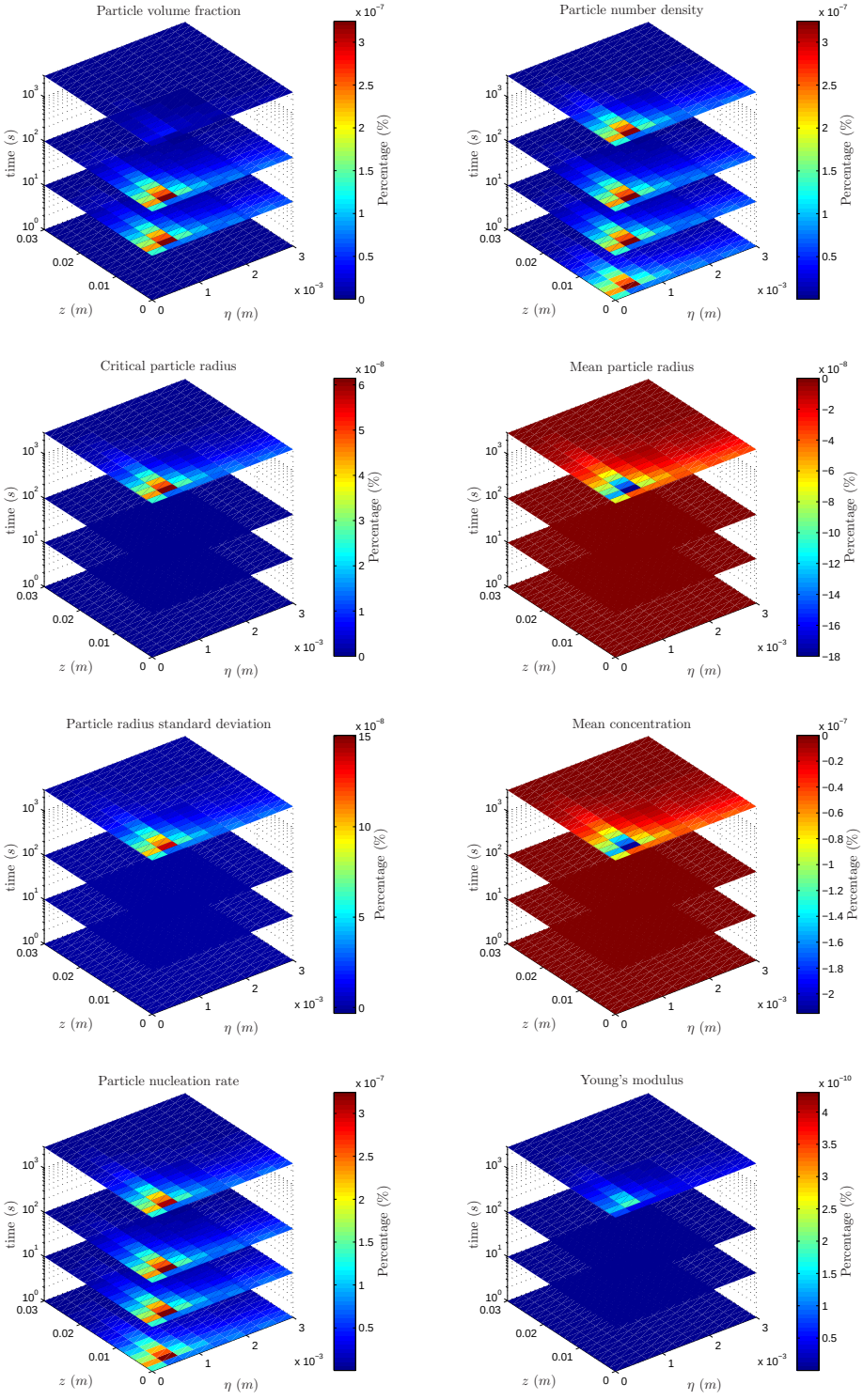

Figure 6.13: Percent differences under tensile test.

Figure B.21 shows that again the solution converges to the physical equilibrium. Figures 6.12 and 6.13 show that there are slight differences with the reference simulation, with the largest differences present at the location with the highest values of the elastic strain energy. This coincides with the results from the one-dimensional simulation and the preliminary results from three-dimensional simulations.

As with the one-dimensional simulation, the differences with the reference simulation are small. To investigate the influence of higher strains, we replace the force exerted at the top of the cylinder with its

thousandfold, for which the results can be found in Figures B.22, 6.14 and 6.15. The latter figures show that the percent differences with the reference simulation follow the shape of the elastic strain energy due to deformations. This indicates that the value of this variable can be used to predict other variables.

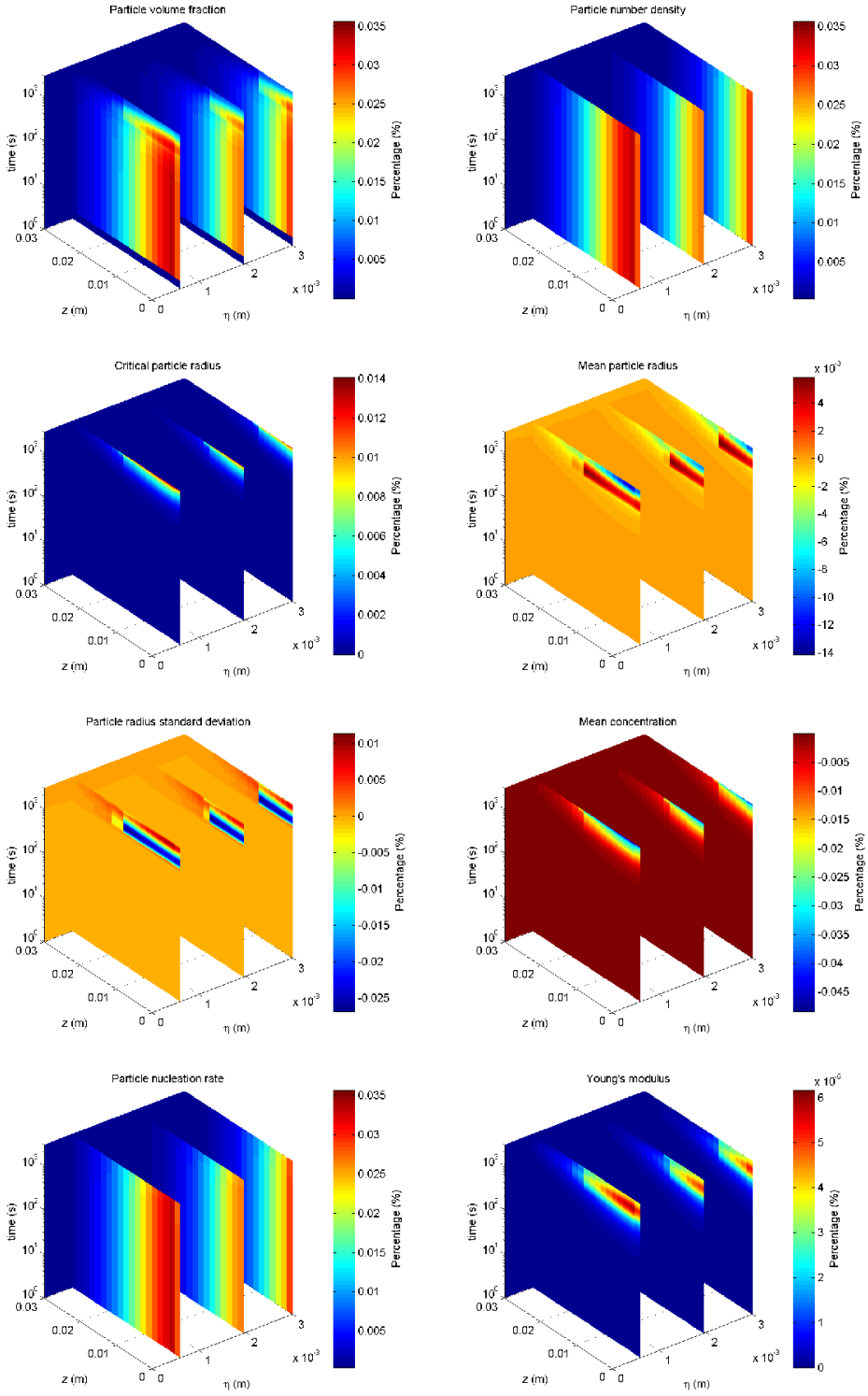

Figure 6.14: Percent differences under tensile test.

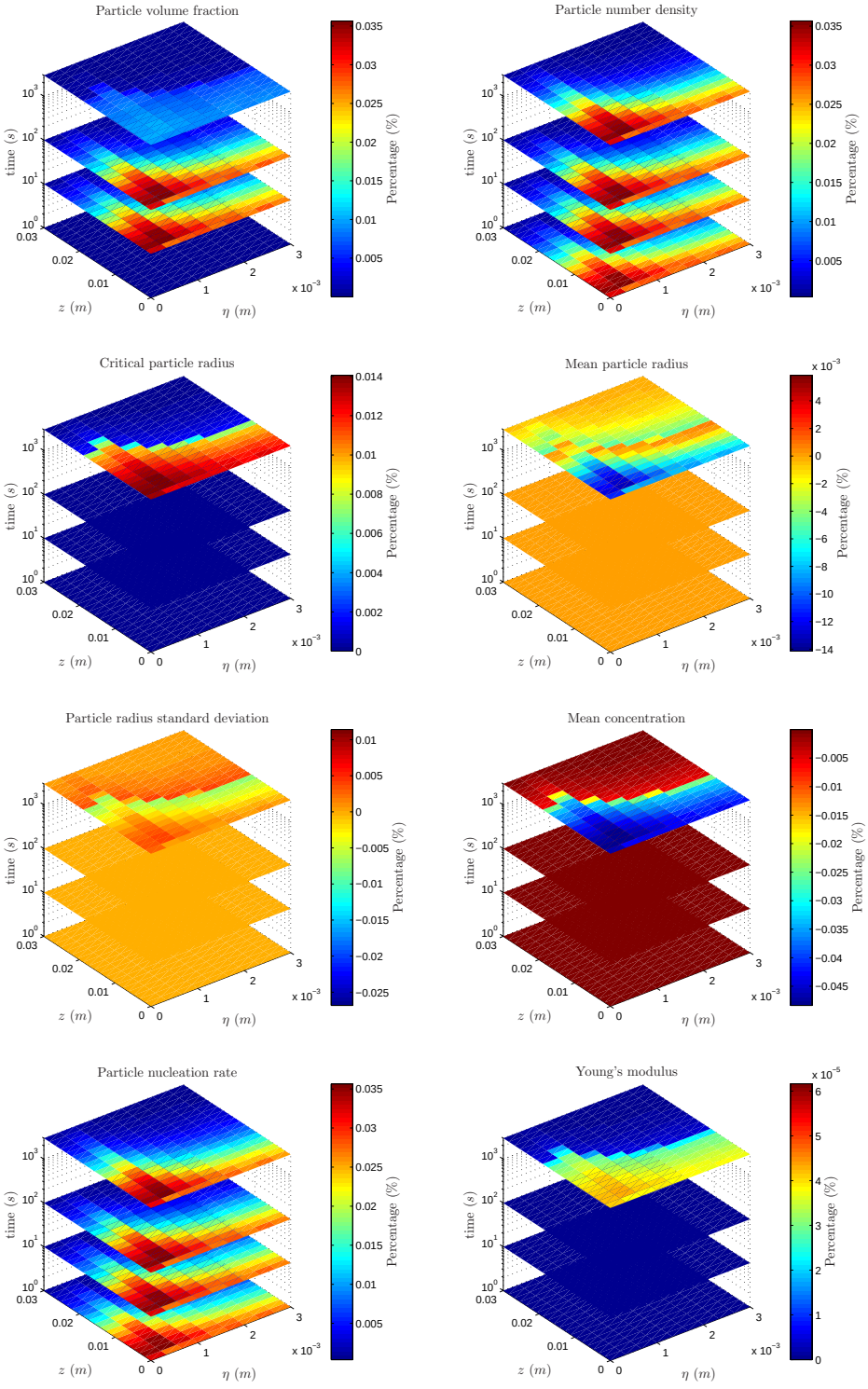

Figure 6.15: Percent differences under amplified tensile test.

6.8 Conclusions from simulations

During the previous sections various simulations with the proposed nucleation-deformation model are performed. The simulations under gravity (Section 6.4) indicate that the presence of gravity give rise to very low elastic strain energies, causing numerically no differences with simulations without the presence of gravity. Therefore the effect of gravity can be assumed to be insignificant and therefore needs not to be modeled.

The subsequent simulations with the one-dimensional, three-dimensional and cylindrical model indicate that applying a tensile force to an system causes extra nucleation of particles, due to a lower heterogeneous nucleation energy barrier. This causes in turn a higher nucleation rate, which influences the overall nucleation model. With stresses in the elastic region of the material simulated the resulting elastic strain energy causes percent differences of an maximum order of 10^{-7} percent in all variables. Increasing the applied tensile force to its thousandfold to ensure stresses outside the region of elasticity causes higher differences, which are of an maximum order of 10^{-2}. This indicates that if the tensile force is multiplied with a factor 10^n, all percent differences can be expected to increase with at most a factor 10^{2n}.

The results from the simulations indicate that the proposed model describes the influences of elastic deformations on the nucleation process to a fair extent, but no conclusions can be made on the physical correctness of these results, as no comparison with experimental results of tensile tests has been performed.

Chapter 7

Summary and future work

7.1 Summary

During this master thesis we have compared two models for nucleation and growth of particles in metallic alloys, the first proposed by Myhr and Grong (2000), the second by Robson et al. (2003). The comparison has been based on the numerical simulation of the nucleation and growth of Mg_2Si particles inside a block of the aluminum alloy AA 6082. The results indicated that both models had different merits and drawbacks. Using the found merits and drawbacks of both models, we formulated a new model for the nucleation and growth of particles. This model has been based on the model by Myhr and Grong (2000) and adapted using the properties of the model by Robson et al. (2003), such as the incorporation of the correct chemical volume free energy and possible elastic misfit strain energy between a particle and the matrix.

Thereafter three models were derived which describe the elastic deformations inside a material due to external and internal forces. The first model assumes only deformations in one principle direction, leading to a one-dimensional model. Second a model was derived assuming all principle directions play an important role in elastic deformations, resulting in a three-dimensional model. The last model describes elastic deformations on the assumption of circle symmetry, which led to a two-dimensional model. From the solution of these models the value of the elastic strain energy density can be found at any point in the material.

As this master thesis had as goal to model the influence of elastic deformations on the nucleation and growth of particles in a metallic alloy, two relations between the derived model for nucleation and growth of particles and the models for elastic deformations were proposed. The first relation consisted of incorporating the presence of the elastic strain energy density in the formula for the particle nucleation rate. As the particles present in the system can also influence the elastic behavior of the material, the second relation proposed formulas for the elastic parameters used in the model which describe the influence of the particle volume fraction on these parameters.

After all four models and the proposed relations between these models has been formulated, these models have been discretized using various numerical methods. On the model for nucleation and growth of particles a first order upwind method in combination with a theoretical first order IMEX θ-method was applied, whereas the models for elastic deformation was discretized using linear finite element techniques. After discretization the found linear systems are implemented in MATLAB.

The results from simulations with the combined models indicated that, first of all, that the influence of gravitational body forces on the nucleation process can be neglected. Further results from the one-dimensional model and the cylindrical model and the preliminary results from the three-dimensional model of tensile testing indicate that the incorporation of elastic strain energy due to deformations influences the nucleation process to some extend. Increasing the elastic deformations and the corresponding elastic strain energy showed that higher levels of strain energy cause higher differences in comparison with nucleation under absent deformations.

The derivation, discretization and simulation of the model which connects elastic deformations with the process of nucleation and growth of show that this model can predict the influence of elastic deformations on the nucleation process and can therefore be used to form a starting point for other models, such as the influences of plastic deformations on the nucleation process.

7.2 Recommended future work

Although various results are obtained from the proposed model, improvements and further studies can be suggested. Possible improvements for the proposed model include:

- Extending the model for nucleation and growth to model more than one particle configuration.
- Adapting the model such that it can model other alloys than AA 6082, as the parameters A_0 and j_0 are only known at present for the alloy AA 6082. This can possibly be done by using the nucleation rate formula of Robson et al. (2003) instead of the formula proposed by Myhr and Grong (2000).
- Improving the implementation of the linear equations resulting from numerical techniques applied to the models. Solution are possibly in the range of faster algorithms to compute the solutions, based on the properties of linear equations.
- Comparing the found numerical data with experimental data, to ensure correct physical behavior of the model.

Subjects that can be further studied are:

- Modeling the influence of plastic deformations on the process of nucleation and growth of particles.
- Combining the model for heterogeneous nucleation with models for the homogeneous nucleation and growth of particles.
- Combining the model with models for determining the grains inside a material, thereby increasing the physical correctness of the models.

Appendix A

Eigenvalues

Let the matrix A^n be defined as in Section 5.1 and denote by Ω^* the numerical interval with interval number i^* in which r^* at time t^n lies. The region on which the discretization is applied can now be divided into three sets:

Set 1: All Ω_i with $i < i^*$;

Set 2: Ω^*;

Set 3: All Ω_i with $i > i^*$.

Now choose any interval Ω_i from set 1, with the corresponding radius r_i and velocities $v^n_{i-1/2}$ and $v^n_{i+1/2}$. Using the definition of the critical radius r^* we can see that both velocities are negative. The row of the matrix A^n corresponding to Ω_i contains at most three nonzero entries. These entries are

$$\begin{aligned} A^n_{ii} &= -((v^n_{i-1/2})^- + (v^n_{i+1/2})^+) \\ A^n_{i,i-1} &= (v^n_{i-1/2})^+ \\ A^n_{i,i+1} &= (v^n_{i+1/2})^-, \end{aligned}$$

which give, using the velocities

$$\begin{aligned} A^n_{ii} &= v^n_{i-1/2} \\ A^n_{i,i-1} &= 0 \\ A^n_{i,i+1} &= -v^n_{i+1/2}. \end{aligned}$$

The above indicates that for each row $i < i^*$ of the matrix A^n only the main diagonal and the upper diagonal are present.

Now choose any interval Ω_i from set 3, with the corresponding radius r_i and velocities $v^n_{i-1/2}$ and $v^n_{i+1/2}$. Using the definition of the critical radius r^* we can see that both velocities are positive. The row of the matrix A^n corresponding to Ω_i contains at most three nonzero entries. These entries are

$$\begin{aligned} A^n_{ii} &= -((v^n_{i-1/2})^- + (v^n_{i+1/2})^+) \\ A^n_{i,i-1} &= (v^n_{i-1/2})^+ \\ A^n_{i,i+1} &= (v^n_{i+1/2})^-, \end{aligned}$$

which give, using the velocities

$$\begin{aligned} A^n_{ii} &= -v^n_{i+1/2} \\ A^n_{i,i-1} &= v^n_{i-1/2} \\ A^n_{i,i+1} &= 0. \end{aligned}$$

The above indicates that for each row $i > i^*$ of the matrix A^n only the main diagonal and the lower diagonal entries are present.

Now choose the interval Ω^* from set 2, with the corresponding radius r_{i^*} and velocities $v^n_{i^*-1/2}$ and $v^n_{i^*+1/2}$. As the radius $r_{i^*-1/2}$ is smaller than r^*, we have that $v^n_{i^*-1/2}$ is negative. As the radius $r_{i^*+1/2}$ is larger than r^*, we have that $v^n_{i^*+1/2}$ is positive. The row of the matrix A^n corresponding to Ω^* contains at most three nonzero entries. These entries are

$$\begin{aligned} A^n_{i^*i^*} &= -((v^n_{i^*-1/2})^- + (v^n_{i^*+1/2})^+) \\ A^n_{i^*,i^*-1} &= (v^n_{i^*-1/2})^+ \\ A^n_{i^*,i^*+1} &= (v^n_{i^*+1/2})^-, \end{aligned}$$

which give, using the velocities

$$\begin{aligned} A^n_{i^*i^*} &= v^n_{i^*-1/2} - v^n_{i^*+1/2} \\ A^n_{i^*,i^*-1} &= 0 \\ A^n_{i^*,i^*+1} &= 0. \end{aligned}$$

The above indicates that for row i^* of the matrix A^n only the main diagonal entry is present. Assessing the sign of the main diagonal entries, we see that in all cases these entries have a negative sign.

The above discussion of the properties of the matrix A^n shows that A^n is of the form

$$\begin{pmatrix} U & \emptyset \\ S & L \end{pmatrix},$$

where U is an $i^* \times i^*$-matrix, $\emptyset$ is the $i^* \times N - i^* - 1$-matrix filled with zeros, S is an $N - i^* \times i^*$-matrix and L is an $N - i^* \times N - i^*$-matrix. U contains only the main and upper diagonals, where L only contains the main and lower diagonal. The matrix S contains one nonzero entry at the most upper right location. Now let I_k be the $k \times k$-identity matrix. Then the characteristic polynomial of A^n is given by

$$\begin{vmatrix} U - \lambda I_{i^*} & \emptyset \\ S & L - \lambda I_{N-i^*} \end{vmatrix} = \left|U - \lambda I_{i^*}\right| \cdot \left|L - \lambda I_{N-i^*}\right|.$$

The eigenvalues of A^n can now be found by finding the eigenvalues of U and L, using the above identity. These eigenvalues are the diagonal entries of U and L, and a a result the eigenvalues of A^n are it's diagonal entries. To conclude, we have found that the eigenvalues of A^n are positive.

Appendix B

Figures

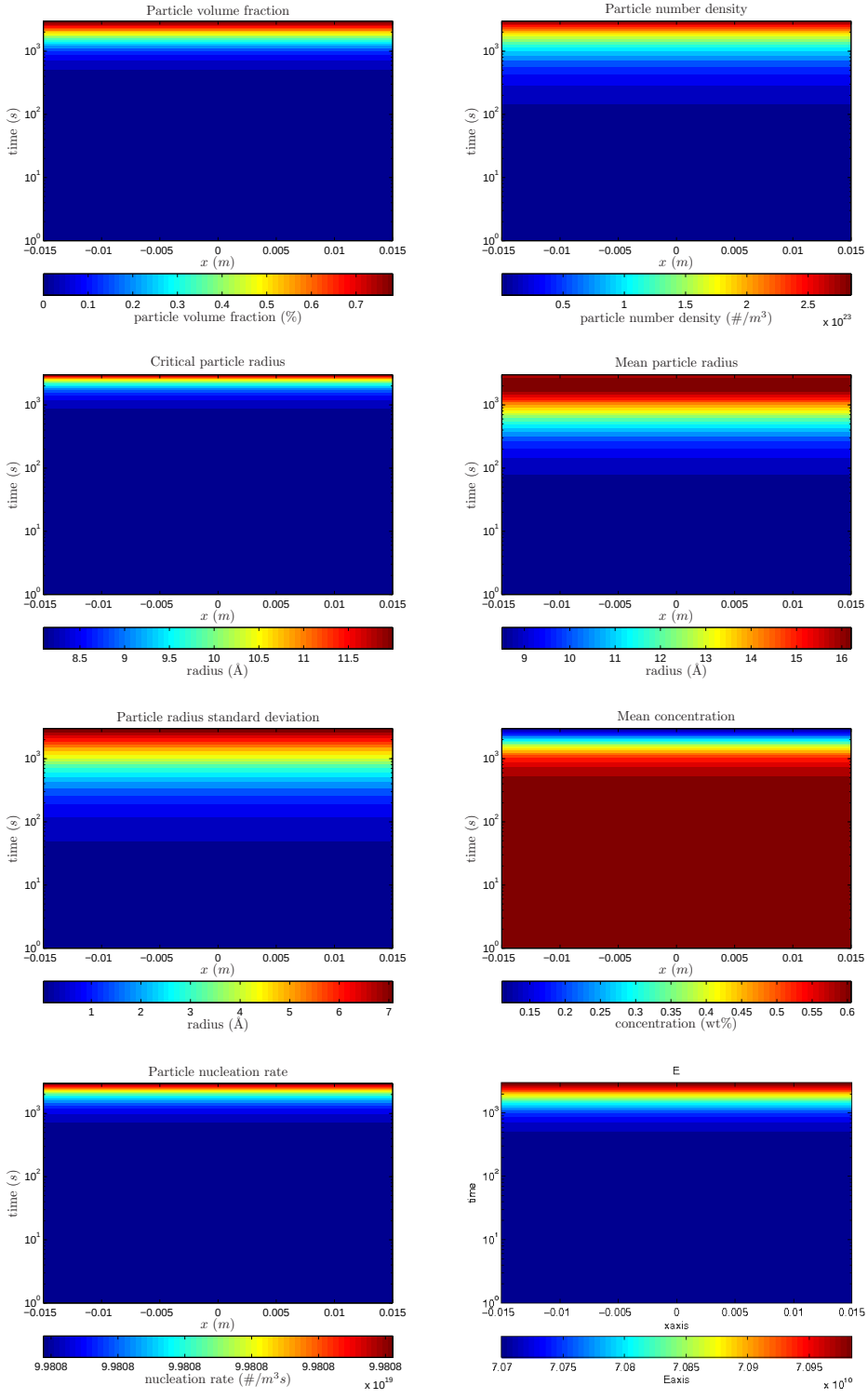

Figure B.1: Results from Section 6.4 under normal gravity.

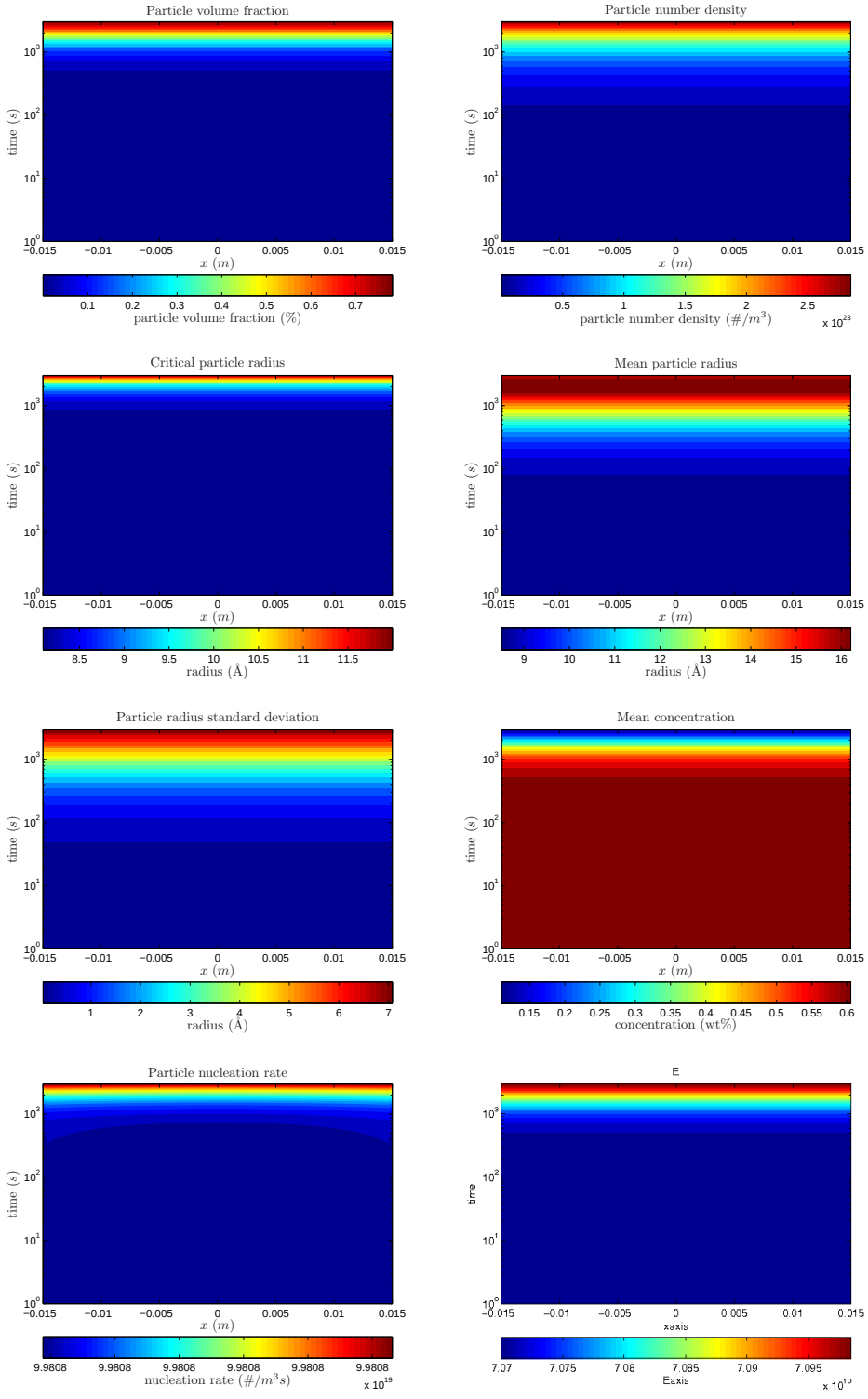

Figure B.2: Results from Section 6.4 under amplified gravity.

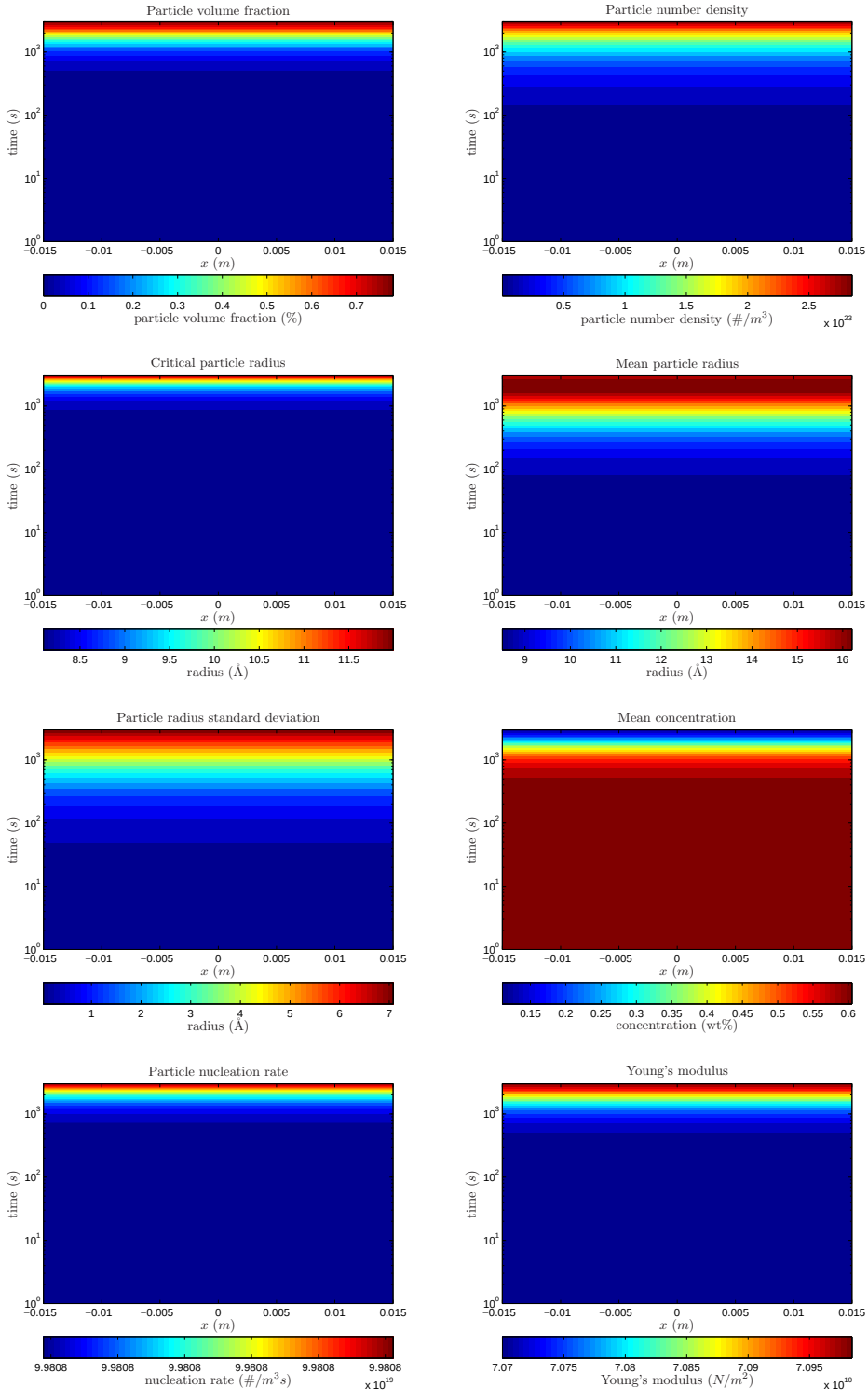

Figure B.3: Results under tensile test.

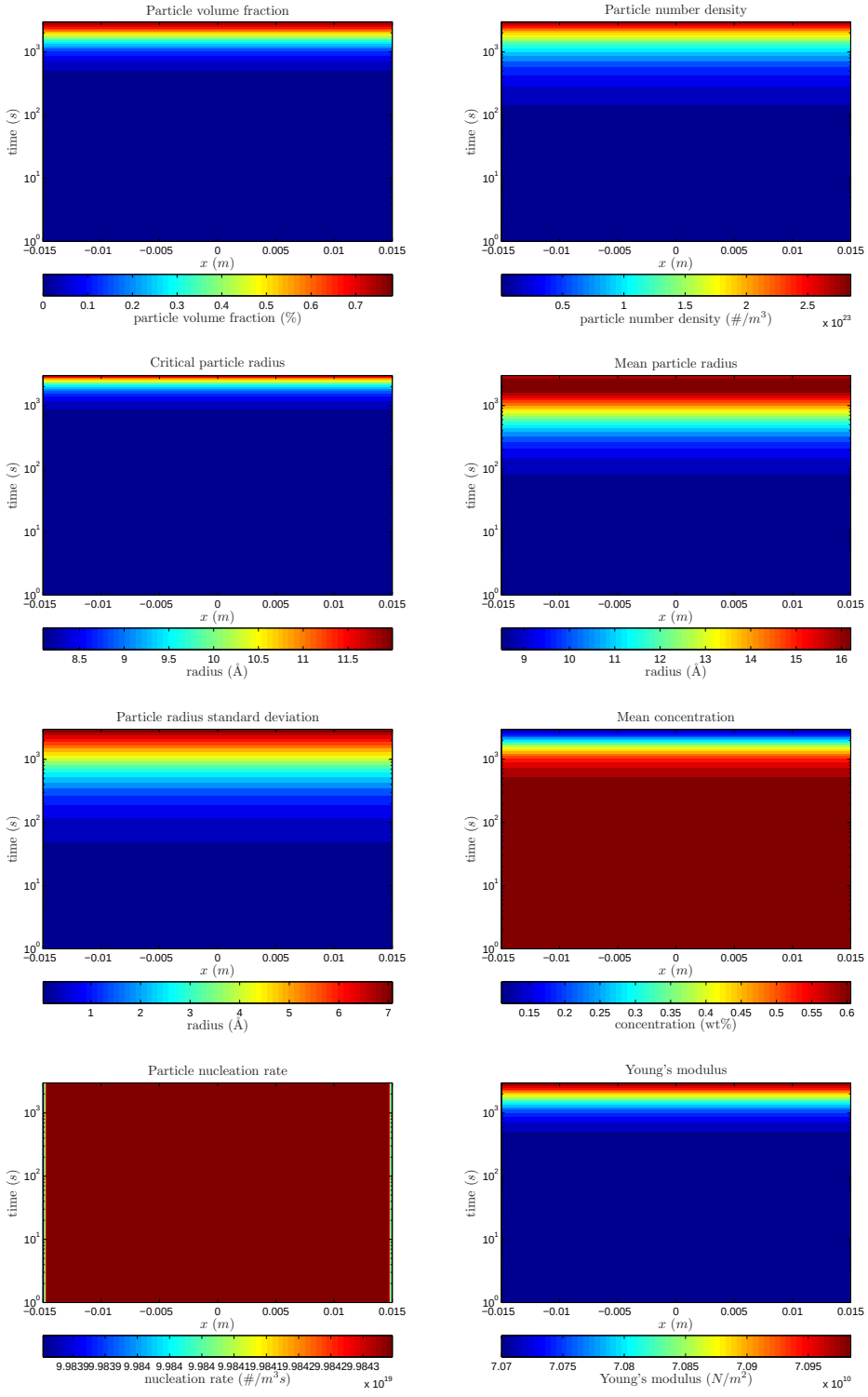

Figure B.4: Results under amplified tensile test.

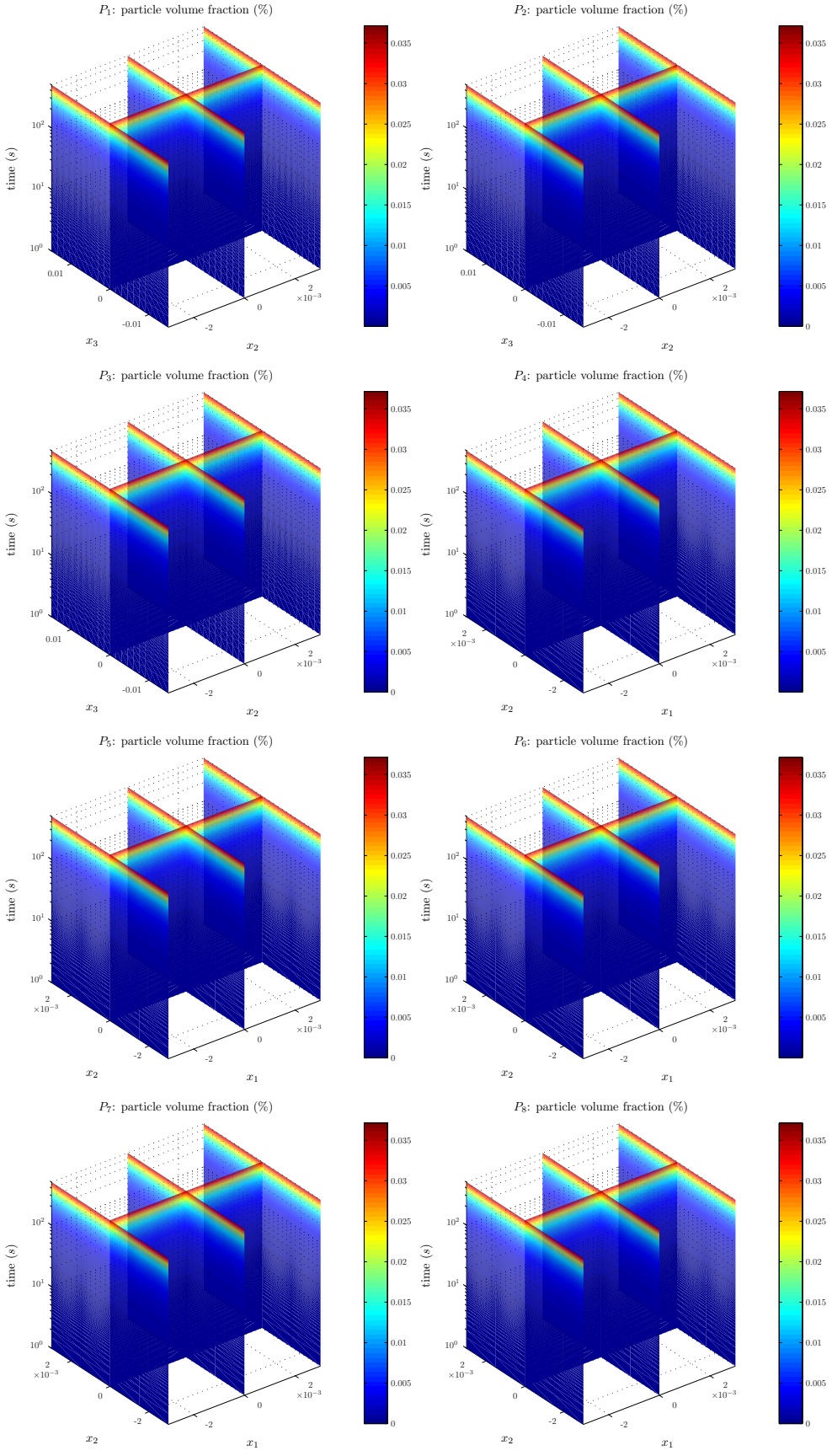

Figure B.5: Results under tensile test of the particle volume fraction.

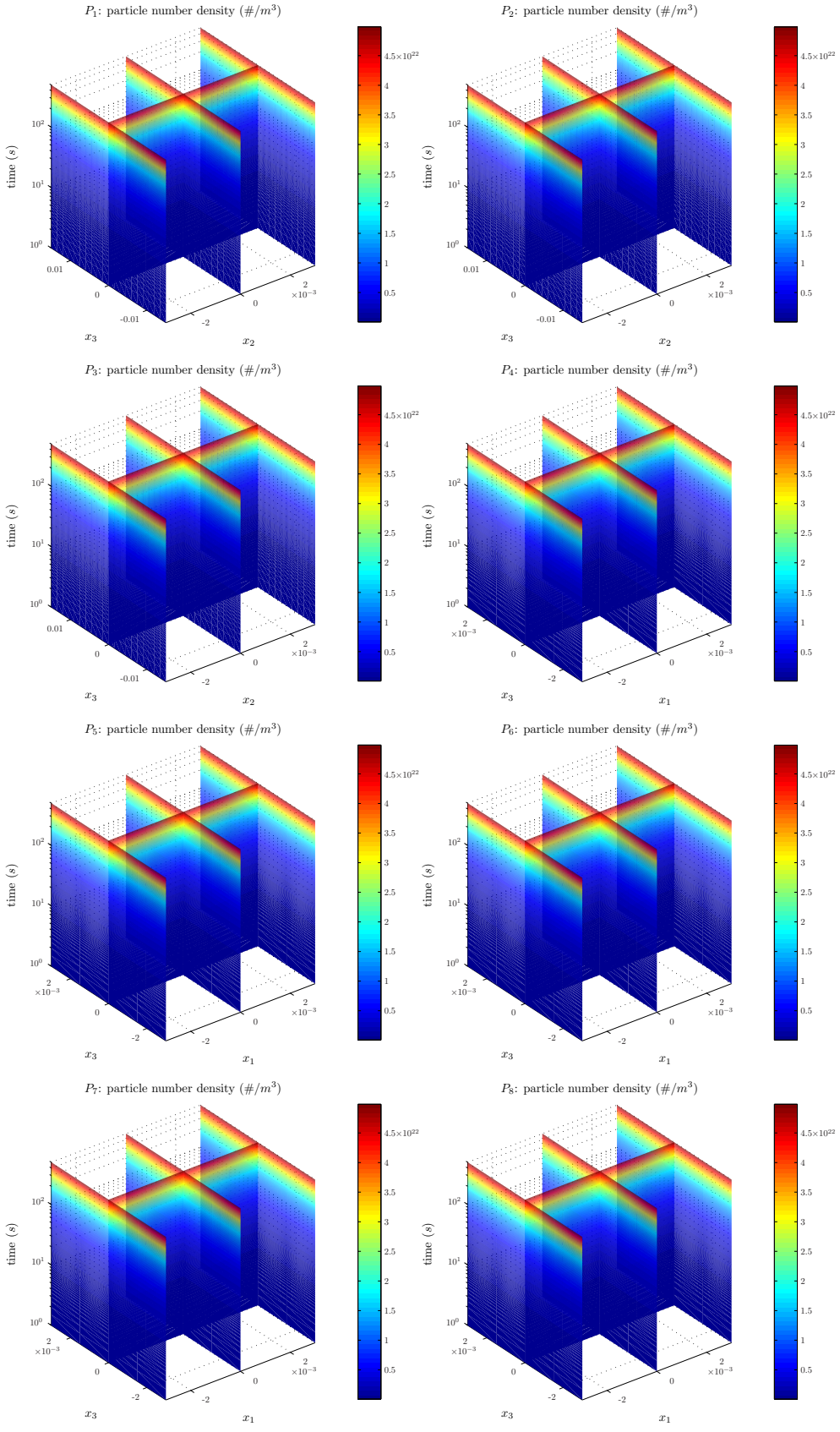

Figure B.6: Results under tensile test of the particle density.

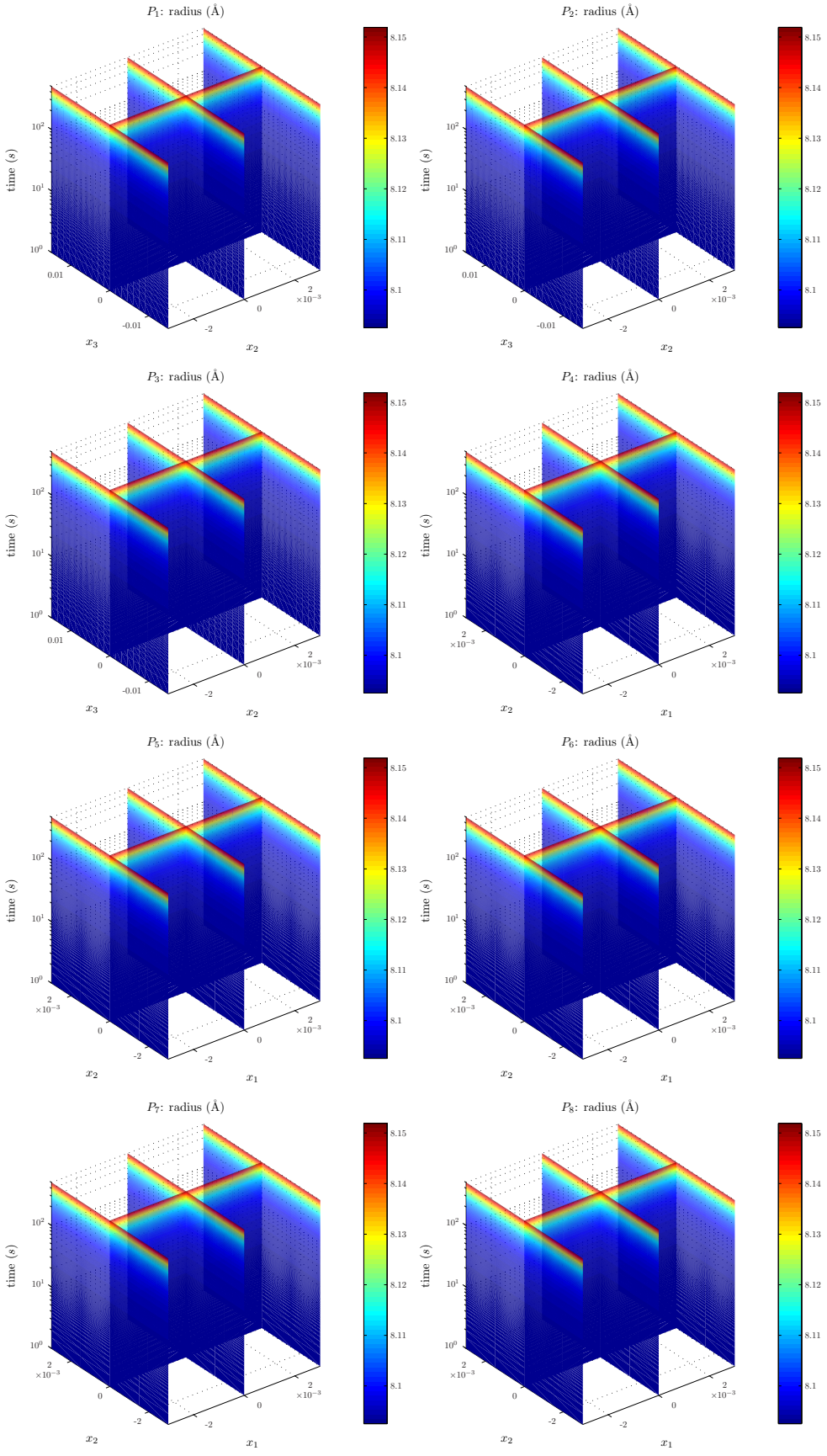

Figure B.7: Results under tensile test of the critical particle radius.

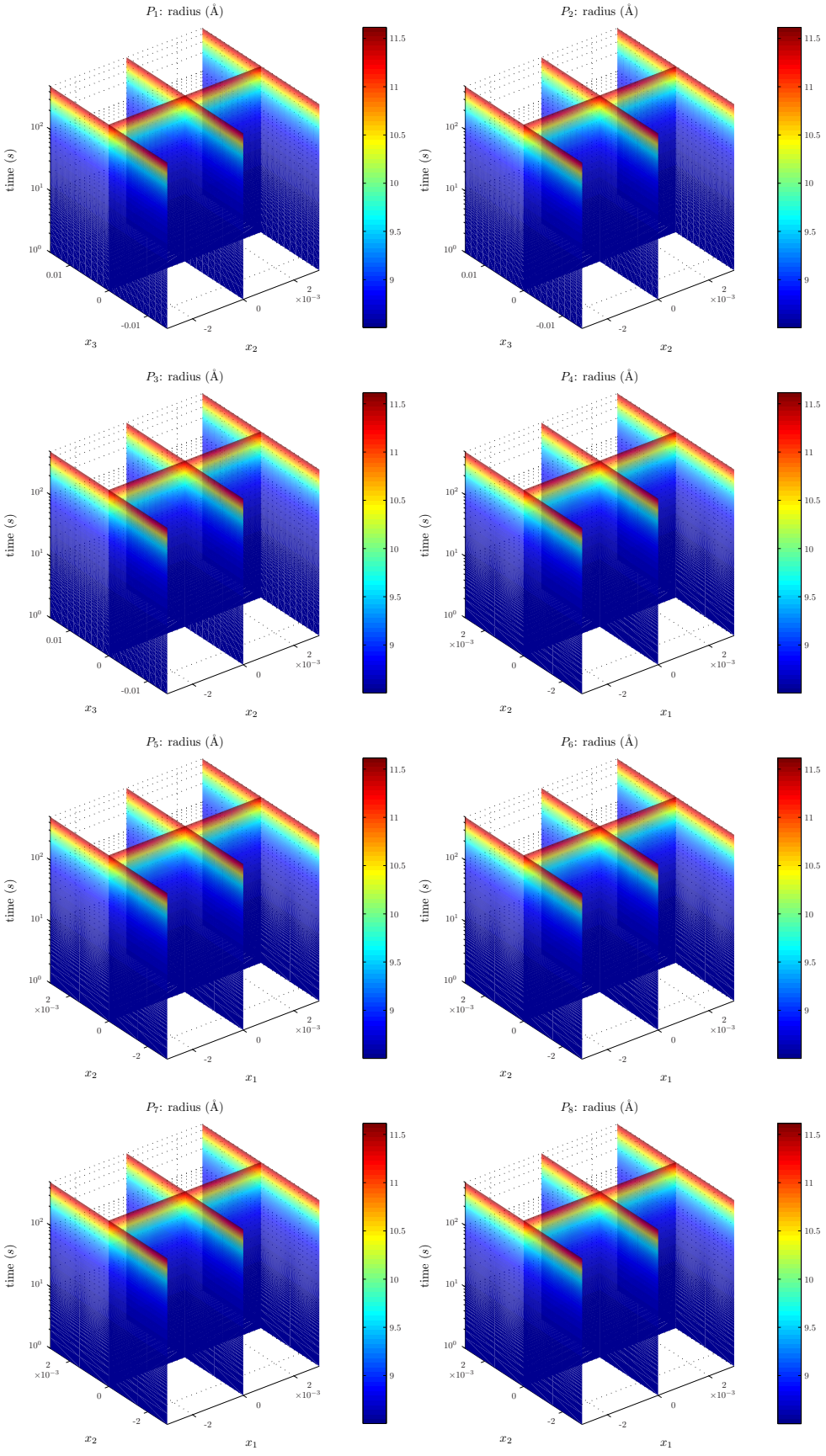

Figure B.8: Results under tensile test of the mean particle radius.

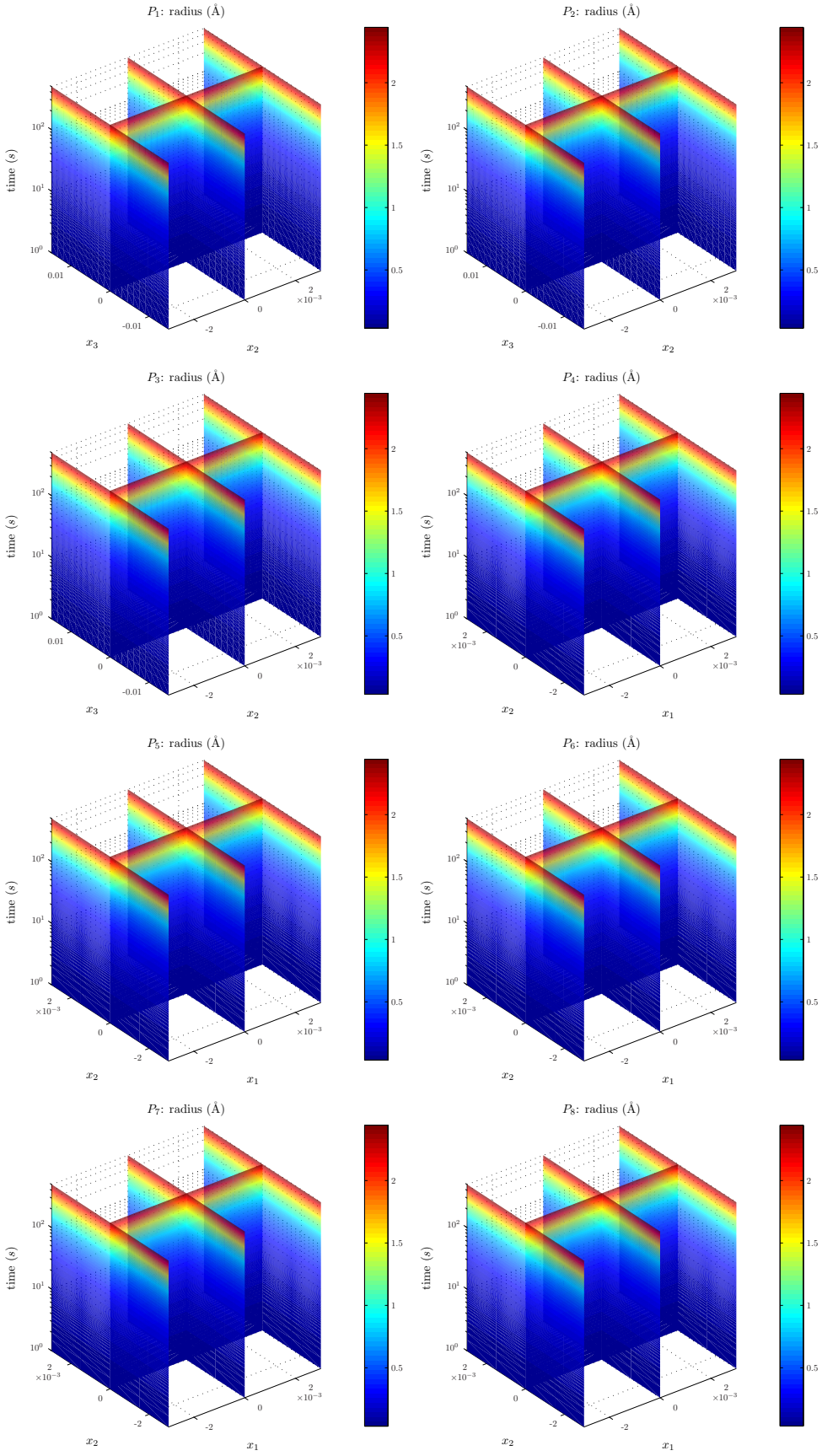

Figure B.9: Results under tensile test of the particle standard deviation.

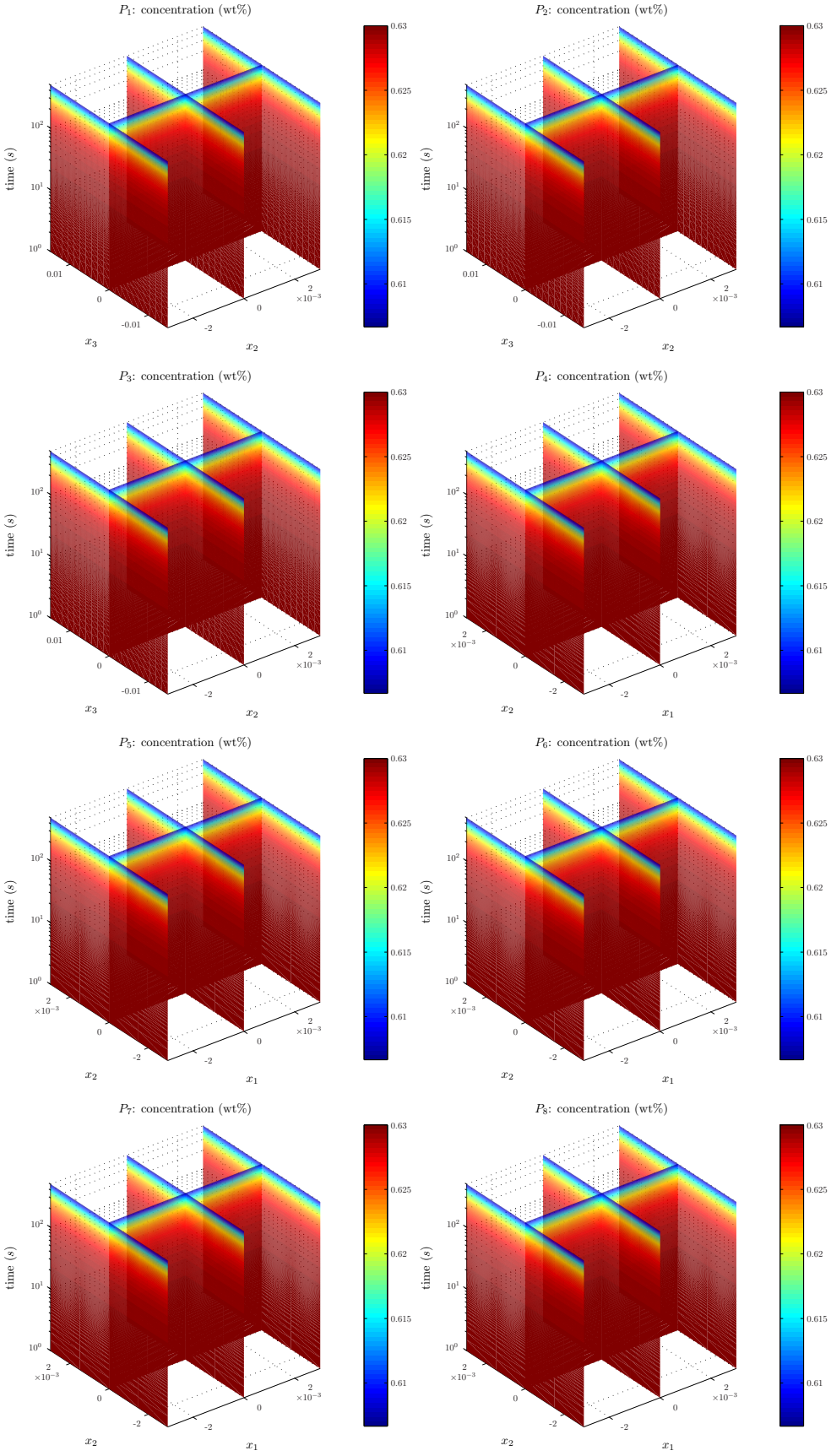

Figure B.10: Results under tensile test of the mean concentration.

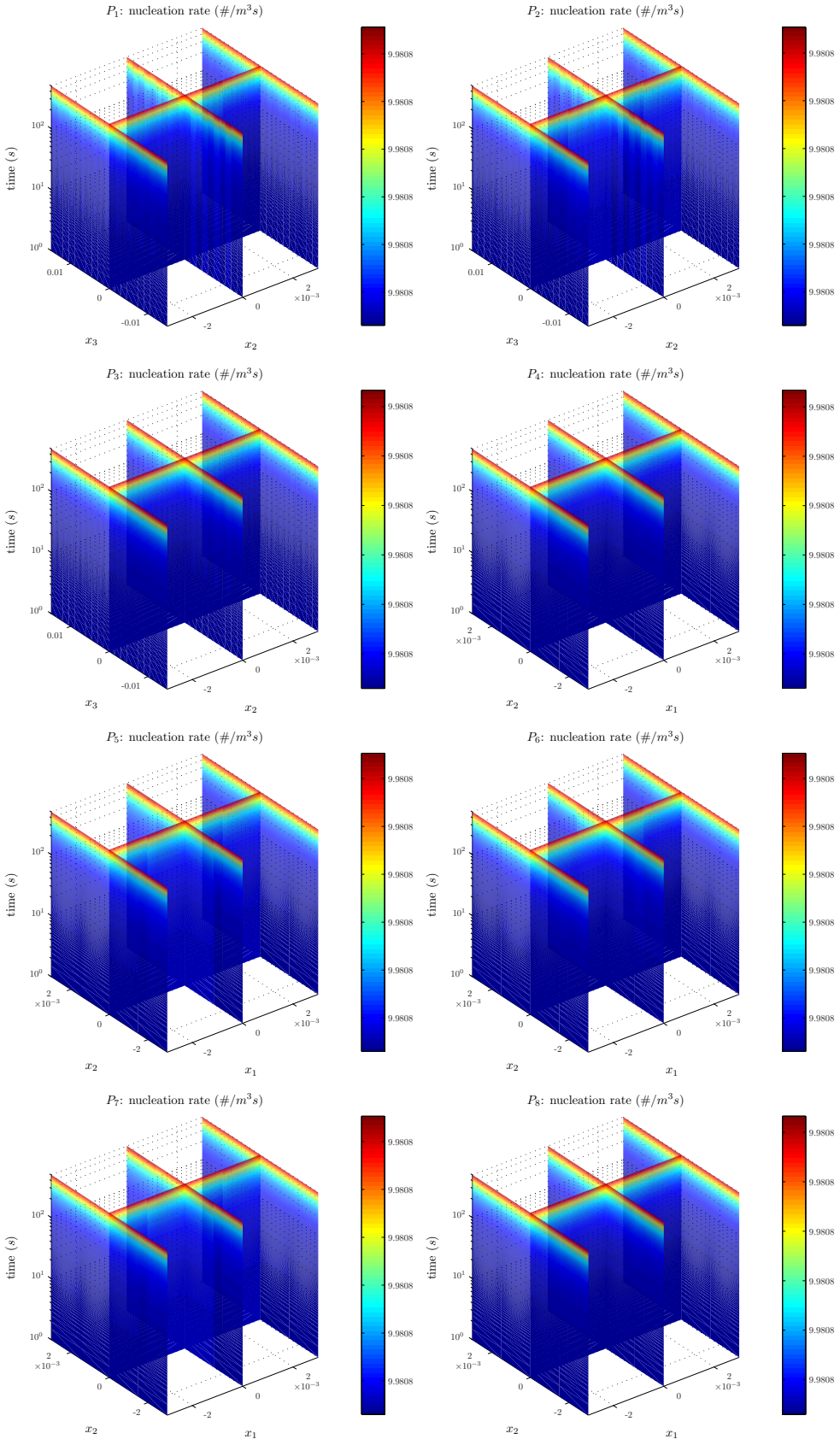

Figure B.11: Results under tensile test of the nucleation rate.

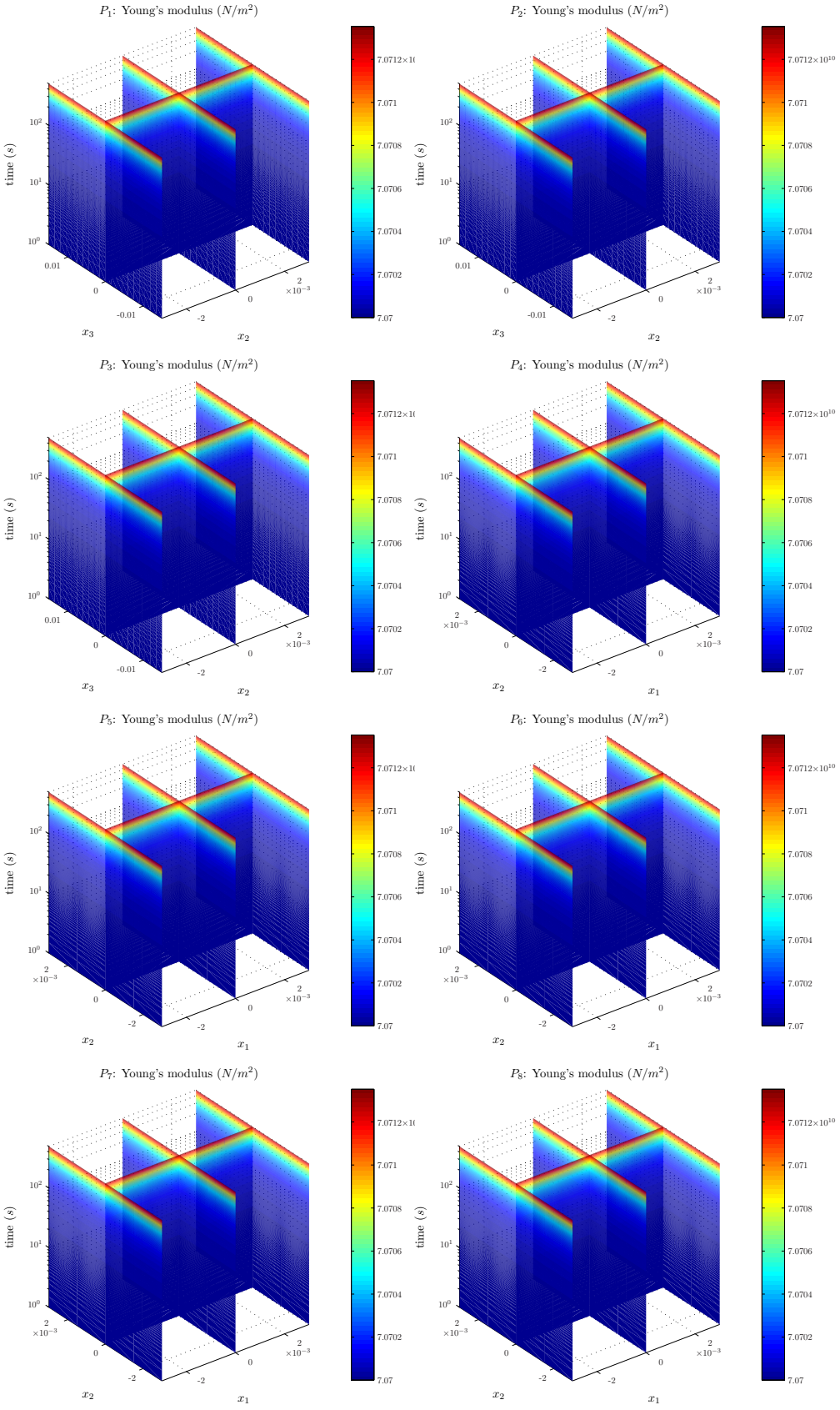

Figure B.12: Results under tensile test of the Young's modulus.

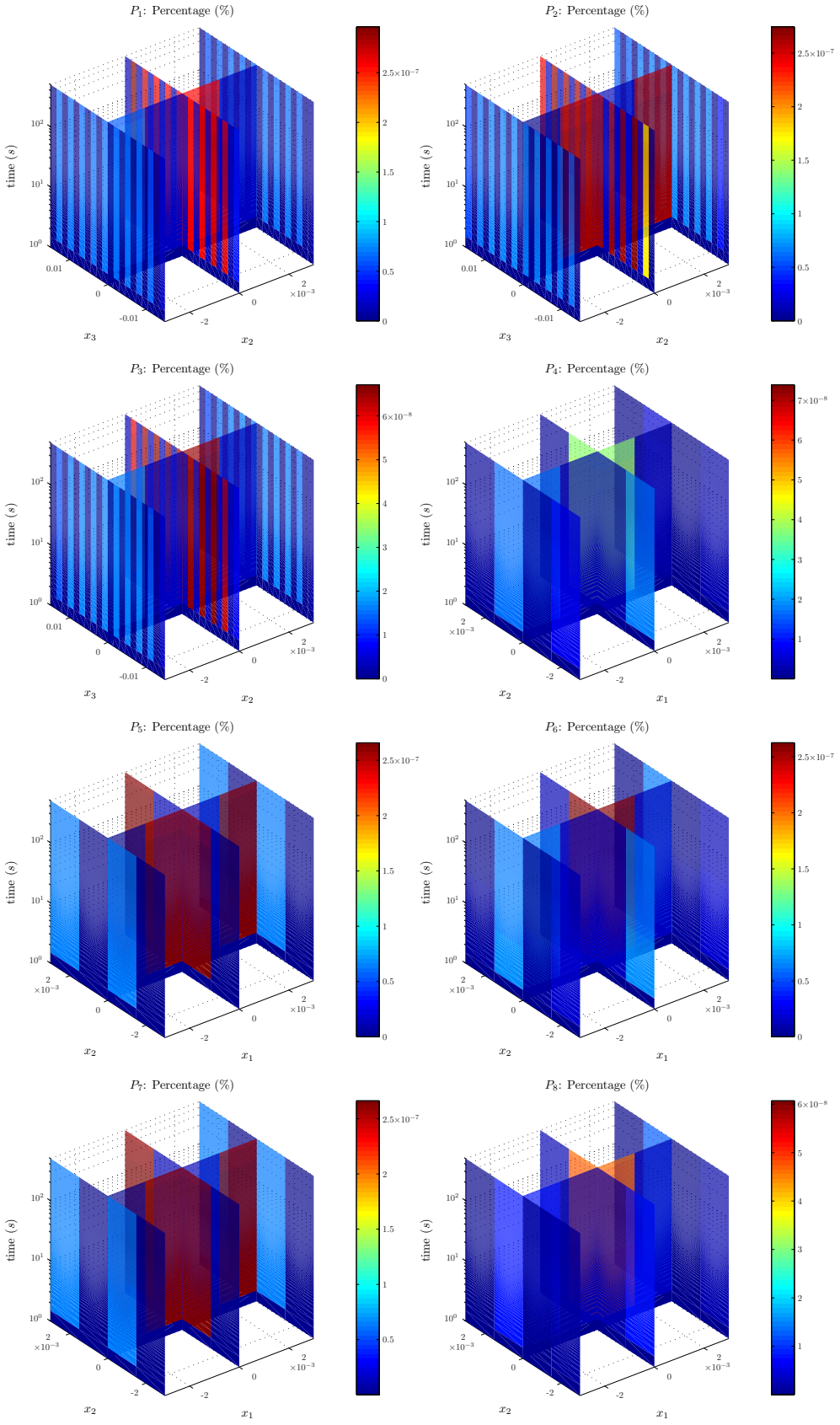

Figure B.13: Percent differences under tensile test of the particle volume fraction.

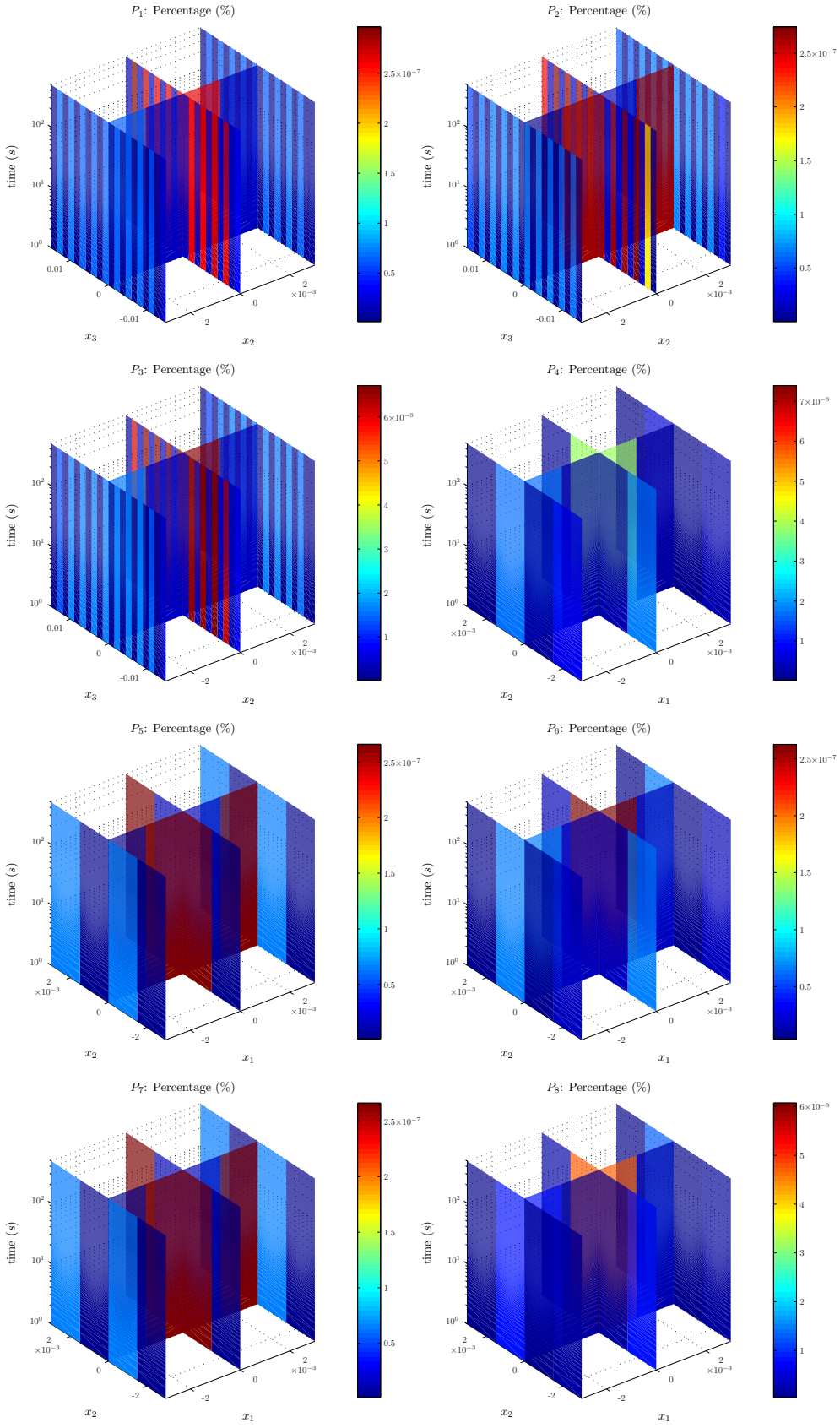

Figure B.14: Percent differences under tensile test of the particle density.

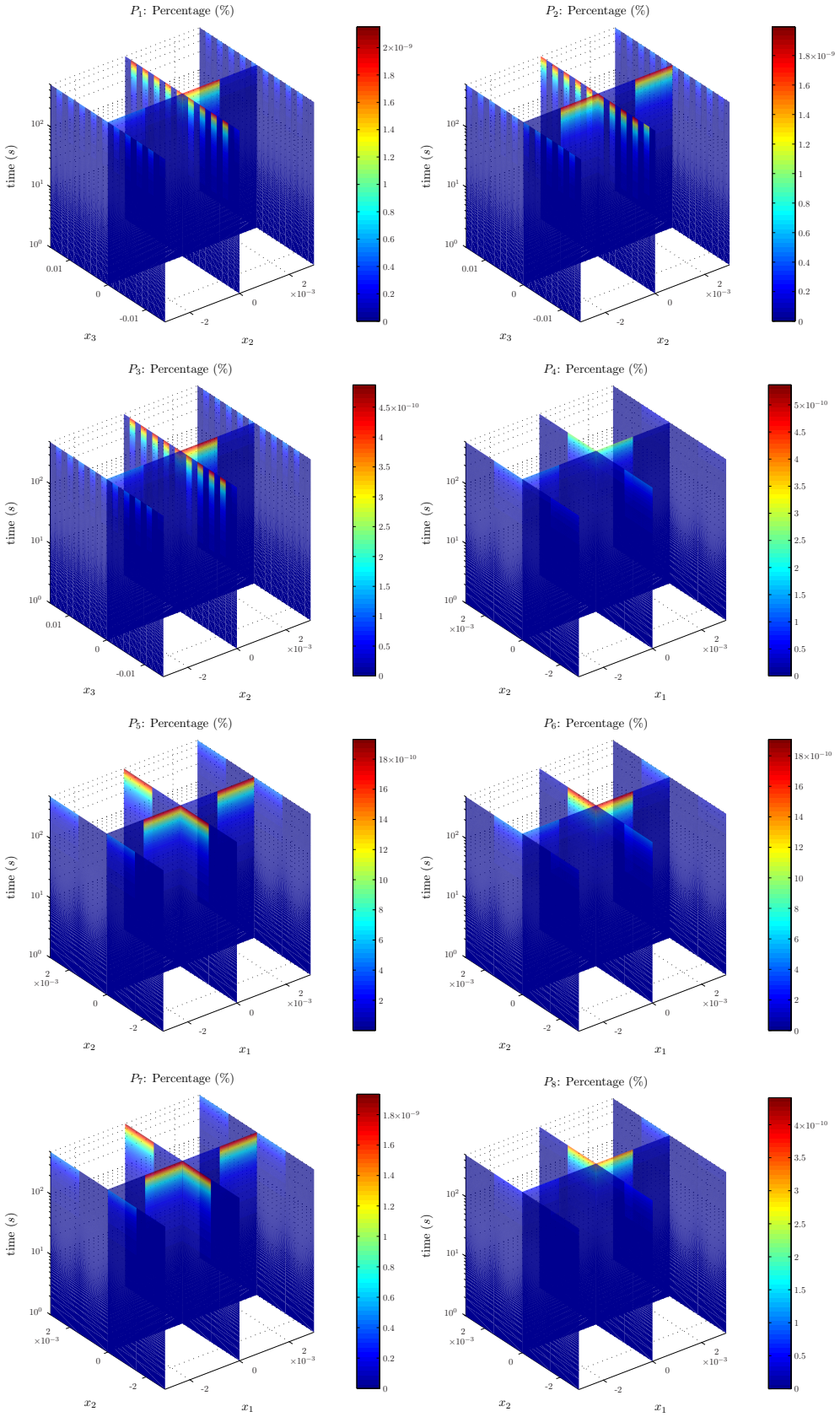

Figure B.15: Percent differences under tensile test of the critical particle radius.

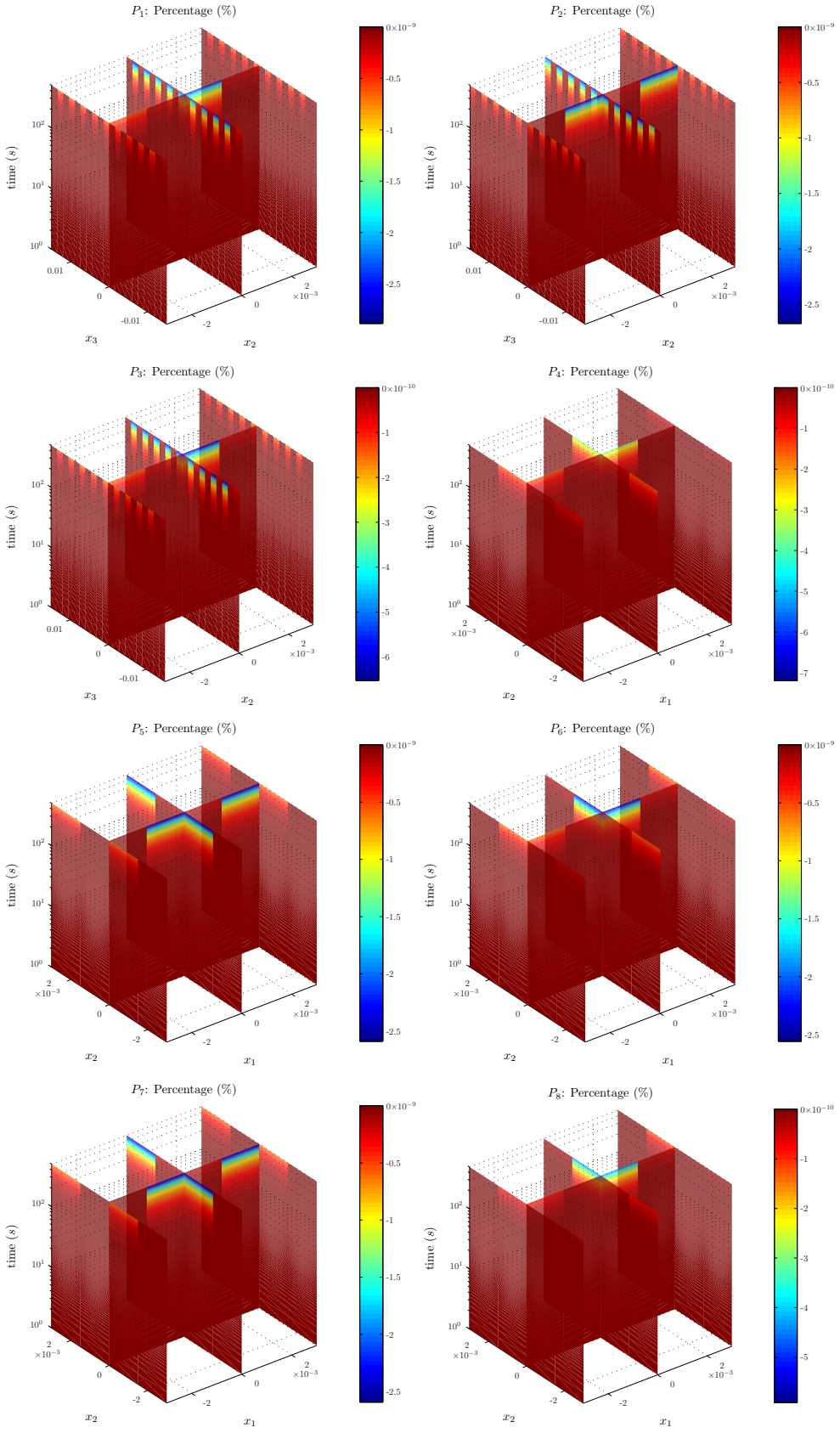

Figure B.16: Percent differences under tensile test of the mean particle radius.

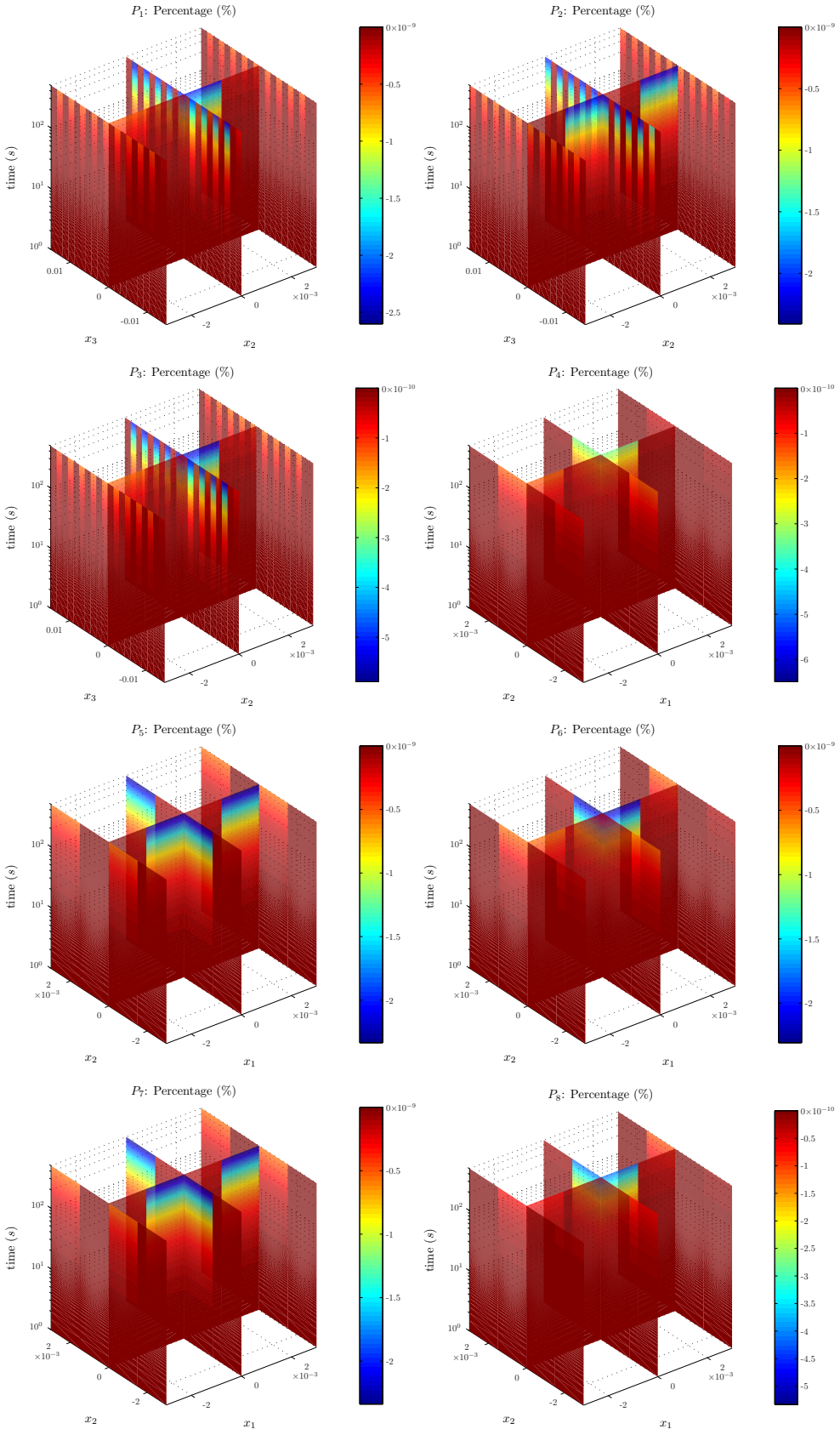

Figure B.17: Percent differences under tensile test of the particle standard deviation.

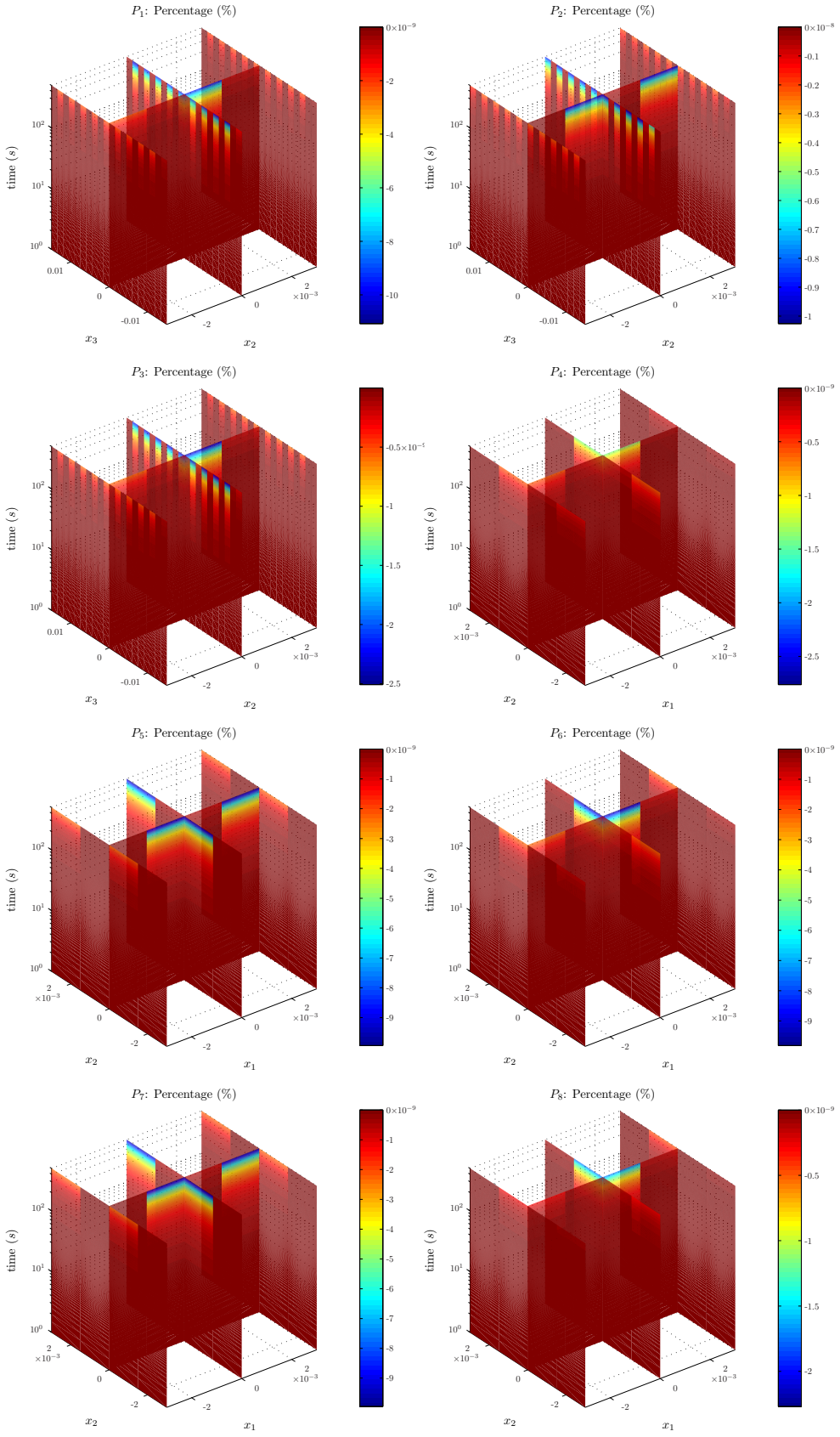

Figure B.18: Percent differences under tensile test of the mean concentration.

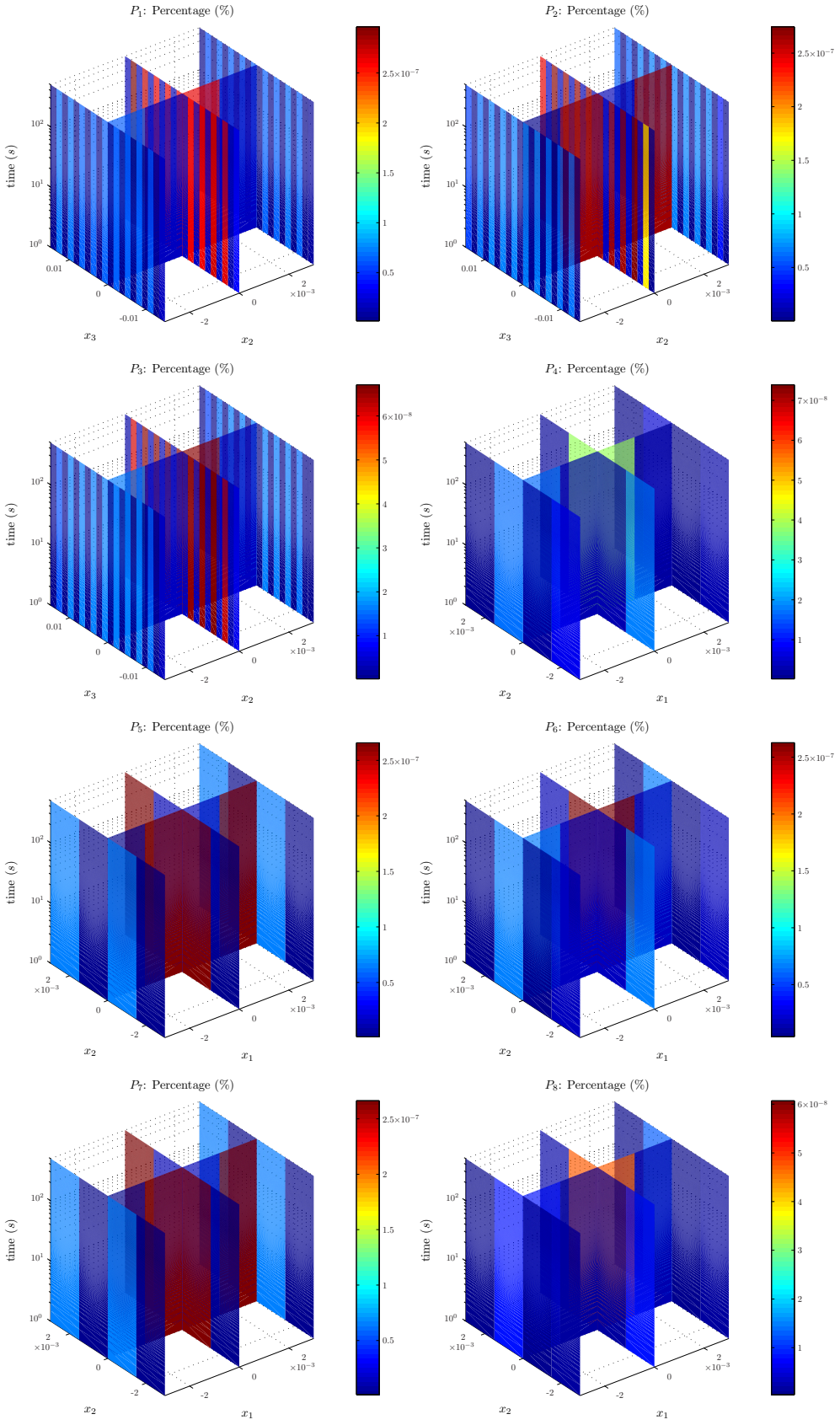

Figure B.19: Percent differences under tensile test of the nucleation rate.

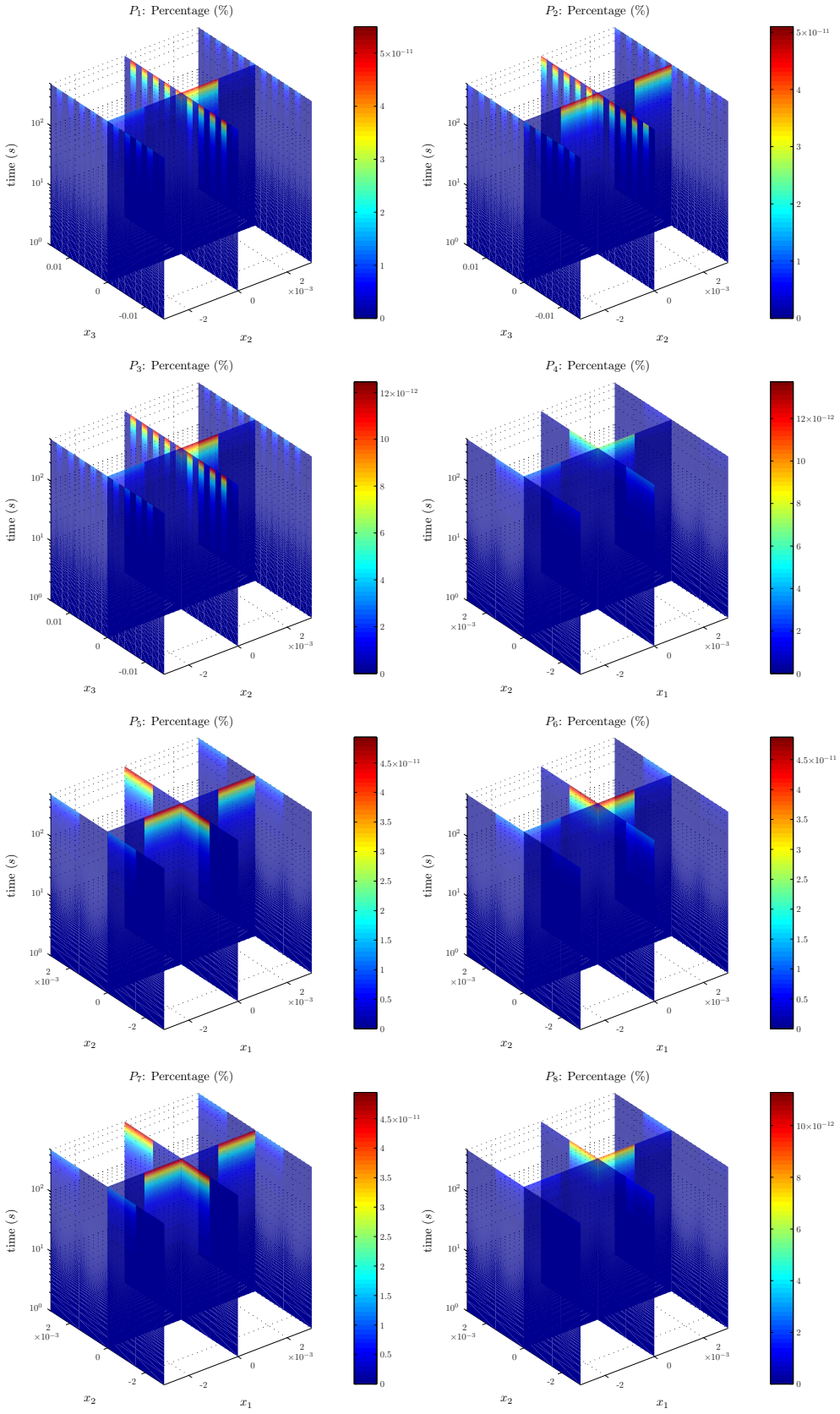

Figure B.20: Percent differences under tensile test of the Young's modulus.

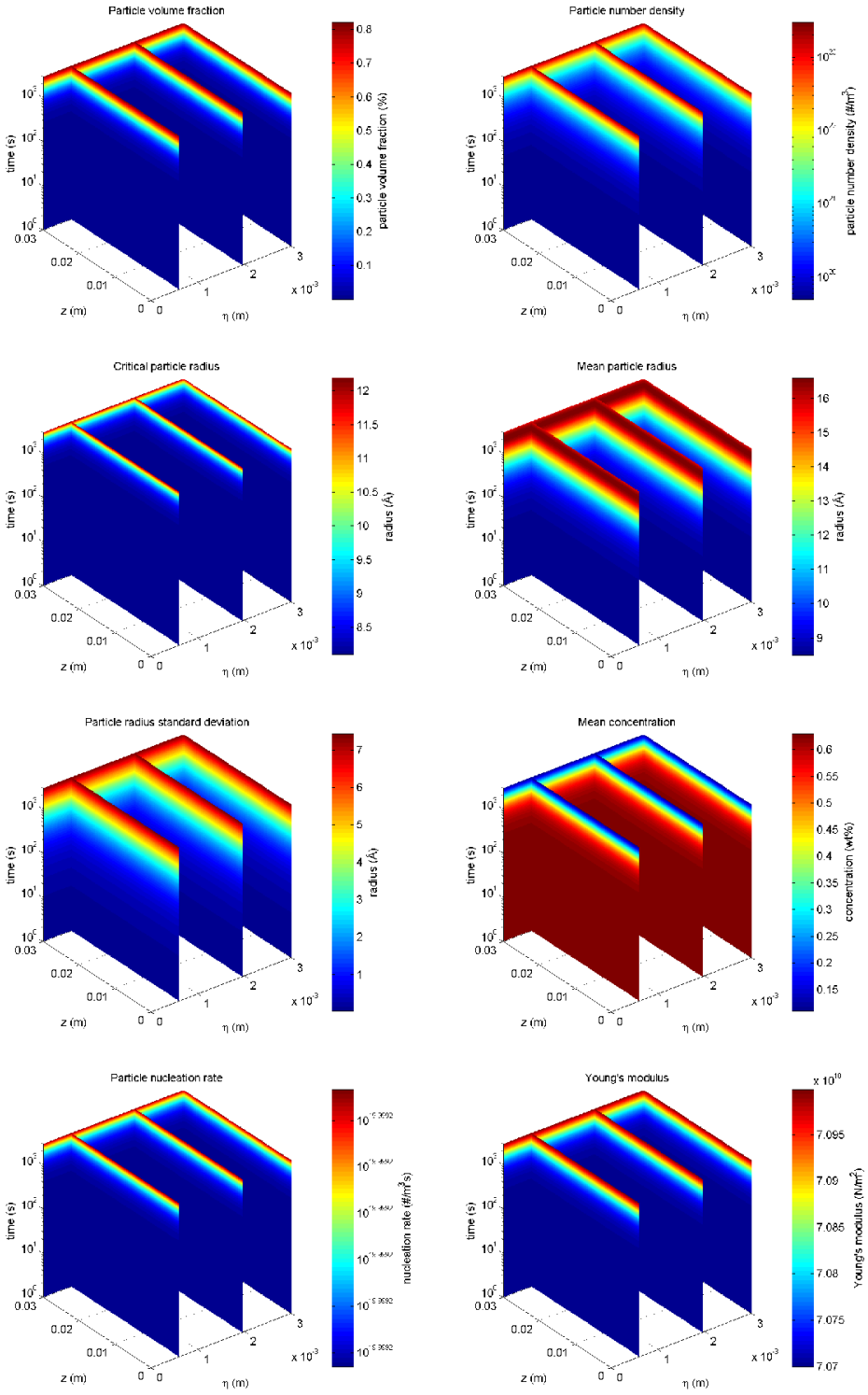

Figure B.21: Results under tensile test.

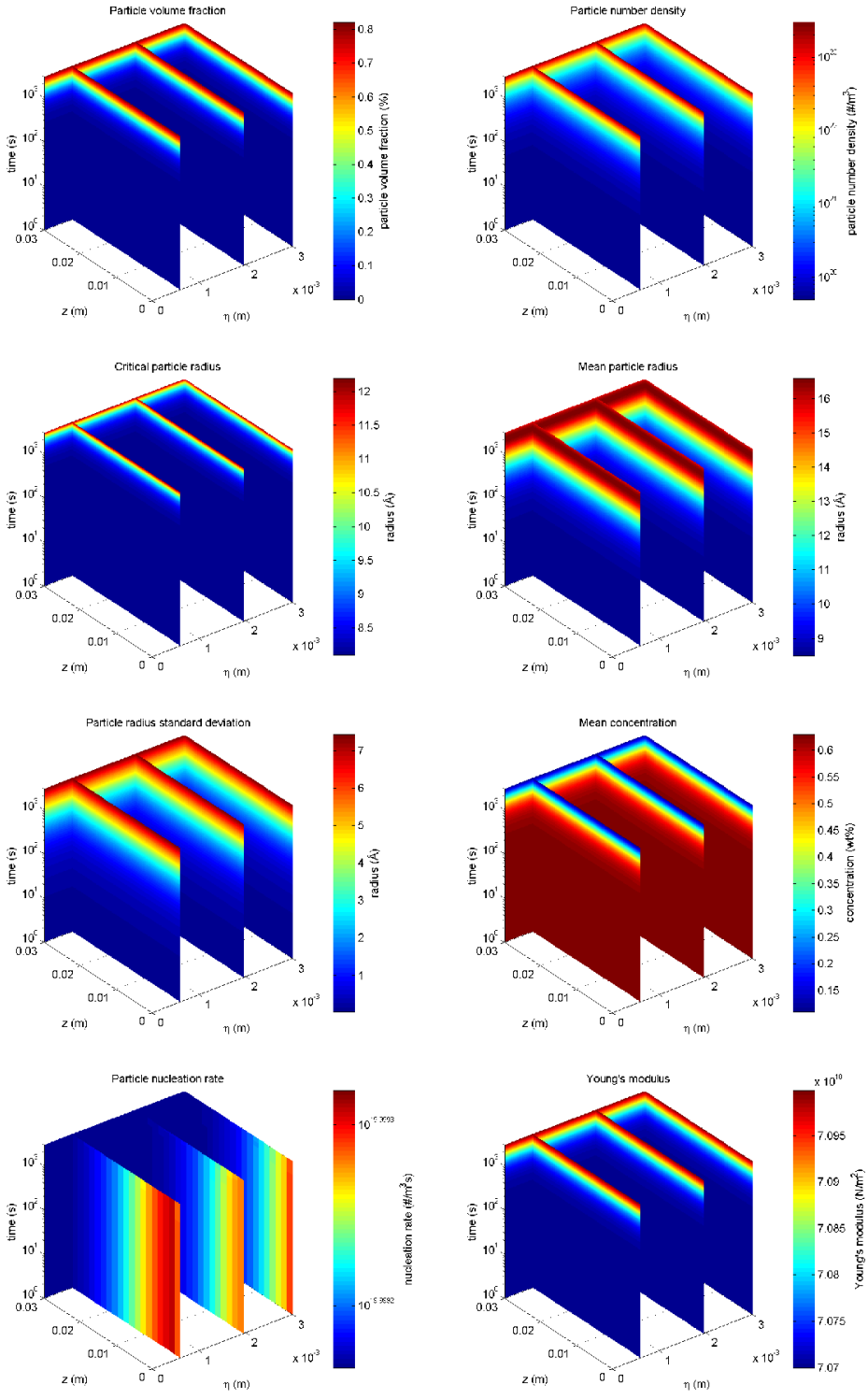

Figure B.22: Results under amplified tensile test.

Bibliography

Aaronson, H. I. , Kinsman, K. R. , and Russell, K. C. . The volume free energy change associated with precipitate nucleation. Scripta Metallurgica, 4(2):101–106, 1970.

Abrantes, J.P. , Clia de Lima, C.E. , and Batalha, G.F. . Numerical simulation of an aluminum alloy tube hydroforming. Journal of Materials Processing Technology, 179(1-3):67–73, 2006.

Barnett, D.M. , Lee, J.K. , Aaronson, H.I. , and Russel, K.C. . The strain energy of a coherent ellipsoidal precipitate. Scripta Metallurgica, 8(12):1447–1450, 1974.

CFD-Online. Tridiagonal matrix algorithm - TDMA (Thomas algorithm), 2005. Available at: `http://www.cfd-online.com/Wiki/Tridiagonal_matrix_algorithm_-_TDMA_(Thomas_algorithm)`. Last visited at: 7 March 2009.

Chau, K.T. and Wei, X.X. . Finite solid circular cylinders subjected to arbitrary surface load. Part I – analytic solution. International Journal of Solids and Structures, 37(40):5707–5732, 2000.

Hyland, R.W. Jr. Homogeneous Nucleation Kinetics of Al_3Sc in a Dilute Al-Sc Alloy. Metallurgical and Materials Transactions A, 23(7):1992–1947, 1992.

Jaeger, J.C. , Cook, N.G.W. , and Zimmerman, R.W. . Fundamentals of rock mechanics. Wiley, Blackwell, 2007.

Kampmann, R. , Eckerlebe, H. , and Wagner, R. . In: Materials Research Society Symposium Proceedings, volume 57, page 525. MRS, 1987.

Langer, J.S. and Schwartz, A.J. . Kinetics of nucleation in near-critical fluids. Phys. Rev. A, 21(3): 948–958, 1980.

Myhr, O. R. and Grong, Ø. . Modelling of non-isothermal transformations in alloys containing a particle distribution. Acta Materialia, 48(7):1605–1615, 2000.

den Ouden, D. . Particle nucleation and coarsening in aluminum alloys. Literature study, TU Delft, 2009.

Pal, R. . New models for effective Young's modulus of particulate composites. Composites Part B: Engineering, 36(6-7):513–523, 2005.

Porter, D.A. . Phase Transformations in Metals and Alloys. Chapman & Hall, London, 1981.

Ratel, N. , Bruno, G. , Bastie, P. , and Mori, T. . Plastic strain-induced rafting of γ' precipitates in Ni superalloys: Elasticity analysis. Acta Materialia, 54(19):5087–5093, 2006.

Robson, J.D. , Jones, M.J. , and Prangnell, P.B. . Extension of the N-model to predict competing homogeneous and heterogeneous precipitation in Al-Sc alloys. Acta Materialia, 51(5):1453–1468, 2003.

Robson, J.D. . Modelling the overlap of nucleation, growth and coarsening during precipitation. Acta Materialia, 52(15):4669–4676, 2004.

Seagrave, S. and Canty, T. . Part I Crystallography Tutorial - Diffusion, 1999. Available at: `http://www.soton.ac.uk/~engmats/xtal/diffusion/index.html`. Last visited at: 5 March 2009.

Tani, J. and Kido, H. . Lattice dynamics of Mg_2Si and Mg_2Ge compounds from first-principles calculations. Computational Materials Science, 42(3):531–536, 2008.

Uguz, A. . Determination of the crystallographic parameters of a fcc metal by means of electron channelling patterns. Crystal Research and Technology, 38(6):515–527, 2003.

Wagner, R. and Kampmann, R. . Materials Science and Technology - A Comprehensive Treatment, volume 5. VCH, Weinheim, 1991.

Wikipedia. Phase diagram, 2002. Available at: http://en.wikipedia.org/wiki/Phase_diagram. Last visited at: 5 March 2009.

Wikipedia. Tensile strength, 2003. Available at: http://en.wikipedia.org/wiki/Tensile_strength. Last visited at: 3 April 2009.

Wikipedia. Extrusion, 2004. Available at: http://en.wikipedia.org/wiki/Extrusion. Last visited at: 26 March 2009.

Wikipedia. Rolling (metalworking), 2005. Available at: http://en.wikipedia.org/wiki/Rolling_(metalworking). Last visited at: 26 March 2009.

Nomenclature

Nucleation related symbols

a_m, a_p	Lattice constants (m)
A_0	Parameter related to the energy barrier for nucleation (J/mol)
$\tilde{A}_0$	Adjusted parameter related to the energy barrier for nucleation $(J/m^3\sqrt[3]{\text{mol}})$
β^*	Atomic attachment frequency $(1/s)$
$\bar{C}$	Mean solute concentration in the system (wt%)
C_e	Equilibrium solute concentration at the particle/matrix interface (wt%)
C_i	Solute concentration at the particle/matrix interface (wt%)
C_p	Solute concentration inside the particle (wt%)
C_s	Pre-exponential term for C_e (wt%)
C_0	Overall solute concentration in the system (wt%)
D	Diffusion Coefficient (m^2/s)
D_0	Pre-exponential term for D (m^2/s)
δ_m, δ_p	Elastic constant used in ΔG_s (N/m^2)
ΔG_{dis}	Dislocation strain energy (J/m^3)
ΔG^*_{het}	Heterogeneous nucleation energy barrier $(J/\text{mol}$ or $J)$
ΔG_s	Strain energy (J/m^3)
ΔG^m_s	Misfit strain energy (J/m^3)
ΔG_v	Chemical volume free energy (J/m^3)
Δr^*	Factor used in production term (m)
ε_m	Linear misfit strain
f	Particle volume fraction
ϕ	Particle size distribution function $(\#/m^4)$
$\gamma_{\alpha\beta}$	Particle-matrix interface energy (J/m^2)
j	Nucleation rate $(\#/m^3 s)$
j_0	Numerical constant in the expression for j $(\#/m^3 s)$
k	Boltzmann constant $(1.380 \times 10^{-23} J/K)$
n	Total number concentration of particles in the system $(\#/m^3)$
N	Particle concentration $(\#/m^3)$
N_A	Avogrado constant $(6.022 \times 10^{23}$ 1/mol)
N_v	Number density of potential homogeneous nucleation sites $(\#/m^3)$
N^*_v	Number density of potential heterogeneous nucleation sites $(\#/m^3)$
N_0	Initial particle concentration $(\#/m^3)$
ν_m, ν_p	Poisson ratios
Q_d	Activation energy for diffusion (J/mol)
Q_s	Apparent solvus boundary enthalpy (J/mol)
r	Particle radius (m)
$\bar{r}$	Mean particle radius of the system (m)
r^*	Critical particle radius (m)
R	Universal gas constant $(8.314\ J/K\text{mol})$
ρ	Standard deviation of radii of the system (m)
ρ_D	Dislocation density $(1/m^2)$
S	Source term $(\#/m^3 s)$
t	Time (s)
T	Temperature (K)

τ	Incubation time for heterogeneous nucleation (s)
v	Growth rate of particles (m/s)
V_m	Molar volume of precipitates (m^3/mol)
x_p	Solute molar fraction inside the particle
Z	Zeldovich factor

Deformation related symbols

$\alpha_i, \alpha_i, \alpha_\alpha$	Boundary constants for deformations (N/m^3)
b, b_i, b_α	Internal body forces (N/m^3)
ΔG_s^{el}	Elastic deformation strain energy (J/m^3)
E, E_m, E_p	Young's modulus (N/m^2)
$\varepsilon, \varepsilon_{ij}, \varepsilon_{\alpha\beta}$	Strains
F_i, f_i, f_α	Boundary forces (N/m^2)
λ	Lamé first parameter (N/m^2)
μ, μ_m, μ_p	Shear modulus (N/m^2)
$\boldsymbol{n}$	Outward unit normal vector at boundary
ρ_m	Material density (kg/m^3)
$\sigma, \sigma_{ij}, \sigma_{\alpha\beta}$	Stresses (N/m^2)
u, u_i, u_α	Deformations (m)
$u_{bi}, u_{b,i}, u_{\alpha,b}$	Boundary values of deformations (m)
x, x_i, η, θ, z	Spatial coordinates (m)

Numerical symbols

Δt	Time step (s)
Δr	Size of particle radii class (m)
t^n	n-th discrete time (s)
r_i	Center of i-th particle radii class (m)
N_i^n	Short for $N(t^n, r_i)$ $(\#/m^3)$
A_{ij}^n	i,j-th element of discreet matrix at time t^n (m/s)
S_i^n	Short for $S(t^n, r_i)$ $(\#/m^3 s)$
v_i^n	Short for $v(t^n, r_i)$ (m/s)
e	Linear interior element
b	Linear boundary element
a_i^j	j-th component of i-th point of an element
S^e	Element matrix
q^e	Element vector
S^b	Boundary element matrix
q^b	Boundary element vector
l	Related to the length of an element
Δ	Related to the area of an element
V	Related to the volume of an element